Cellulose-based Self-Healing and Conductive Hydrogels for Ammonia Gas Sensors

By

Iman Yousefi

A Thesis submitted to the Faculty of Graduate Studies of

The University of Manitoba

in partial fulfilment of the requirements of the degree of

MASTER OF SCIENCE

Department of Biosystems Engineering

University of Manitoba

Winnipeg, Manitoba

Table of Contents

List of Figures

List of Tables

Acknowledgments

I would like to express my sincere gratitude to my advisor Dr. Wen Zhong for the continuous support and professional guide during my study. Her guidance helped me in research and writing of this thesis. I would also like to thank Dr. Malcolm Xing and Dr. Qiang Zhang for joining as my committee members for their insightful feedback and encouragement.

I thank all my lab colleagues especially Dr. Helen H. Hsu for helping me design the gas sensor and, Dr. Yuqing Liu and Dr. Kaige Xu who helped me with mechanical and rheological tests.

Last but not least, I would like to thank my family for their continuous support and encouragement and unconditional love throughout my life.

This research was supported in part by the Natural Sciences and Engineering Research Council of Canada (NSERC) and University of Manitoba, Graduate Enhancement of Tri-Council Stipends (GETS) program.

Abstract

Conductive cellulose-based hydrogels have attracted much research interests owing to their high conductivity, biocompatibility, cost-effectiveness, environmental sustainability, flexibility, excellent mechanical properties, Chemical or physical properties of conductive cellulosic hydrogel can be designed to change in response to external stimuli. The combination of such unique features makes them promising candidates for different practical applications, including electronic devices and gas sensors.

In the present work, a novel multi-functional hybrid hydrogel was fabricated via a facile two-step process. The flexible, self-healing, and electro-conductive hydrogels were successfully prepared by incorporating conductive nanomaterials (Graphene oxide or Reduced graphene oxide) into carboxymethyl cellulose networks crosslinked by citric acid. The chemical structure and morphology of the resulting conductive nanocomposite hydrogels were characterized using FTIR and SEM. The effect of the conductive nanomaterial contents on the mechanical, rheological, and electrical properties of the hybrid hydrogels was studied. The self-healing efficiency of the prepared hydrogels was evaluated by comparing tensile strength, breaking stress, and storage modulus of the original and healed samples.

The FTIR finding confirmed that the 3D CMC conductive hydrogels are formed as a result of intra- and inter-molecular hydrogen bonding among their constituents. Morphological studies demonstrate highly porous interconnected hydrogels with pore sizes of 100–200 μm. It was found that the mechanical strengths of the CMC hydrogels are significantly enhanced by the incorporation of GO/RGO into the hydrogel network. The tensile strength of CMC-GO and

CMC/RGO hydrogels are up to 2.3 times and 2.15 times stronger than the CMC hydrogels (85 KPa), respectively. Rheological results show a more stable hydrogel network with dominant elastic behavior.

In addition, the multi-functional hydrogels exhibit excellent self-healing ability, with about 91.2 %, 94%, and 93% healing efficiency in tensile strength, tensile strain, and storage moduli, respectively. The self-healing capacity of the hydrogels is endowed by the reversible hydrogen bonds in the abundant oxygen-containing functional groups and ionic interactions between oxygen-containing functional groups existing in both CMC and the conductive agents. The CMC-RGO hydrogels show maximum electrical conductivity of 4.4×10^{-2} S/cm and about 68% recovery of the electrical properties after self-healing. CMC-RGO hydrogel sensors demonstrate high sensitivity and desirable stability upon exposure to ammonia gas. With the combination of such superior features, the developed conductive CMC-RGO hydrogels have great potential for practical applications in gas sensors.

Chapter 1. Introduction

1.1 General overview

Nowadays, the production and emission of toxic, explosive, or flammable gases are increasingly growing due to their relevance in a wide variety of industries, including food and agriculture, automotive, and pharmaceuticals [1,2]. Ammonia (NH_3) is one of the most common and harmful air pollutants that may cause respiratory tract irritation at a low concentration from 50 to 100 ppm[3,4]. The development of highly sensitive, reusable, portable, and cost-effective gas sensor devices that enable the effective monitoring of environmental pollutants and the detection of trace chemicals is of great importance for a broad spectrum of applications, including industrial hazardous gas monitoring, food quality/safety monitoring, and healthcare monitoring[1,5]. Various materials, including metal oxide semiconductors, conjugated polymers, carbon-based nanomaterials, and conductive hydrogels, have been research and developed as gas sensing elements[6].

Hydrogels have highly hydrated and three-dimensional (3D) crosslinked networks that entrap substantial water, saline, or physiological solutions [1]. The hydrogels possess their unique physical characteristics, such as hydrophilicity, large specific surface area, and tissue-like structure. These 3D-networks have drawn tremendous attention in the various potential applications, including supercapacitors[2], energy storage devices[3], biosensors[4], tissue engineering[5], drug delivery and wound dressing [6–8], and gas detectors[9].

The gas sensor is a sensing device that enables monitoring of environmental pollutants, and the detection of trace chemicals is essential for both industrial and civilian purposes[10,11]. An ideal gas sensor device is usually expected to be highly sensitive, selective and stable, cost-effective, and able to work at room temperature[12]. Numerous sensing materials for gas detection have been used. It includes metal oxide semiconductors (Tin dioxide, titanium dioxide), conjugated polymers

(Polyaniline, polypyrrole), and carbon-based nanomaterials (Graphene, Carbon nanotubes)[13]. But there are still some main challenges that limit their use for practical application. The high working temperature of metal oxide, expensive doping modification process of conductive polymers, and the inability to produce carbon-based nanomaterials with desired quality and uniformity restrain the application for gas detectors[14]. The development of a new smart gas sensor able to combine many features has gained great attention. An alternative approach for these disadvantages is designing and utilizing new gas-sensitive materials based on hybrid inorganic–inorganic [11], organic–organic [12], and inorganic-organic materials. For example, Hu et al. [15] fabricated the SnO_2/RGO-based sensor demonstrated a noticeably enhanced sensitivity compared with the responses of pure SnO2- or RGO-based sensors toward H_2S at room temperature. It is well known that the electrical conductivity of conducting polymers is affected by exposure to a diverse gas analyte. For instance, Graphene can be incorporated into the PANI matrix to form a hybrid thin film that possesses enhanced, reversible, and stable ammonia gas sensing performance [16]. Among hybrid sensing materials, Conductive Hydrogels are becoming attractive alternative materials for sensor devices as they can be endowed with such unique properties as high elasticity, self-healing, and conductivity.

1.2 Problem Definition

Conductive hydrogels have gained much attention as an advanced electronic platform for sensors by synergizing the advantageous features of soft materials and organic conductors[17]. Electrically conductive hydrogels (ECHs) can be produced by combining a hydrophilic matrix with electrically conductive fillers, such as metallic nanoparticles, conductive polymers (CPs), or carbon-based materials[18]. The nature of the conductive hydrogel structure, including the high surface-to-

volume ratio and porous structure, results in the fast adsorption and diffusion of gas molecules onto the hydrogel's surface and rapid electrical response to external stimuli. It is worth noting that the chemical or physical properties of conductive hydrogel can be significantly changed in response to external stimuli (such as temperature, pH, stress, moisture, electric fields, magnetic fields, light, chemical compounds, etc.)[19]. Among Conductive polymers, polypyrrole (PPy) and polyaniline (PANI) are commonly used to fabricate conductive hydrogels-based sensors. However, conductive polymer-based hydrogels showed weak mechanical strength, and the electrical conductivity of pure conductive polymer is too low to function as gas sensing materials[17]. Hence, Conductive carbon-based nanomaterials have been used in conductive hydrogel fabrication to meet the needs for numerous applications owing to their distinct properties. The introduction of carbon-based materials such as carbon nanotubes (CNT), graphene, and graphite into the hydrogel network enhances mechanical strength and significantly affects the electrical conductivity of hydrogels[20]. However, the development of conductive hydrogels with superior eco-friendliness, self-healing ability, and easy-to-fabricate processes is still a challenge. Another problem is that the uniform dispersion of carbon-based materials into the hydrogel matrix is difficult.

1.3 Objective

To date, demands for environmentally friendly and conductive hydrogel-based products with specific competent properties are considerably growing. However, particular unpredicted challenges often emerge in the case of sensor application, such as low conductivity, weak mechanical performance, lack of self-healing ability, non-sustainability, which cannot satisfy the actual needs.

The objective of this current study was to develop multifunctional cellulose-based hydrogels that exhibit excellent mechanical properties, high conductivity, self-healing capacity, and gas-sensing efficiency toward ammonia gas. In particular, a novel conductive hydrogel with self-healing ability and superb mechanical performance will be fabricated using a sustainable resource of cellulose. Reduced graphene oxide and Graphene oxide nanoparticles will be integrated into the hydrogels via a facile two-step method to impart both conductivity and self-healing capacity. This work may open a new door for the fabrication of multi-functional ammonia gas sensors.

Chapter 2: Literature review

2.1. Introduction

Hydrogel, as a kind of soft material with a three-dimensional structure, can be prepared through the crosslinking of natural or/and synthetic polymers. Unique features of hydrogels such as a high surface-to-volume ratio and porous structure provide sufficient surface areas and defects for ammonia gas adsorption, making them suitable as ammonia gas sensor devices[19]. Various synthetic polymers have been used for the fabrication of hydrogels. Polyvinyl alcohol (PVA) [21], polypyrrole (PPY) [22], polyethylene glycol (PEG) [23], polyoxazoline[24], polyacrylamide (PAM) [25], and their copolymers [26,27] are the most popular synthetic polymers for hydrogel preparation. Although they allow easy control of hydrogel structure and mechanical characteristics, their low biocompatibility and non-degradability confine their usage for various industrial/clinical purposes. Researchers address these challenges by employing natural polymer-based hydrogels by taking advantage of their excellent hydrophilicity, biocompatibility, biodegradability, and availability from renewable resources[28]. In recent years, structured hydrogels made of natural polysaccharides, such as chitosan, alginate, and cellulose, have been intensively explored for food packaging, wastewater treatment, gas sensing, and energy storage, and biomedical applications[29]. However, weak mechanical properties, brittleness, and reduced flexibility of most polysaccharides hinder their further practical applications [30].

Nevertheless, cellulose and its derivatives have been shown as promising alternatives to synthetic polymers due to their reproducibility, cost-effectiveness, and sustainability [31,32]. Cellulose-based materials also benefit from their abundance of reactive hydroxyl groups. It not only enables the formation of hydrogels via either non-covalent or covalent crosslinking but also offers several opportunities for new modifications, leading to the development of unique functional materials for advanced applications[33,34].

However, cellulose-based hydrogels may still have challenges to be used for specific applications where high mechanical performance is required. There has always been a rising demand for environmentally friendly and biocompatible hydrogel-based products with specific competent properties[35]. Hence, an eco-friendly nano-scale material isolated from native cellulose, known as nanocellulose, has gained much attention to be used as a building block of hydrogels during the last two decades[36,37]. The exceptional characteristics of nanocellulosic hydrogels include low density, excellent mechanical performance, flexibility, renewability, and biocompatibility. These unique features make them promising materials for diverse high-performance applications[38]. Based on source and processing conditions, the nanocellulose family is categorized into three different groups, namely cellulose nanocrystals (CNCs), cellulose nanofibrils (CNFs), and bacterial cellulose (BC) [39,40].

The hydrogels can facilitate the transport of electrons and ions[41]. Hence, remarkable progress has recently been obtained to fabricate advanced hydrogel composed of cellulose and conductive agents. Conductive materials like conductive polymers, carbon-based nanomaterials, and metal particles have been used in conductive hydrogel fabrication to meet the requirements for numerous applications owing to their distinct electrical properties[42,43]. Such conductive hydrogels (CHs) have been broadly employed in the areas of small electronic devices, biomedicine, and supercapacitors [18].

This chapter will, therefore, summarize significant features of the nanocellulose family, including CNF, CNC, and BC, and explore recent advances in the application of conductive nanocellulose hydrogels in the past ten years. The use and impact of each kind of conductive nanocellulose based hydrogel in different areas, including biomedical, energy, and electronics, will be discussed. In addition, conductive hydrogels based on cellulose and cellulose derivative will also be briefly

introduced as their developing methods may be adapted to the development of nanocellulose based conductive hydrogels. Finally, future perspectives, limitations, and possible research potentials on the new applications of these sustainable and conductive hydrogels will be proposed.

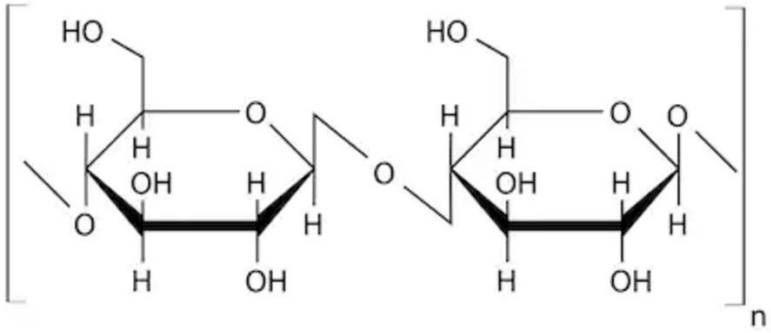

Figure 2. 1 Chemical structure of cellulose

2.2. Cellulose and its derivative

Cellulose is well-known as an oxygen-rich polysaccharide resource in nature. It is found as the primary ingredient of green plants and natural fibers[44]. Cellulose content ranges from 40 to 50% in dry wood, 90% in cotton, and around 60 % in hemp[45,46]. Cellulose fiber has exceptional physicochemical properties, including the possibility for incorporating different chelating groups into the polymeric networks, excellent mechanical performance, sustainability, and low cost, which make them promising materials for various industrial applications[47]. The efficient extraction of high-purified cellulose fibers obtained through the removal of the lignin, hemicellulose, and other impurities as much as possible. Various methods have been adopted for the isolation of cellulose from plant tissue using chemical, mechanical, or combined treatment [48]. The conventional techniques for isolating cellulose fiber include fibers treatment with

alkaline sulfate and acid sulfite, steam, carbon dioxide, and ammonia explosion [49,50]. These methods have also been applied as a pre-treatment to help the hydrolysis procedure to generate nanocellulose materials [51,52].

Cellulose is insoluble in water and common organic solvents owing to extensive intra- and intermolecular hydrogen bonding between its hydroxyl groups [53]. However, the free hydroxyl groups distributed along the cellulose backbone provide possible sites for various chemical modifications [54]. The chemical structure of cellulose is illustrated in Figure 1. By etherification or esterification of the hydroxyl groups on the cellulose backbone, cellulose derivatives such as cellulose acetate (CA), carboxymethylcellulose (CMC), methylcellulose (MC) can be produced [47]. Cellulose ether such as methylcellulose (MC), hydroxypropyl cellulose (HPC), hydroxyethylcellulose (HEC), and carboxymethyl cellulose (CMC) are promising resources for hydrogel preparation, with many applications in the food, pharmaceutical, and cosmetics products since most of them are water-soluble and cost-effective [55]. Most cellulose esters are water-insoluble polymers. Among them, cellulose acetate (CA) and cellulose acetate propionate (CAP) are widely used as stabilizers, thickeners, and viscosity modifiers in many industries, including pharmaceutical controlled release preparations, construction, paper, adhesives, and textiles [47].

2.2.1 Cellulose nanofibers

Cellulose nanofibers (CNF) (Fig. 1c) are also termed nanofibrillated cellulose (NFC), microfibrillated cellulose (MFC), or cellulose nanofibrils. They generally consist of alternating crystalline and amorphous cellulose chains with a diameter varying from several nanometers to 100 nm and a length of a few micrometers. Such flexible CNFs are often isolated from wood sources via high energy mechanical disintegration[56]. To effectively facilitate delamination of

individual nanofibrils from cellulosic fibers, pre-or/and post-treatments including enzymatic hydrolysis of macroscopic fibers 2,2,6,6,-tetramethylpiperidine-1-oxyl (TEMPO)-mediated oxidation or other surface treatments (e.g., carboxymethylation[57], carboxylation[58], quaternization,[59] are required[36].

As a naturally occurring nanomaterial, cellulose nanofibers (CNFs) display excellent mechanical strength and stiffness, low density, and tunable surface chemical reactivity [60]. Also, these physicochemical features of CNF have enabled their use as building blocks or reinforcing agents of hydrogels[36]. Some key characteristics have been imparted to the CNF hydrogel to enhance the performance of the final products. It has been reported that taking full advantage of the exceptional properties of CNF and conductive materials in the form of the hydrogel may provide great opportunities for different functional applications like electronic devices, battery storages, tissue engineering, sensors, and drug delivery[61].

2.2.2 Cellulose nanocrystal

Cellulose nanocrystal (CNCs), also known as nanowhiskers and microcrystals, are one-dimensional rigid crystalline nanorods. They are isolated from semi-crystalline cellulose through acid hydrolysis of cellulose fibers[62]. The geometrical dimensions of CNC are different in length depending on the cellulosic sources, with a diameter ranging from 5-30nm [63–65]. The type of mineral acids used for the hydrolysis influences the surface characteristics of the nanocrystals[66]. For instance, crystals produced via hydrochloric acid have poor dispersibility. In contrast, hydrolysis with sulfuric acid improves the durability of cellulose crystals due to electrostatic repulsive force within the negatively charged sulfate ester groups on the surface [67]. The excellent features of CNCs, including sustainability, non-toxicity, high rigidity, excellent colloidal stability,

and ease of surface modification because of the abundance of surface hydroxyl groups, have made them promising as a reinforcing agent or building blocks of hydrogels for various applications.

2.2.3 Bacterial cellulose

Bacterial cellulose (BC) is a kind of cellulose generated by microorganisms[68]. It is generated by a primary metabolism process of several genera, such as Acetobacter, Agrobacterium, Achromobacter, Aerobacter, Azotobacter, Sarcinaventriculi, Salmonella, Escherichia, and Rhizobium [69]. Compared to plant cellulose, BC benefited from its higher chemical purity and crystallinity, excellent biocompatibility, and biodegradability[70]. BC nanofibers are usually randomly distributed in fibrous layers, with some fibers act as cross-linkers to entangle the fibrous layers, resulting in the formation of a multi-layered structure [71]. These features have made them attractive materials for a variety of practical applications such as foods, electronics, specialty paper, cosmetics, and healthcare[72]. Most importantly, BC, as a biopolymeric hydrogel, possessed 3D networks with high water retention properties.

2.3 Conductive cellulosic hydrogels

2.3.1 Conductive cellulose hydrogels

Conductive cellulose hydrogels can be prepared through blending, coating, or by doping the conductive materials into/onto the cellulosic matrix[33]. Fang et al. [73] synthesized conductive composite hydrogels using oxidative polymerization of pyrrole monomers in the presence of cellulose. They reported that the conductivity of the hydrogel is dependent on the amount of oxidants in the conductive hydrogels. They also found that using dopants with smaller steric

hindrance can effectively increase hydrogel conductivity. Shi et al.[74] prepared a conductive hydrogel from cellulose and Polyaniline (PANI) via the entanglements between PANI chains and crosslinked cellulose networks. The hydrogels demonstrated electromechanical actuation under a low applied electric field. In another work, Xu et al. [75] constructed a hierarchical hydrogel network containing cellulose and PANI. They employed cellulose hydrogel as a template to support in-situ limited interfacial polymerization of PANI, resulting in single-sided conductive hydrogels. As the PANI polymerization process progressed, the electrical conductivity improved due to the contribution of PANI chains, which homogeneously dispersed into the cellulose network. Sun et al. [76] synthesized electroactive conductive hydrogels by co-doping various conductive materials into the cellulose matrix. The obtained hydrogels made of cellulose, carbon nanotube (CNT), MnO_4, and PANI showed a conductivity of 0.083 mS/cm.

Hydrogels based on cellulose derivatives have been considered as promising materials for different practical applications because of their low-cost production, bio-compatibility, and sustainability [33]. George et al. [77] fabricated flexible and conductive biosensors for the acidity level of body fluid. The dispersion of CMC and Graphene sheets were prepared via 3D printing for PH sensors, and Chitosan hydrogels were cast on 3D printed electrodes. Heat-treatment before hydrogel coating was reported to increase the conductivity up to 2.5 times. Hussain et al. [78] designed self-healable and conductive HEC-based hydrogels through interactions among HEC, poly(acrylic acid-co-acrylamide), and ionic crosslinker Fe^{3+}. It was shown that the hydrogen and ionic coordination interactions within the hydrogel network changed the electrical properties of the healed hydrogels. Li et al. [79] successfully constructed conductive composite hydrogels composed of sodium CMC, PANI, and glycerol diglycidyl ether as a biocompatible crosslinker. Their findings demonstrated that increasing concentrations of crosslinker and CMC resulted in a

decrease in conductivity. It might be attributed to the reduction of free space in the hydrogels network that disadvantaged PANI absorption and the formation of an interpenetrating network structure of CMC and PANI. Barras et al.[80] printed conductive flexible hydrogel composed of CMC and carbon fiber (CFs). It was found that the introduction of the conductive component into the printed patterns implied that the electrical conduction was controlled not only by the inherent properties of CFs but also allowing charge transfer through the CMC matrix between adjacent fibers, and therefore improving the conductivity. Rastin et al. [81] developed 3D printed conductive hydrogel bio-inks composed of methylcellulose (MC), kappa-carrageenan, and conducting polymers poly(3,4-ethylene dioxythiophene): poly(styrene sulfonate) (PEDOT: PSS) for tissue engineering applications. The electrical conductivity of products can be varied by tuning the amounts of conducting polymers. The prepared hydrogel bio-inks were also found to be biocompatible and suitable for biomedical applications.

Table 2. 1 Summary of reports on Cellulosic conductive hydrogel

Material components		Features	Swelling porosity Density(ρ)	Electrical properties	Mechanical properties	Application	Ref
Matrix	Conductive component(s)						
Cellulose	PPY	Controllable mechanical/ conductive properties	N/R	9.18×10^{-3} S/cm	CS~26.25MPa	Drug delivery and artificial muscle	[73]
Cellulose	PANI	Electromechanical actuation	N/R	7×10^{-2} S/cm	CS~0.48 MPa	Biomimetic materials	[74]
Cellulose	PANI	Hierarchical micro-nano structure, biocompatible	SR~92%	0.49 S/cm	TS~2.71 MPa	Nerve Regeneration	[75]
Cellulose	MnO_2/PANI/ CNT/RGO	Bioinspired, fast response (actuator)	P~87%	0.083 mS/cm.	TS~2.8 MPa	Artificial muscles	[76]
CMC	Graphene	Flexible, pH-sensitive,	N/R	N/R	N/R	Patch antennas for wireless	[77]

HEC/PAA-PAM	Fe3+	Self-healing, super mechanical strength, moldability	N/R	2.4×10^{-3} S/cm.	TS~3.50 MPa CS~ 32 MPa	Smart device	[78]
CMC	PANI	Non-toxic crosslinking agent	SR~104%	6.31×10^{-3} S/ cm	CS~ 0.448 MPa	electro-stimulated controlled drug release, sensors	[79]
CMC	carbon fibers	Printability	N/R	300 Ω/cm	N/R	Flexible and printed electronics	[80]
MC/kappa-carrageenan	PEDOT: PSS	Printability	N/R	3000 µS/cm	N/R	Tissue engineering	[81]
TEMPO-CNF/ PAA	PPY	Self-healing, stretchable	P~85%	2.4-4.2 S/m	TS~0.6 MPa. CS~1.65 MPa.	Wearable electronics	[82]
PAM/CNF	CNT	Improved mechanical property	SR~710%	8.5×10^{-4} S/cm	TS~0.32 MPa. TM~0.26 MPa.	Biomedical and electronic devices.	[83]
Carboxymethyl CNF	SWCNTs	3D printability	N/R	3.8×10^{-1} S/ cm	N/R	Neural tissue engineering	[84]
PVA/Borax, CNF	Graphene	Self-healing, Stretchable	SR~97% ρ~1.6 $g.cm^{-3}$	3.55 S/m	CS~0.148MPa TS~0.008MPa	Wearable sensing devices.	[85]
PVA, Borax, CNF	PPY	Rapid self-healing, pH sensitivity	SR~ 95% ρ~1.21 $g.cm^{-3}$	3.65 S/m	TS~0.06MPa CS~2 MPa	Flexible bioelectronics	[86]
Agarose, CNF	PPY/Fe_3O_4	Reversible restorability	N/R	6.22×10^{-2} S/cm	N/R	Electronic skin and electrochemical display devices	[87]
PVA, CNF	PANI/$MnFe_2O_4$	Dual conductive and magnetic properties	N/R	8.15×10^{-3} S/cm	N/R	Multi-functional applications	[88]
SA, TEMPO-MFC	PPY	Conductive	SR~26g/g P~95.40% ρ~0.17 $g.cm^{-3}$	8.9×10^{-3} S/cm	CS~1.27 MPa CM~2.34 MPa	Biomaterial applications	[89]
MFC	PPY	Ion-exchange	N/R	1.5 S/cm	N/R	Energy storage devices	[90]
TEMPO-CNF	CNT	3D printability	N/R	216.7 S/cm	TS~ 247 MPa.	Wearable electronic devices	[91]
CNF	CNT	3D printability	N/R	~0.1–0.01 S /cm	N/R	Biomedical application	[92]
CNF/ Alginate	SWCNTs	3D printability	N/R	2.132 S /cm	N/R	Neural tissue engineering	[93]

CNC	PPY	High water retention	SR~ 910%	8.8×10^{-3} S/cm	CS~13.8 MPa CM~4.16MPa	catalyst supports, nerve regeneration, and carbon capture	[94]
Cellulose	PPY	Good electrical conductivity	Sw ~560	7.8×10^{-3} S/cm	CS~26.2MPa.		[95]
CNC	Silver	3D printability,	N/R	1–50Ω	N/R	Electronics	[96]
CNC	MWCNT	3D printability	N/R	N/R	N/R	Microfluidic devices	[97]
CNC/ Gelatin	PANI/RGO	Self-healing, flexible	N/R	5.67 Ω	TS~ 0.017MPa TM~0.004 MPa	Energy storage devices	[98]
BC	PtNPs/ MWCNTs	Good biocompatibility	N/R	0.587 S/cm	N/R	Implantable glucose fuel cell	[99]
BC	PPY	Good conductive and catalytic activity	N/R	N/R	N/R	Microbial Fuel Cells	[100]
BC	PANI	Electroconductive	N/R	10^{-8}-10^{-2} S/cm	N/R	Diverse applications	[101]
BC	c-MWCNTs	Highly stretchable, good cycling stability	N/R	N/R	TS~189.5 MPa TM~ 4.5 MPa	Bio-based sensors	[102]
BC/PVA/ Alginate	c-MWCNTs, Carbon black	Stretchable and durable	N/R	N/R	TS~1 MPa CS~0.337 MPa	Wearable device	[103]

Abbreviations:
N/R: Not Reported;
CM: Compressive Modulus; CS: Compressive Strength; P: Porosity; TM: Tensile Modulus;
SR: Swelling Ratio; TS: Tensile Strength;
BC: Bacterial Cellulose;
CMC: Carboxymethyl Cellulose; CNT: Carbon Nanotube; CNF: Cellulose Nanofiber;
MC: Methyl Cellulose; MFC: Microfibrillated Cellulose; MWCNT: Multi-Walled Carbon Nanotube;
RGO: Reduced Graphene Oxide
PAA: Polyacrylic Acid; PAM: Polyacrylamide; PANI: Polyaniline; PPY: Polypyrrole; PVA: Polyvinyl Alcohol;
PEDOT:PSS: Poly(3,4-ethylenedioxythiophene):poly(styrenesulfonate)
PtNP: Platinum Nanoparticle;
SWCNT: Single-Walled Carbon Nanotube;

2.3.2 Conductive Hydrogels containing CNF

Conductive CNF based hydrogels have attracted lots of attention in electronic devices. CNFs derived from trees have fascinating piezoelectric characteristics and a powerful dipole, making

them aligned using an electric field [104]. Conductive polymeric hydrogels are restricted in practical usage because of their weak processability, biocompatibility, mechanical properties, and non-renewable resources. Hence, mixing them with CNFs alleviate these limitations and lead to hydrogels with tunable conductivity and better mechanical properties. The high surface area of CNFs and their network structure decrease the percolation threshold of conductive materials [105]. Hence, with their large surface areas, flexibility, and ability to reinforce matrices, conductive CNF hydrogels can be developed for sensors, electronics, energy storage, composites, and biomedicine applications. Chen et al. [82] produced self-healable and stretchable conductive hydrogels for damage-free wearable electronics. They prepared uniform dispersion of TEMPO-oxidized CNF into polyacrylic acid hydrogels crosslinked by ferric salts, and the conductive hydrogel was obtained by in-situ polymerization of pyrrole monomers into the hydrogel matrix. A combination of synergistic properties of TEMPO-oxidized cellulose nanofibers (TOCNFs), PAA, and PPy endowed the prepared hydrogels with high tensile strength and fracture strain, conductivity, and self-healing efficiency. The conductivity of hydrogels was almost doubled as Pyrrole polymerization progressed.

Recently, Carbon nanotubes (CNTs)/nanocellulose have been studied for flexible electronic usages. Chen et al.[83] developed conductive hydrogels with good mechanical and electrical properties. The conductive hydrogels were obtained through the polymerization of acrylamide in a CNF /CNT dispersion. The addition of CNT, along with CNF, improved the conductivity of hydrogels up to 8.5×10^{-4} S/cm, which is two-fold higher than the polyacrylamide/ CNT. It may be caused by CNF who improved the dispersion of CNT into the acrylamide solution. The resulting hydrogels can be applied in the fields of tissue engineering and biomedical sensors. Li et al. [91] fabricated carbon nanotube/nanofbrillated cellulose composite microfiber via a 3D-printing

technique. The adjustment of both CNT and CNF in microfibers and the uniform distribution of CNT and CNF improved electrical conductivity. The final conductive products can be employed in smart wearable electronic and energy storage devices. Håkansson et al. [92] printed a Carboxymethylated CNF and CNT hydrogel-based ink. The physical properties and structural integrity of composite can be controlled by the solidification process. 4-point and 2-point probe methods were applied to measure dry- and wet-state conductivity of the hydrogel composite material, ranging from 0.1 (dry) and 0.01 S/cm (wet). Bordoni et al. [93] fabricated conductive neural scaffolds through 3d-printing CNF/ alginate/single-walled carbon nanotubes hydrogel inks. The highest conductivity of the scaffold was around 2.13 S/cm. They showed that the conductivity of hydrogels significantly contributed to neural cell differentiation.

Volodymyr et al. [84] synthesized printable conductive CNF scaffolds for neural cell proliferation and adhesion. CNF functionalized with carboxymethyl groups was mixed with carboxylated SWCNTs at the pH of 8.5 to prepare ink for 3D printed conductive hydrogel with a conductivity of 3.8×10^{-1} S cm^{-1} when CNT concentration was about 20%. The Carboxymethylated CNFs were entangled with themselves and CNTs to build robust hydrogel ink with suitable rheological properties. Zheng et al.[85] fabricated conductive hydrogels that are highly stretchable and self-healing. The final composite hydrogels were formed by hydrogen bonding system and polymer chain entanglements among borax crosslinker, PVA, and Graphene-CNF nanocomposite. CNF, as a nanocarrier, improved the dispersion of graphene into the polymer matrix to make 3D conducting pathways inside the hydrogels. It was reported that the conductivity of 3.55 $S \cdot m^{-1}$ was achieved at a Graphene content of 0.7 wt%. It is reported that the conductivity of hydrogels remained relatively stable under frequent cutting/healing cycles[85].

Ding et al. [86] developed hybrid conductive hydrogels composed of PVA and borax (PB) as a hydrogel matrix and nanostructured CNFs−PPY complexes as both reinforcing and conductive agents. The strong hydrogen and reversible ionic interaction among hydrogel components, as well as chain entanglement, resulted in the formation of a hierarchical 3D structure. The conductivity of the hydrogels enhanced up to 4.8 S m^{-1}, with the addition of pyrrole concentration. It was reported that the efficient dispersion of the PPY-CNF complex within the PB provided a continuous porous conductive network.

In recent years, lots of research efforts have been concentrated on the integration of several advanced functions into a conductive hydrogel for the development of multi-functional hydrogels. For example, the conventional method of mixing conductive and magnetic materials may cause agglomeration within hydrogels. Hence, the fabrication of conductive and magnetic hydrogels has been a big challenge[106]. Recently, Liu et al. [87] synthesized a nanocomposite conductive hydrogel made of agarose, nanofibrillated cellulose, PPY, and Fe_3O_4. Using TEMPO-oxidized CNF as templates not only provided a large surface area to load significant amounts of nanoparticles but also prevented the Fe_3O_4 NPs and PPY from agglomeration in the nanocomposites owing to the network structure and the electrostatic repulsion induced by CNF. The conductivity of the hydrogels varied from 3.39×10^{-2} to 6.22×10^{-2} S cm^{-1} with increasing content of the conductive polymer.

The self-healing feature can be a key feature for multi-functional conductive hydrogels. Liu et al.[88] fabricated self-healable polyvinyl alcohol (PVA) hydrogels containing CNF with both conductive and magnetic functionalities. PANI and $MnFe_2O_4$ nanoparticles were first incorporated onto the modified CNF through in situ polymerization and chemical co-precipitation process, respectively, to form CNF/PANI/$MnFe_2O_4$ nanocomposites. They were subsequently blended with

the PVA hydrogels with the highest saturation magnetization and conductance of about 5.22 $emu \cdot g^{-1}$ and 8.15×10^{-3} $S \cdot cm^{-1}$, respectively. The evenly distribution of the conductive PANI-coated CNF into the PVA hydrogel matrix to provide a continuous electron transport pathway may contribute to the good conductivity of the hydrogel.

Cellulose nanofiber (CNF) has been known to possess appropriate interaction with PPY through plenty of hydroxyl groups on its backbone. Lin et al. [89] investigated the introduction of modified-nanofibrillated cellulose into the sodium alginate hydrogel along with the in-situ pyrrole polymerization. TEMPO-modified CNF can not only act as the strengthening agent but also played a vital role in the formation of the crosslinked networks. It was indicated that the conductivity of the composite hydrogels was significantly improved with a higher amount of functionalized CNF. In another work, Nystro et al. [90] prepared the conductive CNF-PPY nanocomposite hydrogels with a high surface area. The prepared hydrogels in a dry state exhibited a highly porous structure, desirable conductivity, and high ion-exchange ability, making them a great candidate for ion-exchange and energy storage applications.

2.3.3 Conductive Hydrogels containing CNC

As CNCs can form stable hydrogels with more than 98% water content, such hydrogels allow the incorporation of functional components such as conductive materials via electrostatic or hydrogen bonding through the many hydroxyl moieties on the surface of CNC[37]. Thus, the design and fabrication of conductive hydrogels containing CNC have gained attention due to their potentials in a wide variety of applications[29].

Li et al. [94] focused on the fabrication of a conductive composite hydrogel through the incorporation of pyrrole into a 3D matrix of acrylic acid-grafted CNC hydrogel with Fe^{3+} as an oxidant. With the addition of PPy into the transparent hydrogel, the conductivity increased to 1.3 $\times 10^{-4}$ S/cm, which is comparable to those of semiconductors. The conductivity of the prepared hydrogel can be considerably improved when doped with sodium p-toluenesulfonate (TsONa). Liang et al. [95] synthesized Conductive hydrogel formed by microcrystalline cellulose (MCC) and PPY. The conductivity of the hydrogel varied when the TsONa content was increased. The resulting hydrogels demonstrated conductivity of 7.83×10^{-3} S/cm. It was reported that that the hydrogel reached the maximum conductivity at the TsONa content of 0.75 mol/L.

Alizadehgiashi et al. [97] used a 3D-printed microfluidic extruder to prepare the MWCNT/CNC hydrogel-based sheets. In another work, Hoeng et al.[96] fabricated hydrogels from a CNC-based printing solution incorporated with conductive silver particles for electronic applications. The silver nanoparticles and annealing treatment improved the electrical conductivity of the obtained hydrogels. The large surface area of CNC provides a substrate for silver nanoparticles to make a conductive network, leading to a decline in the percolation threshold. Helen et al. [98] synthesized self-healing and conductive hydrogels through a simple two-step process. They first made the self-healing and double network hydrogels through multiple hydrogen-bonding interactions among CNC, Tannic acid, and Gelatin methacrylate. To make the hydrogel conductive, RGO and PANI were coated on the hydrogel surface through in-situ polymerization. The incorporation of RGO/PANI nanocomposite coating into the hydrogels could improve the conductivity. The prepared hydrogels exhibited the lowest resistance after coating with PANI/RGO.

2.3.4 BC Conductive hydrogels

BC-based conductive hydrogels have held great promise to be used for different functional applications due to a combination of their ionic and electrical conductivity. Liu et al.[99] synthesized PtNPs/MWCNTs/BC conductive hydrogels to fabricate electrode materials, taking advantage of the diffusion restriction of the bacterial cellulose, the catalytic activity of platinum nanoparticles(PtNPs), and conductivity of MWCNTs. There was a three-fold increase in the conductivity of the hydrogel when both CNTs and PtNPs were embedded. In another study, Mashkour et al. [100] fabricated a conductive hydrogel anode made of BC and PPY for microbial fuel cells. The obtained hydrogels show surface conductivity and outstanding features as a microbial scaffold, which provides enhanced microbial fuel cells' performance.

The use of BC with conductive materials for the fabrication of conductive hydrogels has got much attention. Shi et al. [101] integrated PANI into BC hydrogels. It was shown that the conductivity of the composite hydrogels was enhanced by doping with different protonic acids. It was suggested that resulting bacterial cellulose–PANI hydrogels can be used in different areas, such as flexible stimulation electrodes and biosensors. Huang et al. [102] fabricated highly flexible conductive hydrogels made of carboxylic multi-wall carbon nanotubes and BC cellulose. The obtained hydrogels showed 70% elongation and excellent cycling stability, providing potentials for biomedical applications. Huang et al. [103] fabricated flexible and wearable hydrogel-based sensors for detecting human motions. Conductive hydrogels were fabricated via loading modified MWCNTs and carbon black into Polyvinyl alcohol/sodium alginate/bacterial cellulose matrix. The prepared hydrogels possessed comparable synchronization between strain and electrical signal, proper stability, cycling repeatability, and durability. It was reported that the stretching of the

hydrogel leads to a decrease in conductivity, and the piezoresistive features of the hydrogels were due to their gradually closing pores and the path of ionic transport.

2.4 Advanced functions of conductive cellulose hydrogels

2.4.1 3D Printability

Three-dimensional (3D) printing has gained much researcher's attention because of its ability to generate intricate and delicate 3D structures. 3D printing, a cost-efficient approach to fabricate materials or structures with complex geometry, have been widely used for fabricating both organic and inorganic materials for various applications[107]. These unique features of 3D printing have significantly increased their potential applications in a vast range of industries, including cosmetics, food packaging, healthcare, agriculture, textile, and aircraft[108–110]. 3D printable hydrogels are usually fabricated from pre-gel solutions or known as 3D printing inks. Many factors can influence the printability of hydrogel inks, including rheological parameters, gelation behaviors, and printing parameters like extrusion temperature, feed rate, and printing distance. [111]. Among them, rheological properties (including viscosity, shear-thinning, fluid flow, and gelation behavior) of the ink are the most important parameters for the 3D printing of hydrogels[112]. However, the low mechanical strength of printed parts remains a challenge to the extended use of 3D printed products for various applications[113]. With the emergence of 3D printing technology, scientists have made more efforts to achieve conductive, flexible, and environmentally-friendly printed products using plant resource-based ink [114–116]. For example, cellulose and its derivatives have become promising “inks” for 3D printing, offering a fascinating pathway that could simplify the fabrication of sustainable structures for various

applications[117]. 3D printing provides a versatile tool to incorporate conductive components into cellulosic ink that can be used for fabricating functional 3D printed materials [91,118]. Knopf et al. [77] printed a flexible pH-sensitive hydrogel composed of graphene-cellulose composites coated with chitosan hydrogel for biosensor applications. In another work, Barras et al. [80] prepared ink through mixing carbon fibers and low-cost and eco-friendly cellulose derivative, CMC. Hadi et al.[81] developed conductive bio-ink composed of conductive polymers PEDOT/PSS and MC/ kappa-carrageenan for 3D printed hydrogels. The results showed that the kappa-carrageenan played a key role in stabilizing printed products, and that it intensified the thixotropic behavior of the bio-ink through the synergistic interaction of MC and kappa-carrageenan.

There have been only a few research works on conductive CNF 3D printing. For example, Kuzmenko et al.[84] printed conductive hydrogel inks containing carboxymethylated CNF and carboxylated SWCNTs for neural guidelines. Håkansson et al.[92] fabricated a 3D network via bioprinting of hydrogel-based ink composed of 2% CNF. The resulting 3D printed structure can collapse or retain via controlling the solidification process. Bordoni et al. [93] fabricated 3D bioprinted hydrogels from conductive inks composed of CNF, alginate, and SWCNTs. The hydrogels containing 10% SWCNTs were found to possess suitable conductivity to promote the maturation and differentiation of SH-SY5Y cells.

The utilization of CNC in 3D printing is becoming attractive because of the excellent hydrogel formation ability of CNC, its biocompatibility, and unique mechanical characteristics[119]. These 3D printed structures can be potentially used in implants, electronic devices, tissue engineering materials, where complex porous structures are required. Recently, 3D printing of CNC with

conductive materials has been explored as a viable route to produce next-generation materials[120]. Hoeng et al.[96] prepared printable CNC/silver particle ink for electronics applications. The nano-size CNC and their unique dispersing and stability eased the production of a conductive 3D printable ink. The use of CNC as a scaffold offers a greenway towards renewable and sustainable electronics.

2.4.2 Self-healing capability

Self-healing is an intrinsic capacity of an organism to automatically repair its damage and restore its function as a mechanism to enhance its chances of survival. Recently there have been extensive efforts to imitating such a natural phenomenon to endow self-healing capacity to non-viable materials as a mechanism to enhance their service life. Fabrication of conductive hydrogels possessing self-healing capability and robust mechanical performance has been a challenge [121]. Hussain et al. [78] fabricated a double network hydrogel based on hydroxyethyl cellulose, which presents around 98% self-healing efficiency. This healing capability of the hydrogel resulted from the diffusion of Fe^{3+} ions along with reconstructing the hydrogen bonding interactions at their cut interface.

Chen et al. [82] demonstrated that TOCNF/PAA-PPy hydrogel benefited from a high self-healing efficiency of 98.3% at room temperature after 6 hours. It was related to the dynamically reversible bonds between ferric ions with PPy and carboxylic groups on TEMPO-oxidized cellulose nanofibers (TOCNFs) and PAA chains, plus the hydrogen bonding between PPy and TEMPO-oxidized CNFs. Zheng et al. [85] demonstrated that the high self-healing efficiency of Graphene-CNF/PVA-borax hydrogels could be attributed to the hydrogen bonding interaction, the multi-

complexation among hydroxyl groups of hydrogel components. In recent work, Ding et al. [86] studied the self-healing mechanism of conductive CNF−PPy/PB hydrogels. They reported that the hydrogel possessed a self-healing efficiency of around 97% and 87% in air and water environment, respectively. It was related to the hydrogen bonding interaction and formation of the reversible network via different borax-based complexes with the nanocellulose and the diffusion of borate in water. Liu et al. [87] reported the blending of nanofibrillated cellulose/PPY/Fe_3O_4 nanocomposites into the agarose hydrogel matrix, which endowed the hydrogels self-healing under the thermal stimuli. The healing efficiency was related to the thermoplasticity of the agarose hydrogel under the thermal stimuli. Liu et al. [88] fabricated self-healable hydrogel containing CNF with both conductive and magnetic functionality. Based on the rheological studies, the self-healing mechanisms include the cross-linking reaction between borax-PVA, the hydrogen bonds between the hydroxyl group of PVA−PVA and PVA−CNF. Helen et al. [98] constructed the conductive hydrogels with proper self-healing capacity. It was reported that the autonomous self-healing caused by multipoint hydrogen bonding and hydrophobic interactions among CNC, gelatin methacrylate, and Tannic acid. The healing efficiency for mechanical strength was around 96%.

2.4.3 High Mechanical Properties

compared with those of solid polymers, the relatively weak mechanical performance of hydrogel has limited their further industrial applications[122]. As a result, there has been extensive development focus on hydrogels with outstanding mechanical properties.

Conductive cellulose hydrogels are usually composite materials. The conductive components sometimes can serve as both conductive fillers and reinforcement to enhance the mechanical

properties of the hydrogels. Fang et al. [73] used a facile method to fabricate conductive cellulose-based hydrogels with compressive strength of 26.25MPa. They showed that mechanical features could be adjusted by varying concentrations of the oxidant and dopants. The PPY was homogeneously distributed in the MCC hydrogel. It was reported that the polymer chain length of PPY played a leading role in the mechanical performance of the as-prepared hydrogel. Shi et al. [74] reported that the incorporation of PANI enhanced the compressive strength of a cellulose hydrogel, with a maximum compressive strength of 0.48 MPa with 15% PANI. Xu et al. [75] investigated the impact of the PANI polymerization progress on the mechanical behavior of the cellulose-based hydrogels. They found that after two hours of PANI polymerization reaction time, the composite hydrogels had higher tensile strength than cellulose hydrogels. Hussain et al. [78] fabricated HEC cellulose-based conductive hydrogels that exhibited tensile stress of 3.50 MPa and stretchability of 1245%, along with a compression strength of 32 MPa. This improvement in the tensile strength was because of the rise in the hydrogen bonding interaction among functional groups of hydrogel components. They reported that the addition of HEC up to 4 wt.% led to around 435% improvement in the toughness of hydrogel. Li et al. [79] showed that the compressive stress and modulus of composite hydrogels enhanced as CMC content in PANI/CMC hydrogels increased. Although the modulus of the PANI/CMC hydrogels improved with more cross-linking agent incorporated, the compressive strength decreased when the crosslinking degree was too high. Huang et al. [102] fabricated highly stretchable hydrogels c-MWCNT/ bovine serum albumin(BSA) /BC hydrogel. They showed that incorporation c-MWCNTs into the BSA-coated BC membrane significantly improved mechanical strength.

Chen et al. [82] incorporated TEMPO-oxidized CNFs and PPy into the polyacrylic acid (PAA) hydrogel network. They reported that combining homogeneous modified CNF into PAA caused a

significant increase in tensile stress and elongation at break. It was due to the uniform distribution of CNF and their chain entanglement with PAA, and the hydrogen bonding system between PPy and TEMPO-oxidized CNFs, plus the ionic interactions between PPy and PAA chains.

Imparting synergistic properties of conductivity and high mechanical integrity remains a challenge in the development of cellulose-based conductive hydrogels. Zheng et al. [85] showed that both tensile and compressive stresses of PVA/CNF hydrogels were considerably enhanced via the incorporation of graphene. The non-covalent and ionic interaction among hydrogel components helped to distribute the load from the polymer matrix to Graphene-CNF nanocomplexes, therefore suppressing the growth of microcracks. Ding et al. [86] synthesized CNF/PPY nanostructured complex and incorporated them into polyvinyl alcohol/borax (PB) hydrogel matrix to fabricate a conductive hydrogel with high mechanical performance. They reported that enhancement of mechanical strength was caused by the hydrogen and ionic interaction via the complexation of borate ions acting as a crosslinker among hydrogel components. Lin et al. [89] demonstrated that introduction of 5% modified cellulose nanofiber into alginate-based hydrogel followed by in situ polymerizations of pyrrole significantly increased the mechanical characteristics of the obtained hydrogels. TEMPO-CNF not only acted as reinforcement in the hydrogel matrix but also provided excellent affinity with PPY/alginate hydrogel to form a strong and crosslinked network structure. Li et al. [91] constructed a highly aligned CNT/CNF composite microfiber through a 3D-printing technique. They reported that the dual alignment of both acid-modified CNT and CNF in microfibers, hydrogen bonding, and hydrophobic interactions of functionalized CNT and CNF led to excellent mechanical performance.

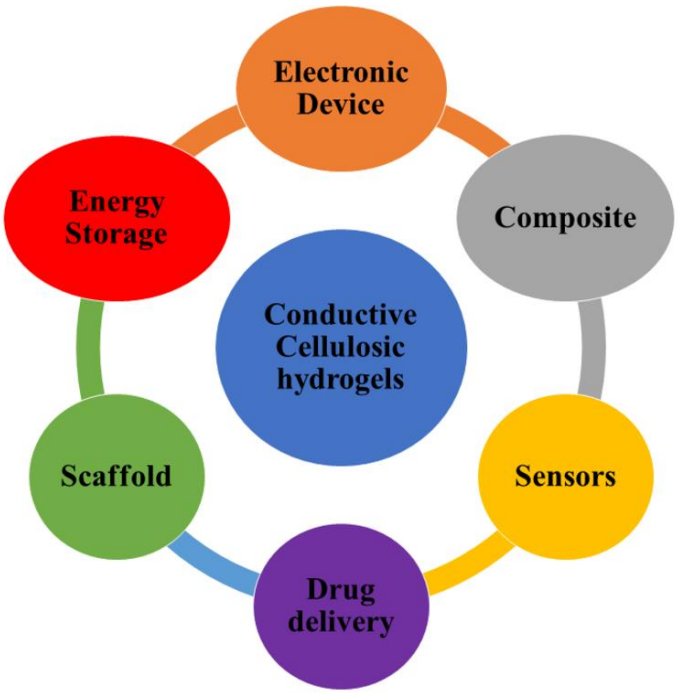

Figure 2. 2 Applications of conductive cellulose-based hydrogels

2.5 Application of cellulosic conductive hydrogels

Nanocellulose or cellulose-based conductive hydrogels have been extensively studied and developed and are finding applications in a wide variety of areas (Figure 2). They represent promising new materials in these areas because of their combination of excellent biocompatibility, biostability, environmental sustainability, and versatility.

2.5.1 Biomedical application

Conductive hydrogels containing cellulose and its derivatives have recently been used for a vast range of biomedical applications because of their superb biocompatibility, mechanical and conductive features.

Conductive hydrogels have been used in biomimetic/tissue engineering scaffolds. For example, Shi et al.[74] prepared polyaniline–cellulose hydrogels with a rapid electrical response to be used in the field of biomimetic materials. Lin et al.[89] showed that a Polypyrrole (PPY)/sodium alginate/TEMPO- microfibril cellulose composite hydrogels demonstrated high mechanical, conductive properties, tunable swelling behavior, and excellent biocompatibility. These features make them emerging materials for the use of biomimetic tissue scaffolds. Xu et al.[75] constructed a single-sided conductive micro-nano structured PANI incorporated cellulose hydrogel for applications in nerve regeneration. The in vivo results exhibited that the developed conductive hydrogels accelerated the healing processes of the injured nerve at three months after surgery. Sun et al. [76] constructed highly sensitive nanocomposite hydrogels through the co-doping treatment of cellulose hydrogels with CNT, MnO4, and PANI. It was reported that the resulting hydrogels have great potential for accelerating the actuation performance of artificial muscles.

It has been found that the conductivity of some stretchable conductive hydrogels can vary with their strains, making them good candidates for developing strain/motion sensors. Chen et al.[82] designed strain sensitive CNF/PAA hydrogels to detect small/large-scale human motions and physiological signals. The results showed that massive resistance changes occurred during stretching. For example, when a finger was bent at various angles, a gradual decrease in the current occurred because of the increased resistance of the hydrogel sensor attached to the finger. Volodymyr et al. [84] 3d-printed CNF/SWCNTs hydrogels ink. They Showed that the nanosized structure and conductivity of 3d-printed scaffolds played a key role in cell behavior. This low-cost and 3D printable cellulose-based hydrogel ink can be applied in tissue engineering fields. Zheng et al. [85] fabricated a strain-sensitive hydrogel-based sensor that had great potential to be used for

monitoring the movements of the finger, arm, and leg. Graphene-CNF/PVA hydrogel was embedded in a closed circuit equipped with a light bulb. The illumination of the light varied with applied strain, which increases the space between the conducting particles inside the hydrogel, leading to enhanced hydrogel resistance. Huang et al. [102] worked on the fabrication of highly stretchable and environmentally-friendly hydrogel strain sensors composed of modified MWCNTs and BC. They demonstrated that the as-prepared hydrogel strain sensor exhibited proper accuracy and signal repeatability during large-scale deformation. Based on the obtained results, the renewable substrate can be used for monitoring large-scale human motions like finger and knee joint movements. Huang et al. [103] fabricated dual-mode wearable sensors by introducing BC and carbon materials into hybrid hydrogels. It was attributed to quickly piezoresistive strain and capacitive pressure responses of the final hydrogels to the motions.

2.5.2 Sensors, energy storage, and electronics device

The sustainability, high strength, and flexibility of cellulose and nanocellulose based hydrogels are of interest in smart sensing systems. Hussain et al.[78] constructed self-healing and conductive hydrogels via Fe^{3+} ion coordination among HEC and P(AA-co-AAm). The multi-functional hydrogel with re-shape capability, conductivity, excellent mechanical properties is useful for intelligent electronic devices. Barras et al.[80] fabricated 3D printed and flexible electronic paper made of water-soluble CMC cellulose and carbon fiber. They found that the conductive 3D printed constructs were sensitive to temperature and humidity. Ding et al.[86] fabricated multi-functional CNF−PPy/PB hybrid hydrogels that have fast self-healing capacity, high water content, biocompatibility, and pH sensitivity, which may be promising for flexible bio-electronic devices. Knopf et al. [77] fabricated an interdigitated capacitive biosensor composed of graphene/ CMC

via 3D printing and then coated it with pH-sensitive chitosan. Results showed that the hydrogel could swell/de-swell in response to changes in pH over the interdigitated electrodes causing a measurable difference in circuit. Li et al. [91] used a scalable 3D-printing technique to fabricate CNT–CNF composite as promising smart materials for wearable electronic products. Hoeng et al.[96] found that 3D printing of nanocellulose–silver hydrogels onto nanocellulose coated cardboard offered new, low-cost, and sustainable materials for the development of electronics.

The design and development of stable cellulosic hydrogel with both conductive and magnetic characteristics to be used for electronic devices remained a challenge. Liu et al.[87] took the advantages of magnetic and conductive properties plus reversible restorability of the nanofibrillated cellulose/PPY/Fe_3O_4 loaded agarose hydrogels for diverse applications like electrochemical device and electronic skin. In another research[88], both conductive and magnetic functionalities were introduced into self-healable PVA hydrogels containing NFC/PANI/$MnFe_2O_4$. It is expected that such hydrogels are promising materials for a broad spectrum of applications, such as smart electronic devices and electromagnetic interference shielding.

There are also a few developments on cellulose hydrogels for energy storage devices. Nystro et al.[90] constructed conductive PPY/CNF hydrogels via PPY polymerization on CNF hydrogels to be used for paper-based energy storage devices. Hsu et al.[98] constructed a self-healable conductive GelMA-CNC hydrogel coated with PANI/RGO for the development of all-in-one supercapacitors. The hydrogel-based supercapacitor demonstrated good mechanical and electrochemical performance, showing its promise in sustainable energy storage devices.

BC is a naturally biocompatible nanocellulose and has found its applications in biomedical applications, including fuel cells. Liu et al.[99] designed a conductive BC/CNTs hydrogel

electrode with excellent biocompatibility and selective glucose oxidation ability. They showed that the prepared hydrogel electrode exhibited a fuel cell performance of 2.24μW/cm^2. Based on the obtained results, it holds a promise for applications in implantable glucose fuel cells.

2.5.3 Composites and coatings

Quite a few conductive agents are found to enhance the composite hydrogels both mechanically and electrically. Fang et al. [73] fabricated conductive composite hydrogels made of PPY and cellulose. They showed that the electrical and mechanical properties of hydrogels could be controlled by altering oxidant and dopant contents. Li et al. [79] constructed CMC/PANI composite hydrogels by using glycerol diglycidyl ether (GDE) as the biocompatible crosslinker. Chen et al. [83] generated the CNF-reinforced polyacrylamide/ CNT composite hydrogels via in situ polymerization. They suggested the composite hydrogels can be applied for a broad range of practical applications. Håkansson et al. [92] constructed 3D-printed hydrogels composed of CNT and CNF. The sustainable 3D structure can be suitable candidates for packaging, textiles, biomedical devices, and furniture with conductive parts. Li et al. [94] synthesized conductive composite hydrogels through in-situ polymerization of pyrrole monomer into a 3D matrix acrylic acid grafted nano crystal cellulose hydrogel. It was reported the prepared sustainable hydrogels could be promising materials for various applications. Liang et al. [95] incorporated natural biomass into the conductive polymer to fabricate CNC/PPy composite hydrogels using for various applications. Alizadehgiashi et al. [97] 3D-printed the CNT/CNC hydrogel-based sheets. It was suggested that the patterned composite hydrogel has the potential for the growth of stem cells, sensors, and functional tattoo printing. Shi et al. [101] synthesized the composite hydrogels made of BC and PANI, which potentially be used for different applications. Mashkour et al.[100]

fabricated conductive BC/PPY nanocomposite hydrogels as anodes in a dual-chamber microbial fuel cell device. They indicated that the PPY coating could significantly improve the capacitance and electrochemical properties of BC. It was comparable to those unmodified BC and commercial ones.

2.6 Ammonia gas sensors

Significant growth of industry and agriculture has led to the production and emission of poisonous and harmful gases (NO_x, O_3, SO_2, CO, and NH_3), which threaten human health and the ecosystem in the long term [9]. Among them, Ammonia gas is considered a colorless, corrosive gas with a pungent smell. It is a prevalent chemical owing to its widespread use and existence in household cleaners and (most abundantly) industrial fertilizers. Exposure to ammonia gas at one ppm may lead to slight irritation. In comparison, concentration levels of more than 25 ppm may cause severe skin burns and hurt the respiratory system. Acute exposure to a high level of ammonia may cause death[123]. As a result, it is essential to develop cost-effective sensors for ammonia detection. Low sensitivity and high working temperature restrain the application of metal-oxide-based gas detectors [19]. Hence, there have been increasing demands for the development of cost-effective sensors with high sensitivity for environmental air pollutants and chemicals for both industrial and civilian purposes. Conductive hydrogels have emerged as an advanced platform for gas sensors by combining the advantageous properties of both hydrogels and conductors. The critical function of conductive hydrogel-based gas sensors is fast responses to gas molecules with a corresponding change in the electrical signal output. The porous nanostructures of conductive hydrogels with high surface areas provide more sites for gas molecule adsorption and reaction, leading to a fast response to external stimuli [124].

For instance, Wu et al. [10] prepared 3D reduced graphene oxide hydrogel that could monitor nitrogen dioxide and ammonia at low concentrations of 200 ppb and 20 ppm, respectively. They employed a local micro heater to enhance gas-sensing performance. They showed that the miniaturized microheater was placed in the hydrogel-based gas detector to evaluate temperature effect on gas sensing performance[10].

Wang et al.[125] fabricated a room-temperature ammonia gas sensor including Cerium(IV) oxide ($CeO_{2)}$ nanoparticles conformally coated by cross-linked phytic-acid-doped PANI hydrogel. They showed the hybrid hydrogel sensor exhibited a proper gas sensitivity and long-term stability. It was due to the doping and crosslinking effects on the PANI polymer chains. Wang et al.[126] constructed wearable hydrogel sensor for ammonia gas detection. The PAA–rGO–Ca^{2+} hydrogel was able to respond to a much lower ammonia gas concentration and has the potential to be used as an artificial electronic nose for ammonia gas that communicates with a smartphone to display the detection via wireless connections.

Although much research has been done on using conductive materials for the gas detector[126,127], there have been very few attempts to utilize cellulose-based conductive hydrogels for the development of the gas sensor. There has been an increasing demand for developing sensing platforms using cellulose-based substrates due to their cost-effectiveness, excellent mechanical strength, stiffness, ease of surface modification, non-toxicity, and sustainability [50,128]. Aldalbahi et al. [7] constructed a hydrogel-based gas sensor for detecting methane. They first prepared the magnetic nanocomposites by the reaction of Fe_3O_4 NPs containing carboxymethyl cellulose with polyvinyl alcohol. Then, the conductivity of the magnetic nanocomposites was enhanced by adding conducting materials such as MWCNTs and PANI. The gas sensing findings showed the hydrogels containing MWCNTs, and Fe_3O_4

responded to the methane gas at the lowest concentration detected, five ppm. They also reported that higher sensitivity was achieved at a slightly high operating temperature. To the best of our knowledge, there has been no research on using conductive cellulose hydrogels for ammonia gas detection. In this work, we report a self-healing and flexible reduced graphene oxide embedded-carboxymethyl cellulose hydrogel capable of detection of ammonia gas in ambient temperature with very high sensitivity and low detection limit. This method of fabricating 3D conductive cellulose-based gas sensor is facile, cost-effective, and simple compared to previously reported strategies for traditional sensor. The electrical resistance changes at different test conditions (such as vapour concentrations and conductive agent concentration in hydrogel) are analyzed. The sensitivity and reusability of these materials as vapour sensors are investigated.

2.7 Summary

Cellulosic conductive hydrogels benefit from a combination of superior properties such as non-toxicity, biodegradability, sustainability, cost-effectiveness, and superb mechanical strength. They show great promises for a wide range of industrial applications, where environmental sustainability, toxicity, and mechanical performance issues are concerned. Integration of novel functionalities to the conductive hydrogels, such as high mechanical properties, 3D printability, and self-healing capacity, opened new opportunities for conductive cellulose hydrogels to be used as a matrix for various applications, including those for ammonia gas sensors. Key challenges to practical applications of ammonia gas sensors still reside in the requirement for cost-effective sensors with high sensitivity at room temperature. Mechanical properties and such advanced functions as self-healing also play key roles in extending all types of gas sensors to wearable devices.

Therefore, in the current study, we developed an innovative type of flexible, cost-effective, self-responsive, and conductive cellulose hydrogels with desirable mechanical performance, enhanced conductivity (fast response), and self-healing efficiency (91.2% in tensile stress), which was highly sensitive to ammonia gas at room temperature. It is expected that the research on cellulosic conductive hydrogels will continue for the development of new, ultra-strong, highly conductive, and lightweight materials with exceptional features for practical ammonia gas sensors.

Chapter 3: Materials and Methods

3.1 Materials

Sodium Carboxymethyl cellulose (CMC, M.W. 700,000, D.S. = 0.9, 2500–4500 mPa s) was supplied by Sigma-Aldrich in a powder form and used as received. Citric acid was obtained from Sigma-Aldrich. Graphene oxide powders were provided by Wuxi Chemical Company. An aqueous solution of Ammonia (28 − 30% (w/w), Sigma Aldrich) was used as a source solution for ammonia vapor generation. Citric acid, Sodium hydroxide, and sodium borohydride were obtained from VWR and used without further purification.

3.2 Choice of Materials

A vital step in developing ammonia gas sensors is the choice of the sensing materials that display changes in their chemical or physical properties upon exposure to ammonia vapor [129]. Conductive hydrogels stand out as an advanced platform for various sensor technologies via synergizing the features of soft materials and organic conductors [19,130]. The nature of the conductive hydrogels, such as the ultra-high surface-to-volume ratio and porous structure, water content, results in the fast adsorption of gas molecules onto the hydrogel's surface and further diffusion into the hydrogel structures. Also, their conductivity makes them highly sensitive to the gas analyte at room temperature[19]. Conductive materials like conductive polymers, carbon-based nanomaterials, and metal particles have been used in conductive hydrogel fabrication to meet gas sensors' requirements due to their distinct properties[131]. Among them, graphene oxide (GO) and reduced graphene oxide (RGO) have recently attracted a great deal of attention in gas sensing， because of their atom-thick two-dimensional conjugated structures, ultra-high surface areas, low electrical noise, high conductivity, and outstanding electronic properties[10,132]. However, the development of ammonia gas detectors with superior eco-sustainability， mechanical strength and facile fabrication processes is still a challenge[133]. There is an increasing

demand for fabricating sensing platforms using cellulose-based substrates due to their cost-effectiveness, excellent mechanical strength, stiffness, ease of surface modification, non-toxicity, and sustainability[50,128]. We, therefore, employed a RGO-incorporated carboxy methyl cellulose hydrogel to fabricate the conductive hydrogel that contains RGO to fabricate self-healing, flexible, and sensitive NH_3 gas sensors.

3.3 Synthesis of Reduced graphene Oxide (RGO)

RGO was synthesized according to a previously reported method [134]. Briefly, 70 mg of GO was dispersed into distilled water and sonicated for two h to achieve well-homogeneous dispersion. Sodium hydroxide (1 M) and sodium borohydride (0.1 M) was added into a resulting graphene oxide mixture and stirred for two hrs followed by heating for one hr at 90 C. The obtained dispersion was then rinsed with distilled water and filtered through a 0.45um nylon membrane filter using a sintered glass filtration system. To eliminate the excess water, the obtained wet reduced graphene oxide was subsequently kept in the oven at 40 ºC overnight. The overall procedure of RGO synthesis is shown in Figure 3.1.

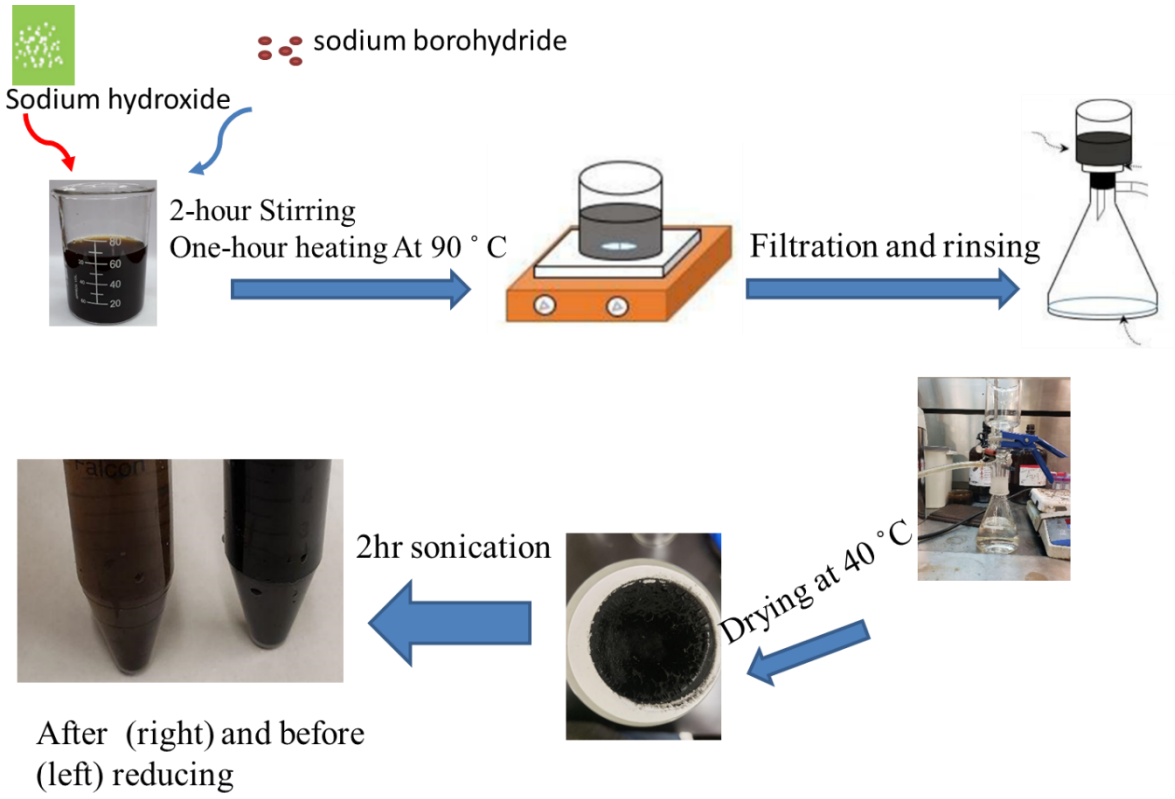

Figure 3. 1 Preparation scheme of RGO.

3.4 Preparation of RGO-CMC hydrogels

Conductive CMC hydrogel was prepared at ambient temperature through a straightforward second-step procedure according to the literature[135]. Firstly, different amount of RGO was redispersed in water by ultrasonication to make a homogeneous 1,2 and 3 mg/mL aqueous dispersion of RGO. Then, the dry Na-CMC powder was gradually added to as-prepared RGO dispersion with a CMC concentration of 20% and stirred as the CMC paste. The CMC content is defined as the weight of dry Na-CMC powder over the weight of CMC/RGO paste. The obtained black paste was placed into a mold, pressed to remove air bubbles, and molded into the desired shape. At this stage, the CMC polymer chains were uncross-linked. In the second step, the black paste was immersed into a citric acid solution at the concentration of 8 mol/L for 9 hours, and then

the as-prepared CMC/RGO hydrogel was made. The CMC hydrogels with the desired shape were formed through physical cross-linking in the second step along with the formation of hydrogen bonds among the CMC and RGO chains. Additionally, the same procedure was applied to prepare GO (0,1,2 and 3mg/ml)- loaded CMC hydrogels as reference samples. Finally, the hydrogels were kept in distilled water for two days to remove any residue and air-bubbles. The fabrication method of CMC hydrogel and Conductive CMC hydrogels were presented in Figures 3.2 and 3.3.

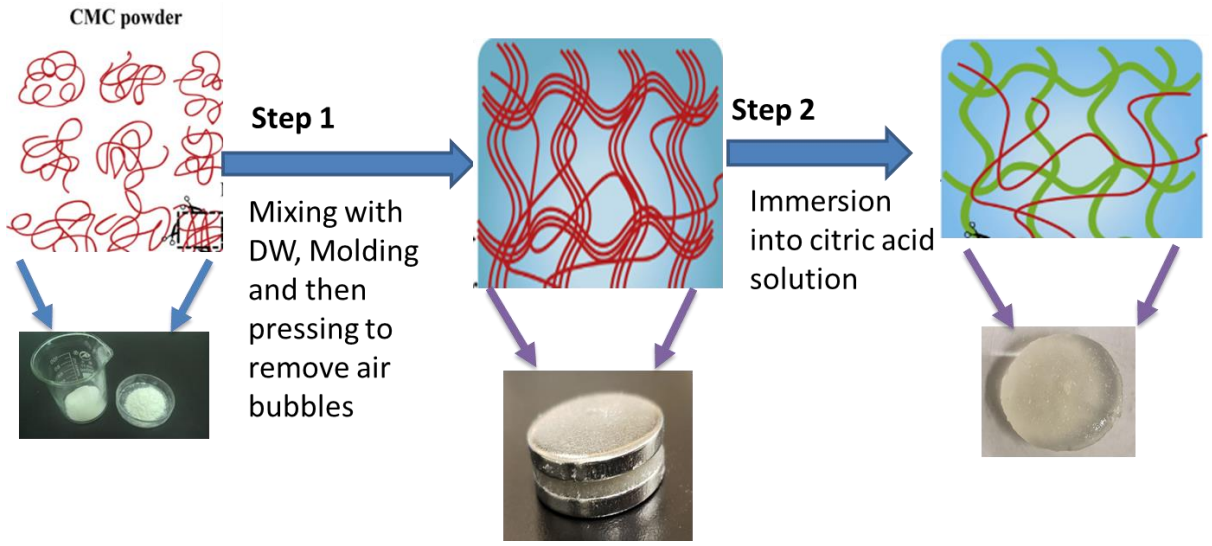

Figure 3. 2 Overall procedure of CMC hydrogel fabrication

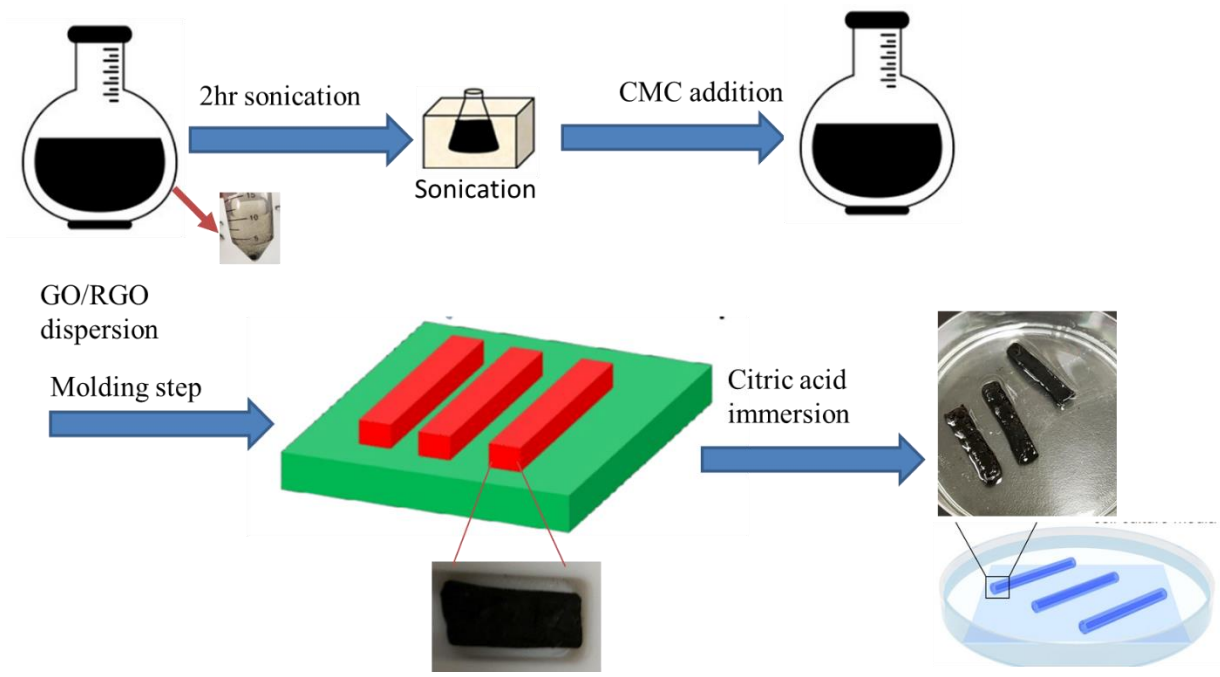

Figure 3. 3 Schematic of preparation of electrically conductive CMC hydrogels

3.5 Characterization of the conductive cellulosic hydrogels

3.5.1 Scanning electron microscopy (SEM) characterization

The morphology of the hydrogel microstructure was characterized using a scanning electron microscope operating (SEM; JEOL, JSM-5900LV) at an accelerating voltage of 10 kV. All hydrogel samples were freeze-dried. For the SEM observation, all hydrogel specimens sputtered with a thin layer of gold and then loaded onto a metal holder for examination under the microscope. The average pore sizes were also measured using the Image J software (National Institutes of Health (NIH), http://imagej.nih.gov.uml.idm.oclc.org/ij).

3.5.2 Fourier-transform infrared (FTIR) spectral characterization

The FTIR spectra were used to characterize the chemical bonds within the hydrogels. The FTIR analysis of the samples was performed using a Fourier transform infrared spectrophotometer (Nexus 670, Nicolet, United States) in the scan range of 4000-400 cm^{-1} with a spectra resolution of 4.0 cm^{-1}.

3.5.3 Mechanical properties: tensile behavior

The tensile tests were conducted on a 3366 Electronic Universal Testing Machine with 10 mm/min speed of crosshead to obtain the stress−strain curves (Figure 3.4). The sample sizes for tensile tests were 30 mm in length, 5mm in width, and 2mm in thickness. All samples were tested at a crosshead speed of 10mm/min at room temperature[136]. The tensile stress (σ) was calculated as $\sigma = F/(W*T)$, where F represents the load, W and T represent the original width and thickness of the tested specimen. The tensile strain (ε) was defined as the ratio of the change in length $L-L_0$ to the original length L_0, or $\varepsilon= (L-L_0)/L_0$. Average values and standard deviations for all sample groups were calculated for statistical analysis.

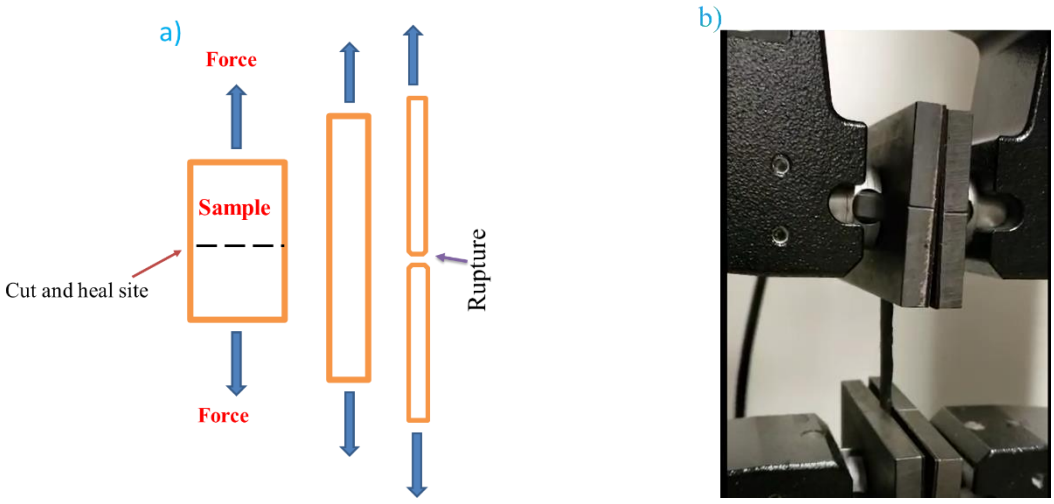

Figure 3. 4 Schematic of tensile Test (a), and tensile machine (b)

3.5.4 Self-healing evaluation

Each freshly prepared strip-shaped and disk-shaped hydrogel were cut into halves. Immediately, two separate semicircles were put together and contacted along with their cut interfaces and put in a covered Petri dish to prevent water evaporation. The self-healing process was carried out at room temperature for nine hrs without any external stimulus. Digital photographs were taken to record the self-healing behaviors of hydrogels.

3.5.5 Rheological measurements

Rheological studies of the composite hydrogels were carried out with a TA HR-1 rheometer equipped with an 8 mm parallel plate system. The cylindrical samples were prepared with a diameter of 8 mm and a thickness of 1mm. Hydrogel samples with different GO (0%, 1%, 2% and

3%) and RGO contents (0%, 1%, 2% and 3%) were prepared for optimizing the parameters. Dynamic viscoelastic parameters such as the storage modulus G' and loss modulus G" as a function of the oscillatory strain, was measured through an oscillatory strain sweep at a fixed strain amplitude of 0.5%. The storage modulus (G′) represents the hydrogel's capacity to store energy elastically, while the loss modulus (G″) is the amount of energy dissipated under the oscillatory stress. All rheological data were obtained at a changing angular frequency ranging from 0.1 to 100 rad s^{-1}. Oscillation torque was ranging from 0.86- 29.68 µN.m. To quantitatively assess self-healing ability, the rheology evaluation was carried out after a specific time of the healing process. The self-healing efficiency in storage modulus was measured by comparing the modulus of the healed hydrogels with the pristine one. The percent self-healing efficiency in the storage modulus was calculated by the following equation [87]:

$$\text{Stress healing efficiency} = \frac{T2}{T1} \times 100 \qquad (3.1)$$

T_2 and T_1 were defined as the ultimate storage modulus of healed hydrogel and the original one, respectively.

3.5.6 Conductivity of hydrogels

The electrical conductivity of the original and healed samples was obtained by measuring the resistance of hydrogels via a Digital Multimeter (Victor 86E, China). The samples were cut into a

rectangular shape of 10 mm (length) × 5 mm (width) with a thickness of 0.2 mm. The electrical conductivity was calculated using the following equation [137]:

$$\delta = \frac{1}{t \times R} \quad (3.2)$$

Where t represents the thickness of the hydrogel, and R (Ohm, Ω) is the sheet resistance of the hydrogel. The hydrogel conductivity (S/cm) was measured at room temperatures.

3.5.7 Ammonia detector

The gas-sensing performance of the conductive hydrogel-based sensors was measured within a sealed gas sensing chamber containing ammonia vapor and evaluated by monitoring the relative resistance change via a multimeter at room temperature as presented in Figure 3.4. The hydrogel sensors were placed on the glass slide, and two copper wires were fixed on both ends of the sensors using conductive copper foil tapes. The hydrogel sensors were exposed to different concentrations (7.5, 15, and 30 ppm) of the ammonia solution. For each concentration, the sensor was placed over ammonia vapor for approximately 20 minutes until the conductivity changes reached a steady level, which usually lasted for an additional 10 minutes.

A digital multimeter (Victor 86E, China) having a measurement range from 10^{-6} to 10^{9} Ω was used to monitor the electrical resistance change of the specimens. Resistance values were collected every 1 s. To measure the sensing properties of samples independently of their initial resistance, the relative electrical resistance change (R_{rel}) was calculated in the following equation[126]:

$$R_{rel} = \frac{R_t - R_0}{R_0} \times 100 \quad (3.3)$$

where R_0 is the initial resistance of the specimen in dry air; R_t is the transient resistance upon exposure to vapor at time t. The samples were tested at 25°C. In each group, the concentrations of gaseous NH_3 were calculated according to the volume of the evaporated ammonia solution, the concentration of ammonia in the solution, and the volume of the sensing chamber. When calculating the vapor concentrations, the pressure of 1 atm and a temperature of 25 ◦C was adopted, and ammonia was assumed to be an ideal gas[126,138]. The Ammonia gas concentration was calculated based on the Raoult's law., following equation[139]:

$$y_i . P = x_i . P_i^{Sat} \quad (3.4)$$

P =total pressure, P_i^{Sat} = saturated pressure of ammonia solution at the room temperature, and x_i and y_i = concentration in the liquid and gas phase.

We also investigated the gas sensing performance when hydrogels contacted with air at atmospheric conditions.

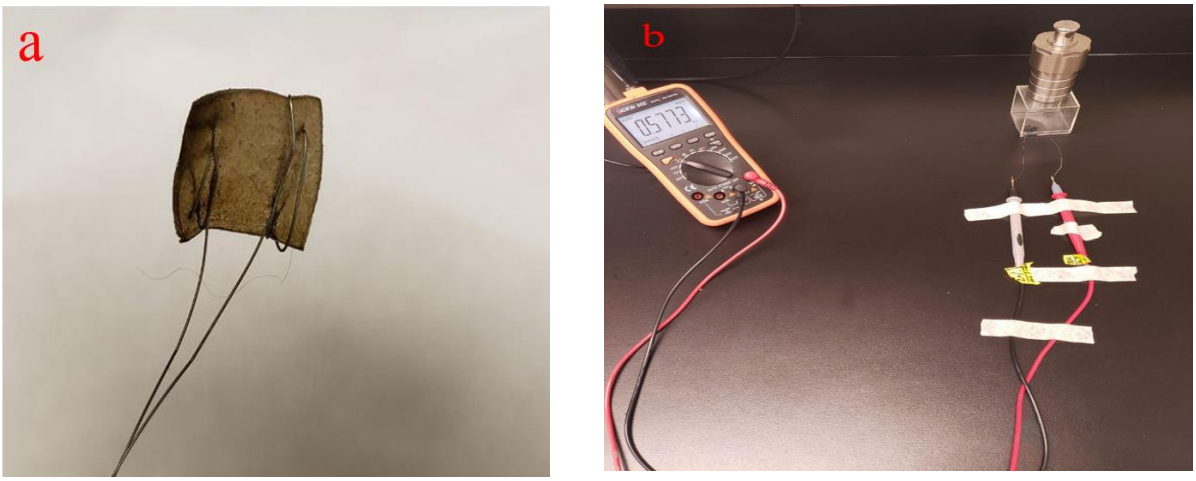

Figure 3. 5 CMC/RGO-2 gas sensor (a) Sealed system of Ammonia detector (b)

3.5.8 Statistics

The measurements were carried out three times for each sample. Values in this study are reported as mean and standard deviation (SD). Statistical analysis was performed using the one-way ANOVA test, with $p < 0.05$ considered as being statistically significant.

Chapter 4: Results and Discussion

4.1 Preparation of RGO

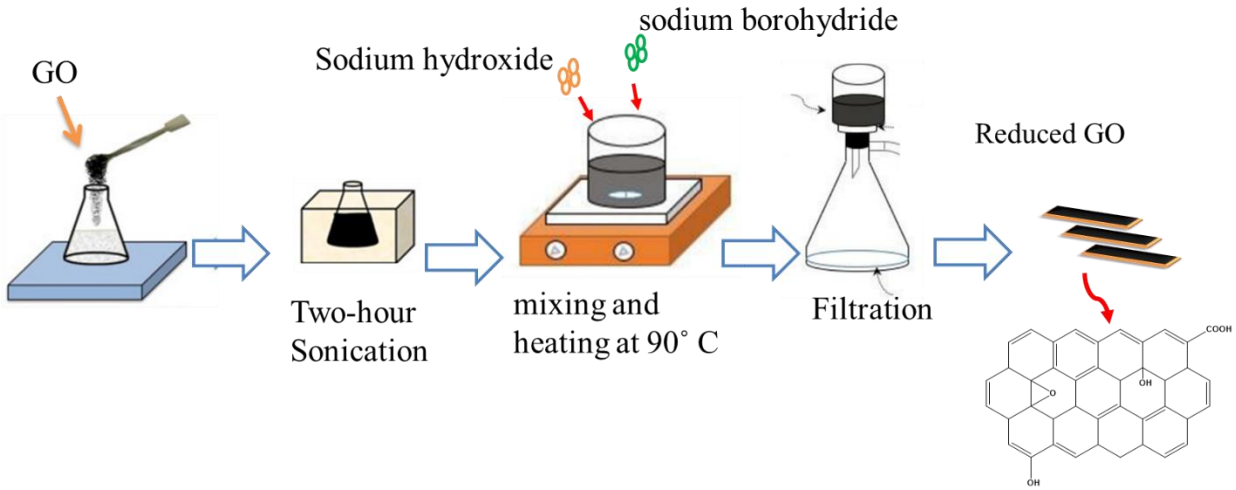

Figure 4. 1 Preparation scheme of RGO.

The graphene-like characteristics of RGO, such as excellent conductive properties, low electrical signal noise, great electron mobility, and cost-effective and scalable production, make them a highly desirable material for a wide range of applications [140,141]. The procedure for producing RGO is shown in Figure 1. The conversion of GO into RGO can be recognized by its color changes from brownish-yellow to black. Pictures of GO and RGO suspensions in the water at a concentration of 3 mg/ml was shown in Figure 2. The color change is a visible characteristic of reduction and suggests the formation of reduced GO. According to the literature [142,143], the amounts of oxygen-containing functional groups located on the GO carbon plane decreased after the reduction.

Figure 4. 2 Pictures of GO and RGO suspensions in water

4.2. Mechanism of CMC conductive hydrogel

The conductive hydrogel-based sensors were prepared by a straight-forward two-step method. The preparation methods for CMC/GO and CMC/RGO hydrogels are illustrated in Figure. 3.

The CMC/RGO hydrogels were made from RGO dispersion, Na-CMC, and citric acid via a facile two-step method. In the first step (molding process), a Na-CMC/RGO paste was obtained by mixing Na-CMC powder with RGO dispersion (Figure. 1a) and then filling the mixture into plastic molds with desired shapes. The next step is an acidification process, in which the CMC/RGO hydrogels were obtained by immersing the pre-shaped CMC/RGO pastes into a citric acid solution for 9 hrs. During the acidification step, the sodium carboxylate (–COONa) groups on the polymer backbones were gradually replaced by H^+, which diffused into the Na-CMC paste from the outside. The 3D hydrogel network was constructed through physical crosslinking of multiple hydrogen bonds between the neighboring CMC polymer chains and RGO. As shown in figure 3b, the same procedure was applied for preparing CMC/GO hydrogels.

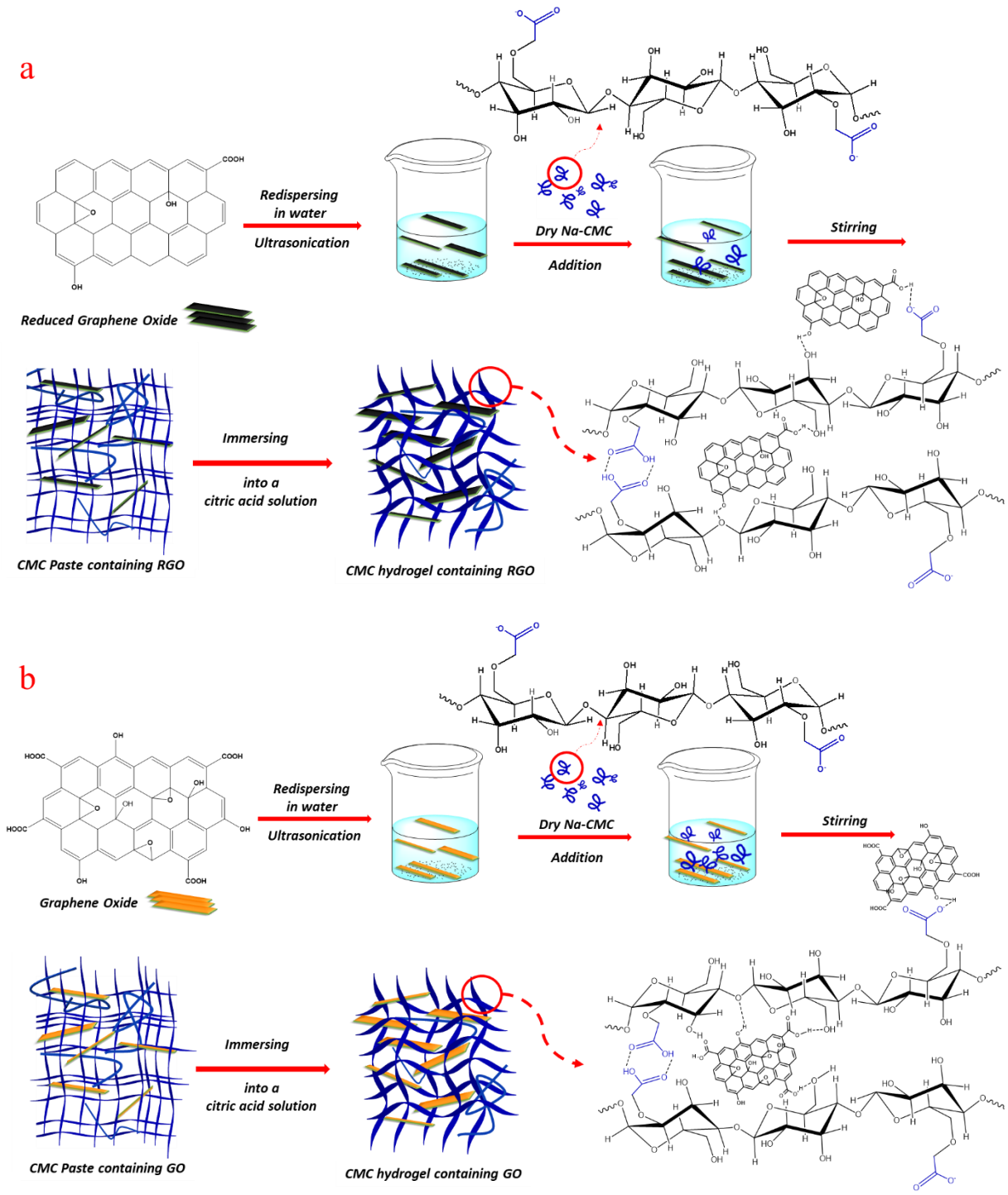

Figure 4. 3 Schematic of fabrication of conductive CMC hydrogels. a) CMC-RGO and b) CMC-GO hydrogels

4.3 Morphology of Conductive hydrogels

A RGO–CMC hydrogels with different RGO concentrations were prepared and denoted by RGO1-CMC, RGO2-CMC, and RGO3-CMC, corresponding to 1, 2, and 3 mg/ml RGO content, respectively. The highly porous morphology of the developed hydrogels contributes to the rapid gas adsorption onto the hydrogel surface and diffusion into the inner structure [144]. To characterize the surface morphology of the hydrogels, the samples were freeze-dried and monitored using the scanning electron microscopy (SEM). SEM images of the hydrogels are demonstrated at different scales in Figure. 4. As illustrated, all hydrogels showed porous 3D structures with pore sizes ranging from 40 µm to 350 µm. As shown in the SEM image of the CMC hydrogel (Figure. 4a), the surface morphology exhibited a rough structure and some wrinkles. Figure. 4b and c show that incorporating RGO into the CMC hydrogel matrix leads to a densely crosslinked network with smaller pores. It may be caused by the non-covalent crosslinking effect of intercalated RGO sheets with the backbone of CMC (hydrophobic interactions) and its hydrogen bonding interactions with functional groups of CMC, which can reduce the expansion of the gel matrixes, resulting in a decrease in the pore sizes [145]. An uniformly interconnected structure with pore sizes ranging from 100–200 µm indicates that the CMC was miscible with RGO. As can be seen from Figure 4 b and c, the RGO sheets in the CMC hydrogels cannot be distinguished easily from the cellulose matrix, which may be related to the ultralow loading of RGO and strong interactions between RGO sheets and CMC matrix. Further addition of RGO up to 3mg/ml resulted in a significant reduction in the specific surface area and average pore sizes of the obtained hydrogel, as shown in Figure 4d. One possible explanation was that the existence of RGO sheets on the surface and inner structures of RGO3/CMC hydrogel leading to the blocking

of some pore structures [146]. Another possible reason may be the aggregation of the RGO sheets [147].

The surface morphology of the CMC-GO hydrogels was also investigated as a reference sample. SEM results of CMC/GO hydrogel (Figure. 4e) showed a porous 3D structure, similar to those of RGO/CMC hydrogels. It proved that the hydrogels possessed good miscibility.

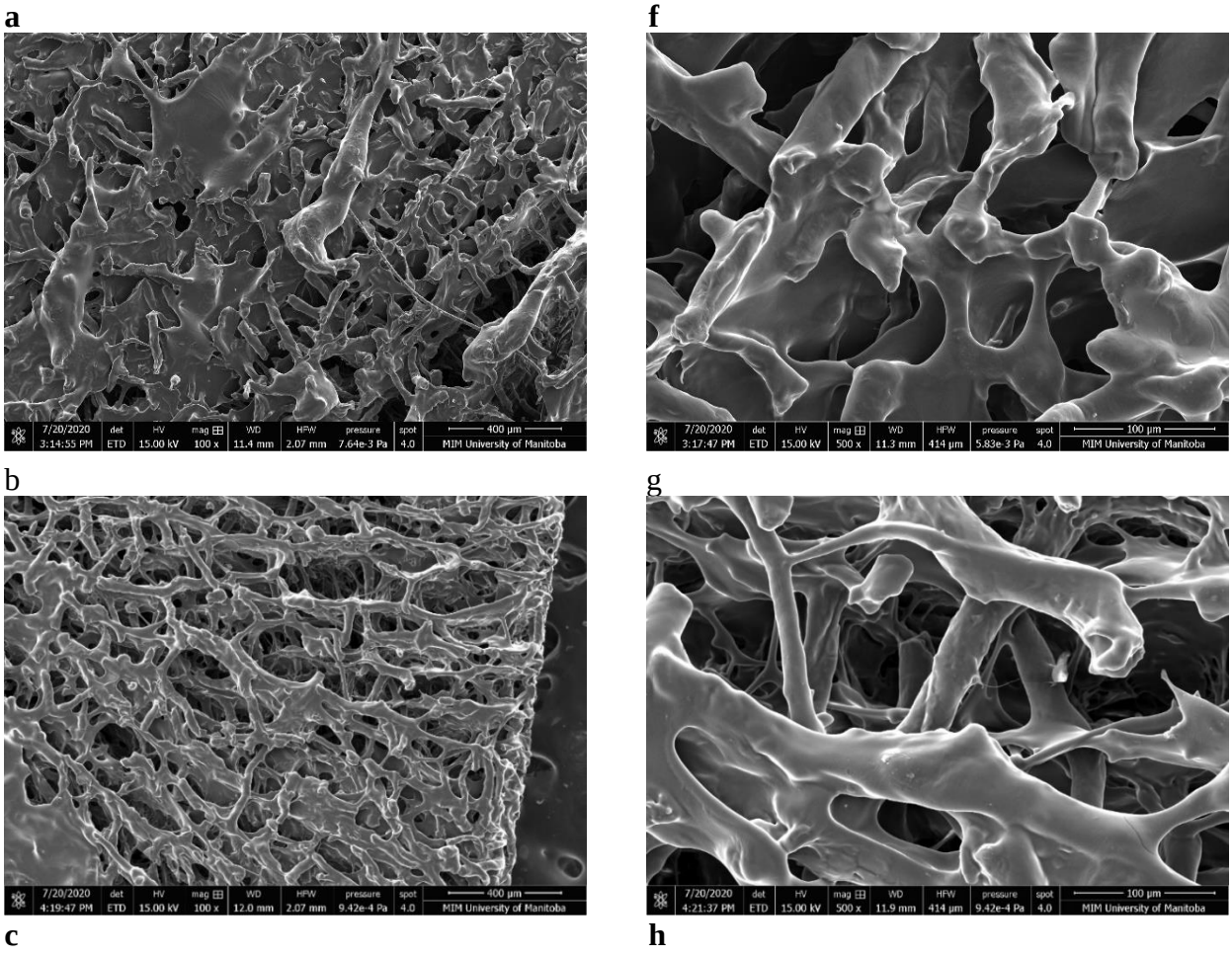

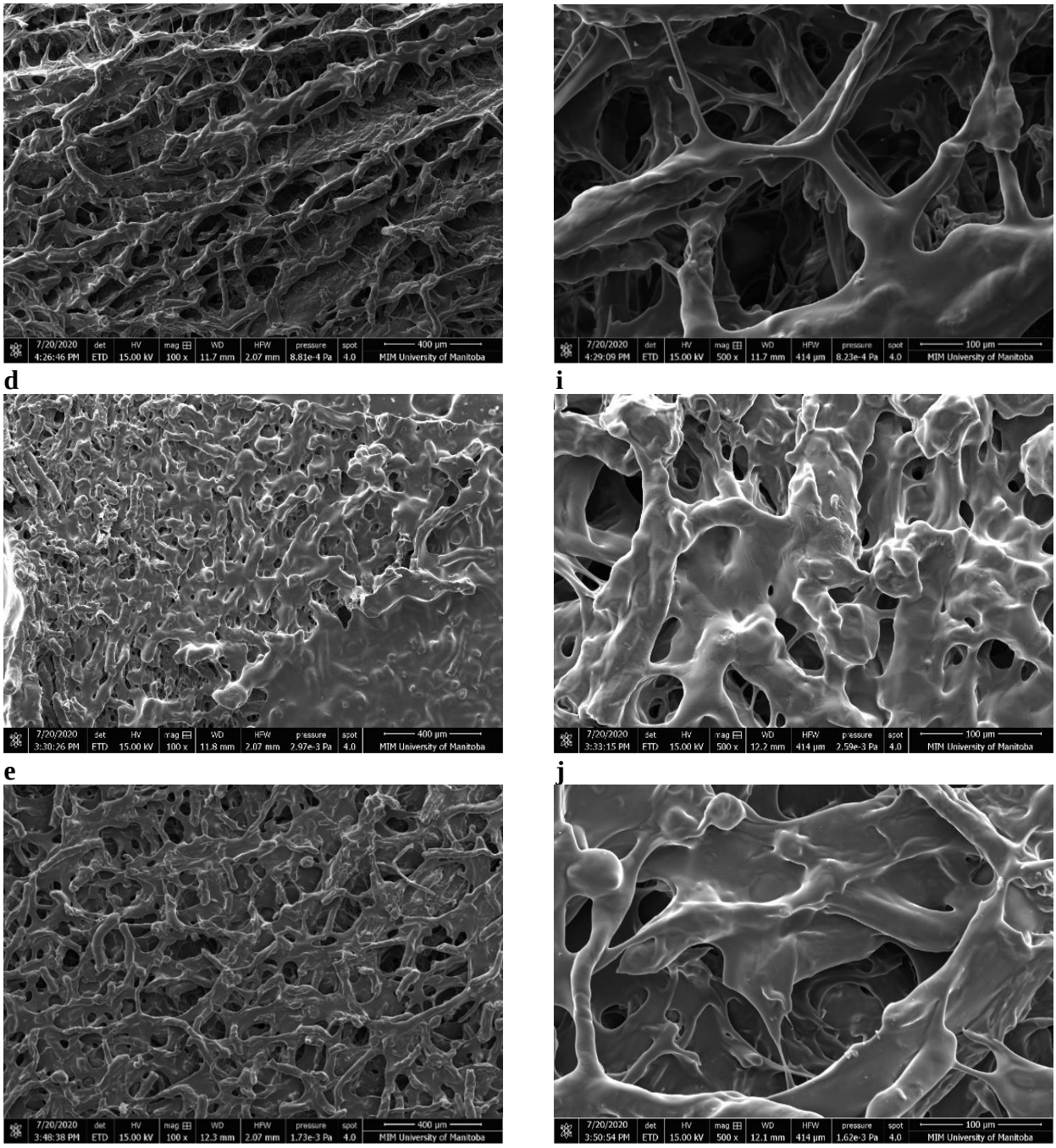

Figure 4. 4 SEM images of freeze-dried conductive hydrogel: a) CMC b) CMC-RGO1 c) CMC-RGO2 d) CMC-RGO3 and CMC-GO2 (f). Figure f-j shows the SEM images of the CMC, CMC-RGO1, CMC-RGO2, CMC-RGO3, and CMC-GO2 at higher magnification (×500).

4.4 FTIR analysis of conductive CMC hydrogels

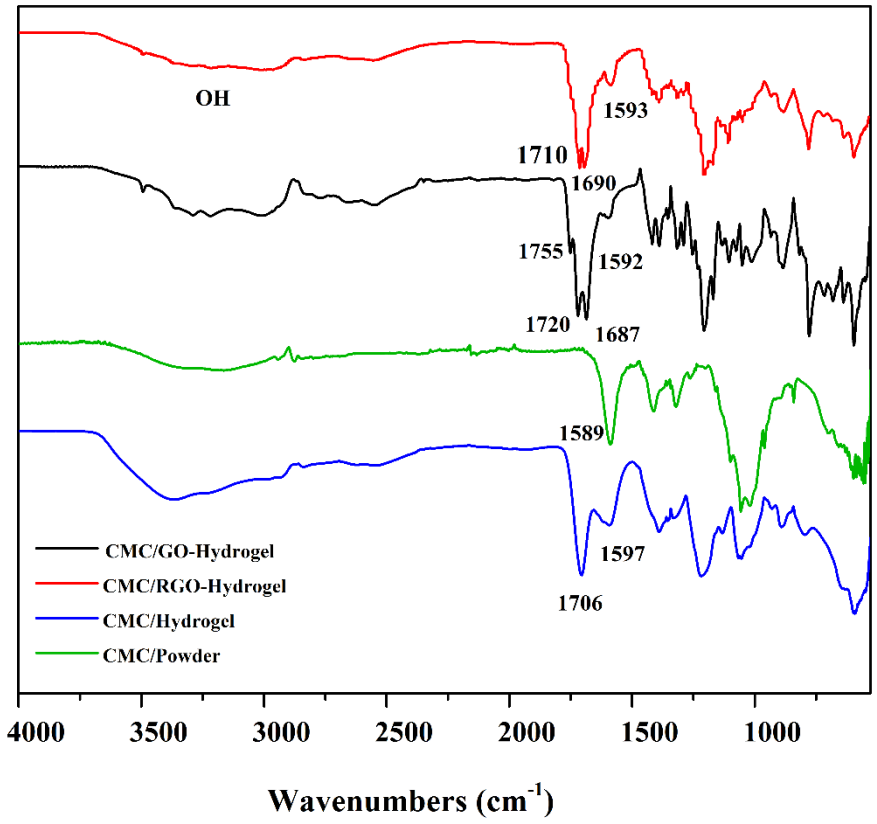

Figure 4. 5 FTIR spectra of CMC powder, CMC hydrogel, CMC/ GO hydrogel and CMC/RGO hydrogel

Figure 5 showed the FTIR spectra of CMC powder, CMC hydrogel, CMC/GO, and CMC/RGO hydrogels. The FTIR spectra for all samples showed the presence of sodium carboxylate (–COONa) as represented by its characteristic peak at 1589 cm^{-1} [148]. For the hydrogel samples, the $–COO^-$ the asymmetric stretching band was shifted to a lower frequency, and the absorption intensity for the sodium carboxylate group decreased. It was because there were still some –COONa groups in the CMC hydrogel after the acidification process. Compared to the CMC powder spectrum, the new and strong peak at 1706 cm^{-1} appeared in the FTIR spectrum of CMC

hydrogels, corresponding to the stretching vibration of the formed carboxylic acid groups, which confirms the success of the acidification step [135,148]. The dominant absorption peaks for CMC/GO hydrogel were identified at 1592, 1687, 1720, and 1750 $cm^{-1,}$ which correspond to –COONa, carboxylic group of CMC, C=O in carboxylic acid and carbonyl moieties on GO, respectively [135,145]. As shown in Figure. 5, the characteristic peaks for hydrogels containing RGO were at 1690, 1710 cm^{-1}. The intensities of the above-peaks corresponding to oxygen-containing functional groups in RGO/CMC hydrogels were decreased compared to their intensities in GO/CMC hydrogels, and C=O peak at 1755 cm^{-1} was disappeared. So the FTIR results confirmed the successful reduction of GO [149,150].

Based on the FTIR results, the main mechanisms of hydrogel formation could be described as follows: First, some free segments of CMC entangle with each other after the CMC powder is dissolved into water[151]. The addition of RGO or GO dispersion caused the viscosity increased, and the flowability decreases, leading to less-effective dispersion of conductive agents in the CMC matrix at higher concentrations[152]. The conductive nanomaterials are trapped among free polymer chains. Hydrogen bonds can be formed among the carboxyl and hydroxyl groups of conductive nanomaterials and polymer chains, and hydrophobic interactions between the basal planes of conductive components (RGO/GO) and hydrophobic regions of CMC can also occur. The second step is the acidification process. After immersing the conductive black paste into an 8 mol/L citric acid solution, the–COONa groups attached to Na-CMC polymer backbones are converted into –COOH groups, thus the CMC polymer chains carry more –COOH groups to allow the formation of more hydrogen bonds and finally leading to 3D cross-linked hydrogel networks [135].

4.6. Macroscopic self-healing test

The self-healing capacities of the hydrogel samples were evaluated by a cut and heal experiment. The two cut pieces were then put together to allow the reconnection of the two cut surfaces in a Petri dish for 9 hours to heal at room temperature. After that, the samples were taken out. The samples were found to restore their original shape with no trace of cut (as shown in Figures 6 and 7). The healed samples also demonstrate sufficient mechanical integrity to withstand bending into a U-shape or semicircular shape, as depicted in Figure. 8.

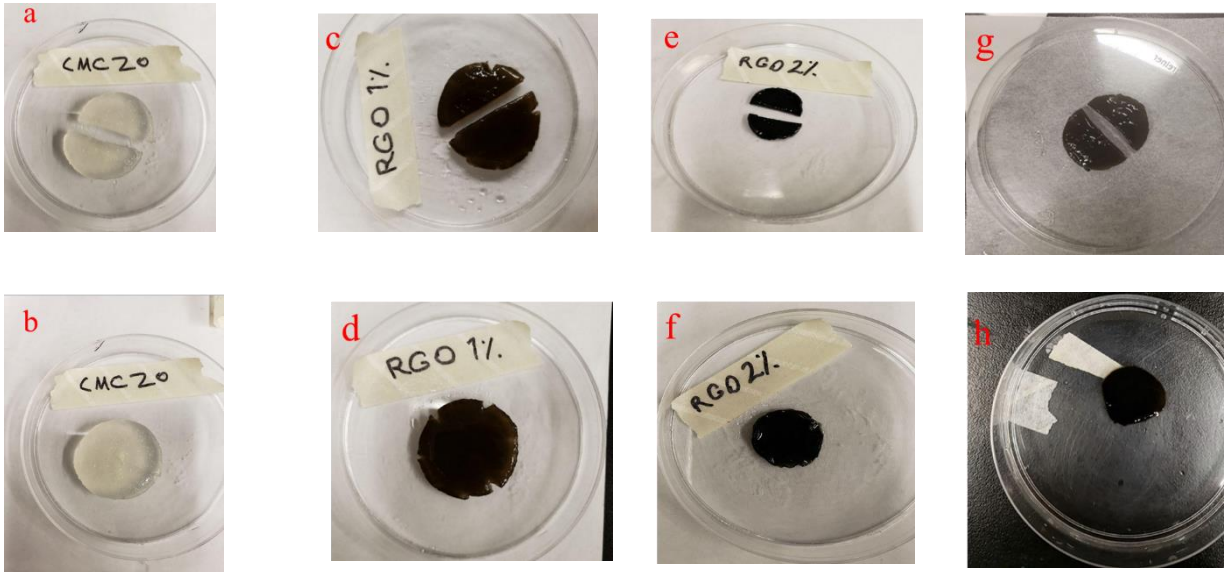

Figure 4. 6 Self-healing ability for CMC hydrogel incorporated with different contents of RGO (0, 1, 2, and 3 mg/ml)

A B C

Figure 4. 7 Self-healing ability for CMC/GO hydrogel incorporated with different contents of GO (1, 2, and 3 mg/ml)

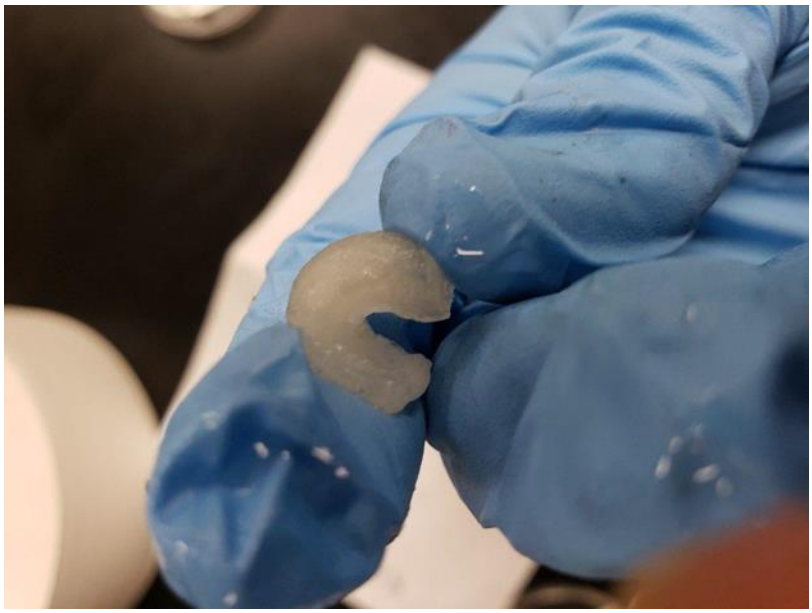

Figure 4. 8 Bending of self-healed CMC, CMC-GO2, and CMC-RGO2 hydrogels.

4.7 Tensile Behaviors and Self-Healing Ability

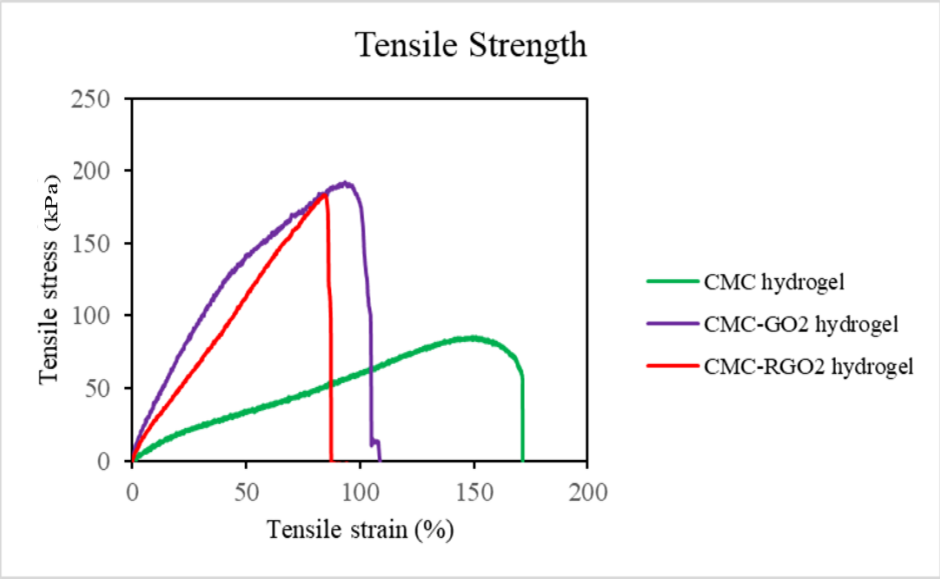

Figure 4. 9 Tensile stress−strain curves of CMC, CMC-GO2, and CMC-RGO2 hydrogels before the cut

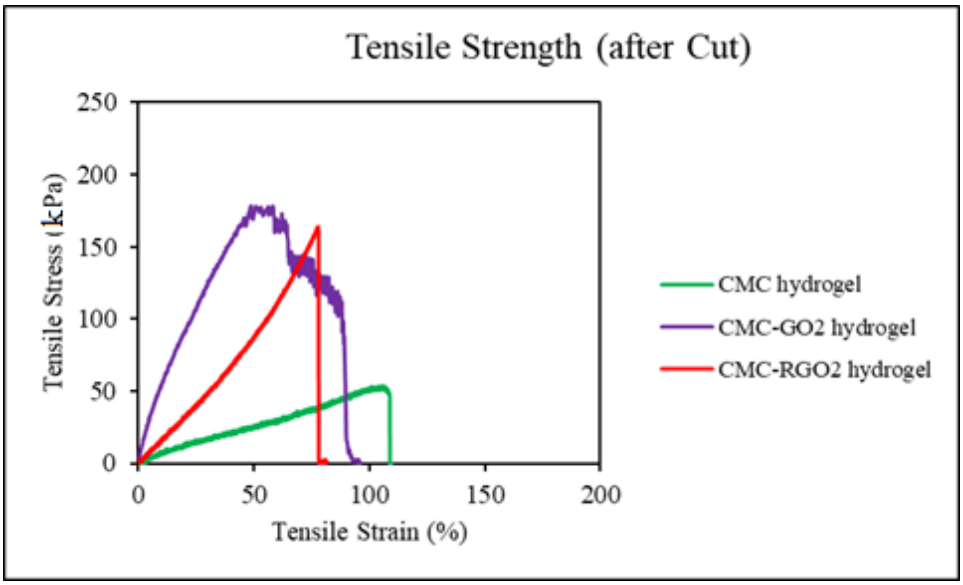

Figure 4. 10 Tensile stress−strain curves of CMC, CMC-GO2, and CMC-RGO2 hydrogels after the self-healing.

Mechanical characteristics are important for practical applications of hydrogel-based sensors. Hence, we evaluated the mechanical properties of the obtained hydrogels using a tensile test machine, with the crosshead rate being set at 10 mm/min. The representative tensile stress-strain

curves for hydrogels are shown in Figure.9. Obviously, the pristine CMC hydrogel possessed a poor tensile strength of around 85 kPa. It is clear from Figure. 9 that the incorporation of GO and RGO with the concentration of 2mg/ml into the CMC hydrogel network significantly enhanced the tensile stresses to 195 kPa and 183.3 kPa, respectively. The tensile strength of CMC-GO2 hydrogel is almost 2.3 times greater than that of the pristine hydrogel, and the tensile strength of CMC-RGO2 was 2.15-fold greater than that of the original hydrogel. These results strongly suggested that Both GO and RGO can act as reinforcement nanomaterials. The remarkable enhancement in the mechanical properties was attributed to the excellent dispersion of the above-mentioned nanomaterials into CMC hydrogel. Another cause of the significant improvement in the tensile strength is the increase in the number of hydrogen bonds formed among the oxygen-containing functional groups of GO or RGO with the hydroxyl groups of CMC[150]. As can be seen from Figure 9, the elongation at break for pristine CMC hydrogel reached around 170%, while the elongation at break was gradually decreased to 101% and 94% with the addition of GO and RGO, respectively. The decrease of elongation at break may result from the increased interaction between CMC chains and nanomaterials, which hindered the migration of the CMC chains[85].

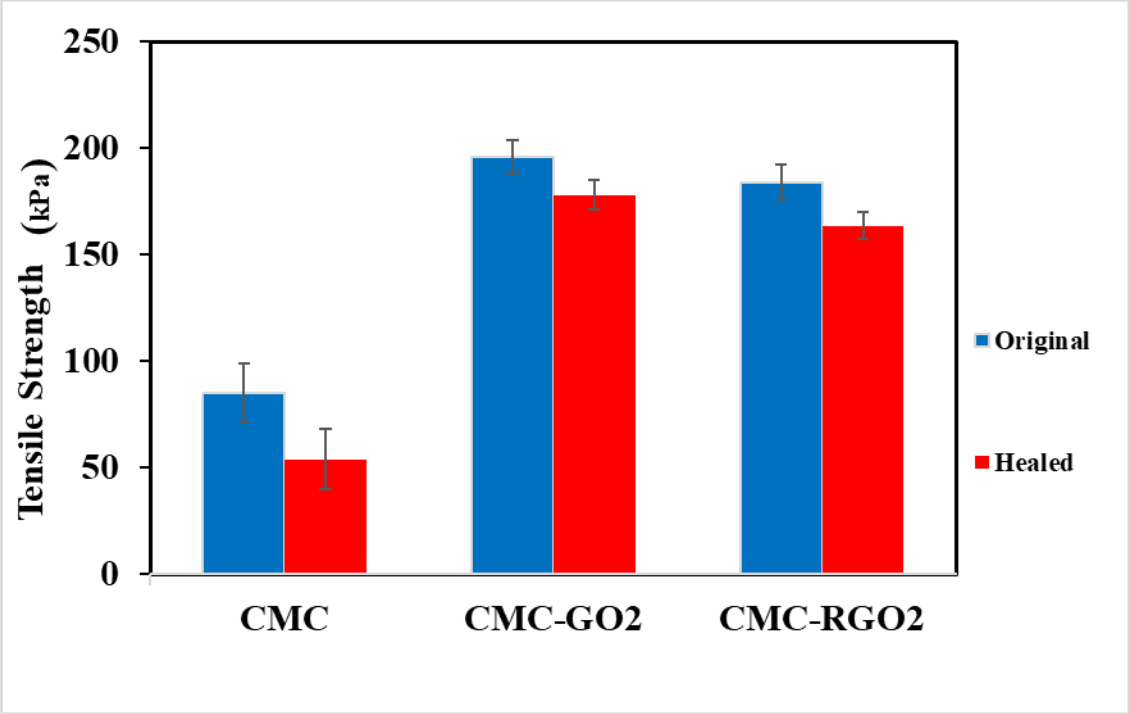

Figure 4. 11 Comparison of tensile strengths of hydrogels before and after healing, with p value < 0.05

Tensile tests of the self-healed samples were also carried out with the same tensile machine used for the original samples at the same crosshead speed. The results are shown in Figures 10 and 11. The self-healing efficiencies (HE) in breaking stress and strain were obtained by comparing the breaking stress and strain of the healed hydrogels with the original one, shown in equation 4.1 and 4.2.

$$\text{Breaking Tensile Stress healing efficiency} = \frac{S2}{S1} \times 100 \qquad (4.1)$$

$$\text{Breaking Tensile strain healing efficiency} = \frac{e2}{e1} \times 100 \qquad (4.2)$$

Where S_2 and S_1 are as the breaking tensile stresses of the healed hydrogel and the original one, respectively; E_2 and E_1 are the breaking tensile strain after and before self-healing, respectively.

Figure 10 illustrates the tensile stress−strain curves of hydrogel samples after self-healing in air. The breaking tensile stress and elongation for the self-healed CMC hydrogel were 53.11 kPa and 111%, respectively. The hydrogels exhibited 63% healing efficiency in breaking stress and 65% recovery in breaking strain. After healing, CMC-GO2 hydrogels showed a breaking tensile stress of 178KPa and a breaking tensile strain of 94.3%. As shown in Figure 12, with the addition of GO into the CMC matrix, the hydrogels showed excellent self-healing efficiency in the breaking tensile stress and tensile strain with 91.2 % and 94.05% recovery, respectively. As shown in Figure.10, when RGO was loaded, tensile strength and rapture strain of the healed CMC-RGO2 hydrogels reached 163 kPa and 82%, respectively. The HE in stress was 88.7%, and HE in strain was around 86% for CMC-RGO2. Compared with the hydrogels containing nanomaterials, CMC hydrogels presented a lower self-healing efficiency. This may be due to the formation of less hydrogen bonds in a CMC hydrogel network than CMC-RGO and CMC-GO hydrogel samples. When the hydrogel is damaged, the broken Na-CMC polymer chains can generate a mobile phase in or around the cracks, and H^+ ions from un-crosslinked polymer chains substitute Na^+ ions of the CMC polymer chains, which cure the broken networks via the formation of new hydrogen bonds, which fill and bridge the damaged area to heal the hydrogel [78,135].

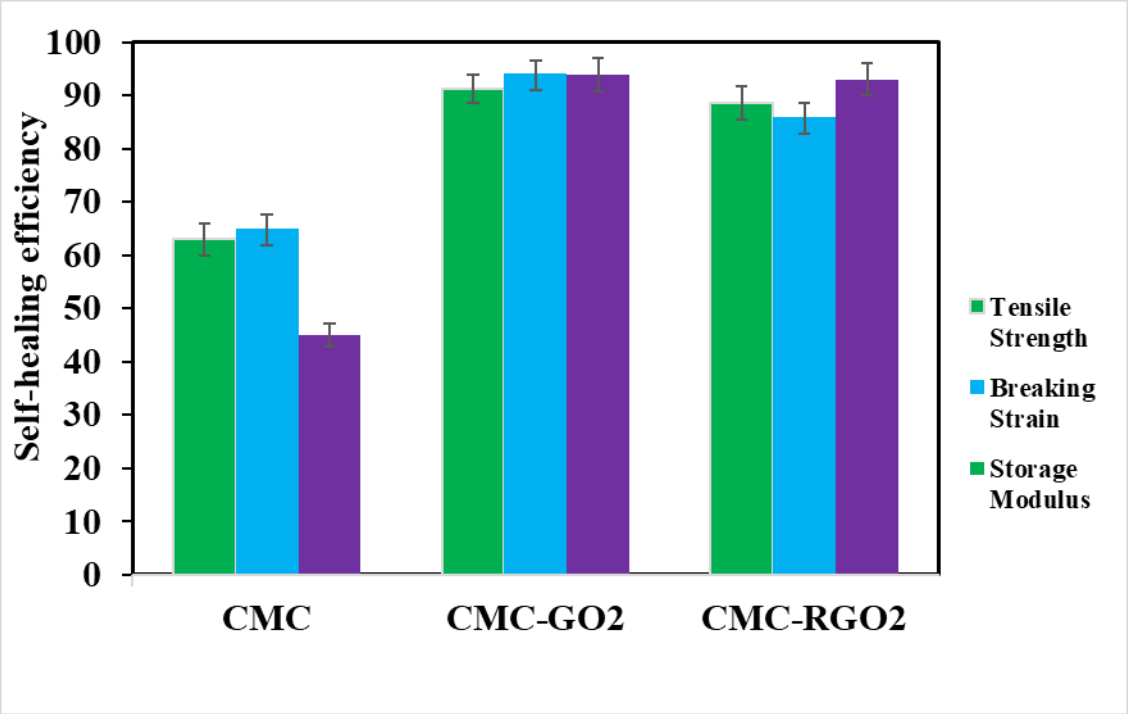

Figure 4. 12 Healing efficiency in breaking tensile stress, breaking strain, and storage modulus

4.8 Rheological study

The rheological study is of primary importance for the characterization of mechanical properties of hydrogels because it is quick, sensitive, and it requires small samples. The rheology test is also conducted to reveal the details of the gelation processes and to provide information on the hydrogel structures and mechanical property changes during gelation[153]. Two important parameters, the storage modulus (G′) and the loss modulus (G″), are monitored in the rheology test for a hydrogel sample. A high storage modulus indicates a tough hydrogel network, which may be achieved by an increased crosslinking density [154]. The loss modulus *G″* exhibited weak dependence on the applied frequency. The value of G″ is gently increased with increase in frequency due to a gradual increase in relaxation of CMC chains at a higher frequency[155,156].

The storage modulus (G′) and loss modulus (G″) of the original and the healed CMC hydrogels were recorded, and the results were shown in Figure. 13. Rheological results show that both original and healed CMC hydrogels have high storage modulus (G′) and exhibit elastic behavior at w = 0.1~100 rad s^{-1} (G′ is substantially higher than G″). The higher storage modulus resulted from a more tightly crosslinked hydrogel[157]. After the cutting/healing operation, the G' and G" values of the healed hydrogels declined, and Storage modulus decreased from 2307 Pa to 1020 Pa. It implies that less crosslinking density occurred after self-healing compared to the original hydrogel. It was due to the formation of fewer hydrogen bonds during the self-healing process. However, the self-healed CMC hydrogel still shows solid-like behavior as G′ is much higher than G″[158].

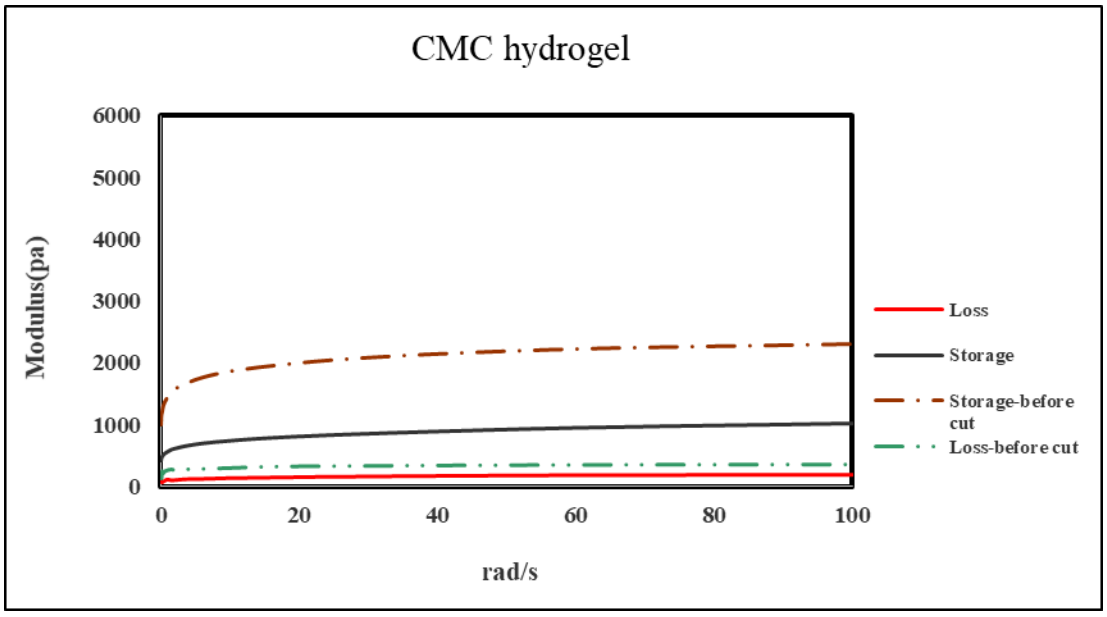

Figure 4. 13 Rheological measurements of CMC hydrogels before and after cut and healing

Figure.14 illustrates the storage and loss moduli of CMC hydrogels containing different amounts of RGO in the strain amplitude sweep test. Over the entire ω range, the G′ values of all hydrogels were always higher than their corresponding G″ values, which indicated that a permanent elastic network was formed in the solid-like hydrogels[159]. It is obvious that G′ and G″ increased significantly when a low dose of the RGO was added. The reason may be that the RGO nanoparticles might affect the crosslinking of the CMC. As shown in Figure 14a, the storage moduli of CMC-RGO1 was about 3906 KPa and 3404 Pa before and after self-healing. The CMC-RGO1 exhibited loss moduli of 557.8 Pa originally 509.14 Pa after self-healing. The healing efficiency in storage moduli of CMC-RGO1 was approximately 87.2% (Figure 14). As shown in Figure 14.b, the G′ and G″ values increased with the further increase of the RGO content at 2mg/ml. It may be caused by the entanglement and crosslinking of CMC in the RGO-CMC hydrogels. Among all samples containing RGO, CMC-RGO2 exhibited the highest storage moduli of 5246.15 Pa and loss modulus of 759.4 Pa. After the cut and healing process, the storage modulus of the CMC-RGO2 hydrogel shows a recovery to 93% of the original hydrogel. This finding agrees with the self-healing efficiency in tensile tests for the CMC-RGO2 hydrogel. Figure 14c demonstrates a slight decrease in storage and loss moduli when the RGO content reached 3mg/ml. It may be caused by excessive nanoparticle contents, which might hinder the formation of the 3D network within the hydrogel, leading to a decline in G′ value. Results also showed that the CMC-RGO3 hydrogel shows a recovery to 76% of its original storage modulus after self-healing.

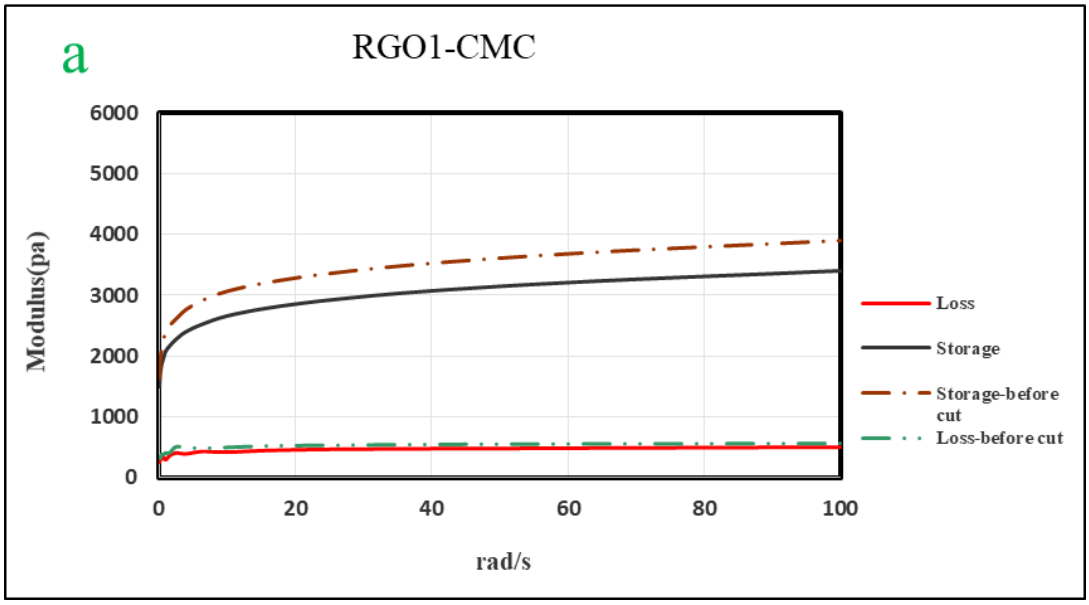
a
RGO1-CMC
Modulus(pa)
6000
5000
4000
3000
2000
1000
0
0
20
40
60
80
100
rad/s
Loss
Storage
Storage-before cut
Loss-before cut

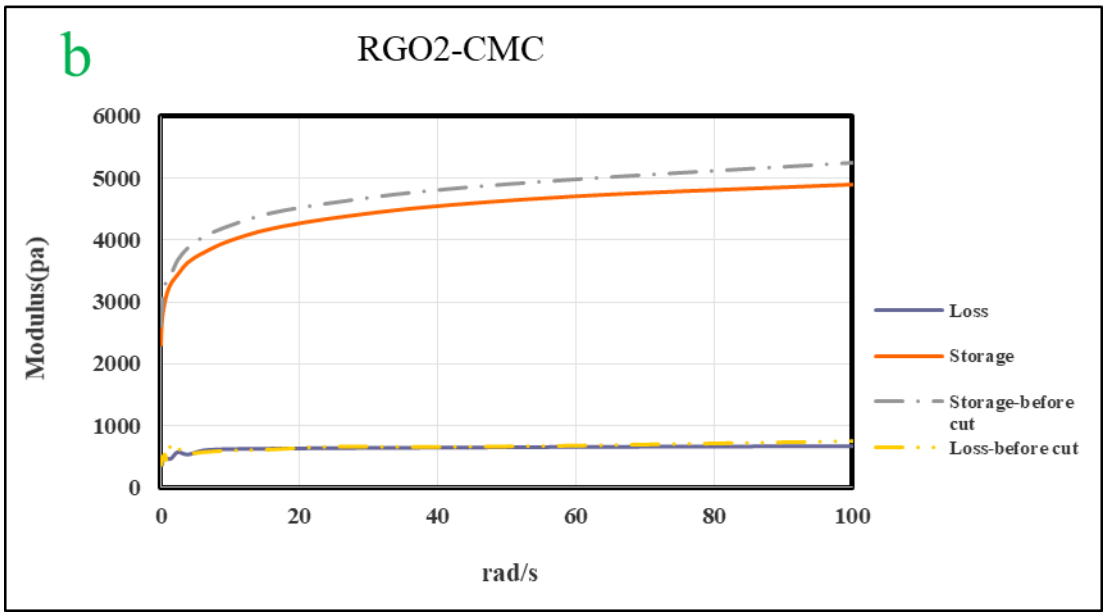
b
RGO2-CMC
Modulus(pa)
6000
5000
4000
3000
2000
1000
0
0
20
40
60
80
100
rad/s
Loss
Storage
Storage-before cut
Loss-before cut

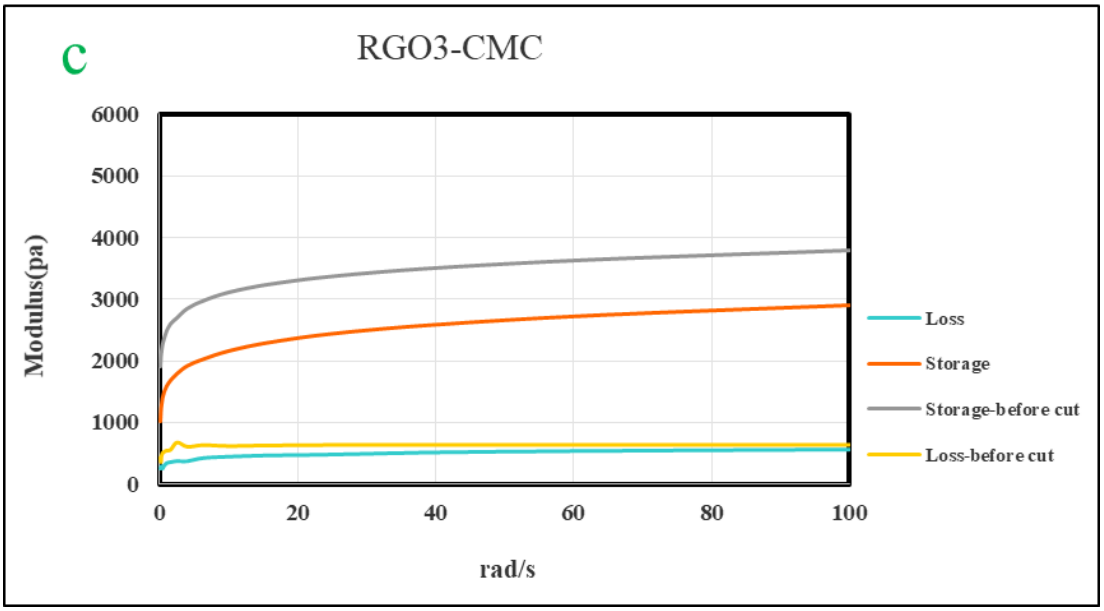

Figure 4. 14 Rheological properties of CMC hydrogels with different RGO contents before and after the cut and healing.

Figure 15 shows the rheological properties of CMC hydrogel incorporated with various contents of GO. Figure 15a presents that adding a small amount of GO to the hydrogel network considerably enhanced both storage (9488 Pa) and loss moduli (1175.4 Pa). Among all CMC-GO hydrogels, the CMC-GO2 had the highest G' (~11449 Pa) and G" (~1105 Pa) values, as shown in Figure 15b, indicating strong interaction and entanglement between the CMC chain and the GO that lead to a more stable and higher crosslink. Compared with the other hydrogels, storage moduli of CMC-GO2 (11449 Pa) was almost 2.1 times higher than that of the CMC-RGO2 hydrogel (Gmax ′ ≈ 5203 Pa) and 5.5 times greater than that of the pristine CMC hydrogel (Gmax ′≈ 2307 Pa). Figure 15c shows that the storage and loss moduli of hydrogels containing 3mg/ml GO gently declined compared to CMC-GO2. G' values of the healed hydrogels show recoveries to about 97% (CMC-GO1), 94% (CMC-GO2), and 92% (CMC-GO3) of that of the original hydrogels, indicating that the nanocomposite hydrogels possess reversible restorability. Storage modulus (G') of all obtained

hydrogels remain much higher than loss modulus (G") over the whole frequency range, demonstrating a more stable hydrogel network with dominant elastic behavior [98].

The major contribution to the high self-healing efficiencies in both CMC/RGO and CMC/GO hydrogels may be the massive hydrogen bonding interactions among the neighboring CMC polymer chains and GO/RGO[126]. After the cutting surfaces were allowed to get into contact, the Na-CMC polymer chains can generate a mobile phase in or around cracks, and the –COONa groups can be converted into –COOH on the CMC polymer chains, which heal the broken networks by reforming of the supramolecular interactions at their points of contact to fill and bridge the damaged zone [78]. Hydrophobic bonds should also be taken into consideration due to interactions between the basal planes of conductive components (RGO/GO) and the hydrophobic regions of CMC [160]. The difference in HE of the hydrogels with different conductive components may be due to the difference in mobility of the free polymer chains and number of oxygen-containing groups in the network, such as carboxyl groups and hydroxyl groups that leading to the formation of new hydrogen bonds[135]. Therefore, the formation of new hydrogen bonds and hydrophobic interactions among CMC and conductive nanoparticles at the cut interface of the hydrogels led to the repairing and recovery of hydrogel along with restoring the mechanical strength to the hydrogel networks.

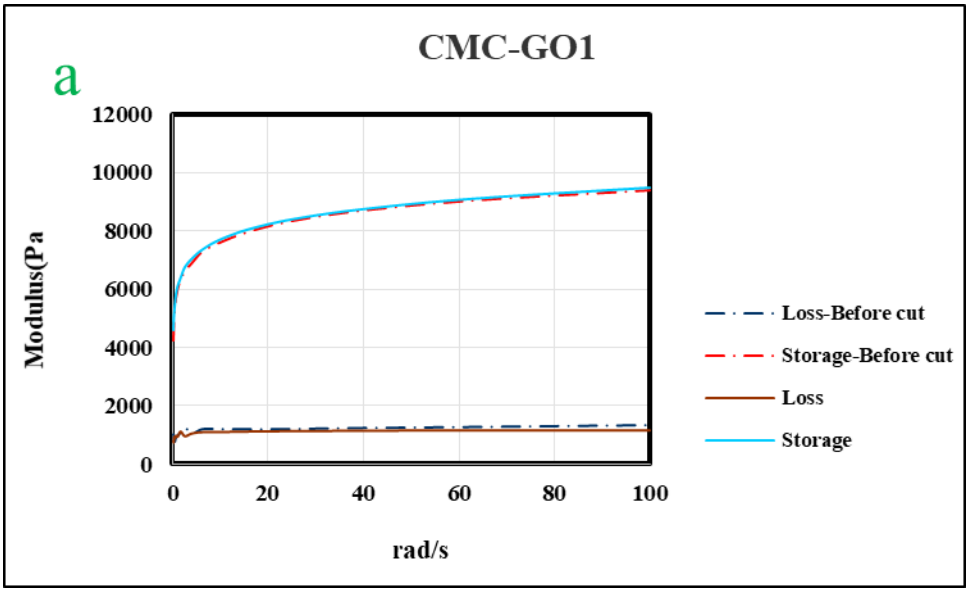
a
CMC-GO1
Modulus(Pa
12000
10000
8000
6000
4000
2000
0
0
20
40
60
80
100
rad/s
Loss-Before cut
Storage-Before cut
Loss
Storage

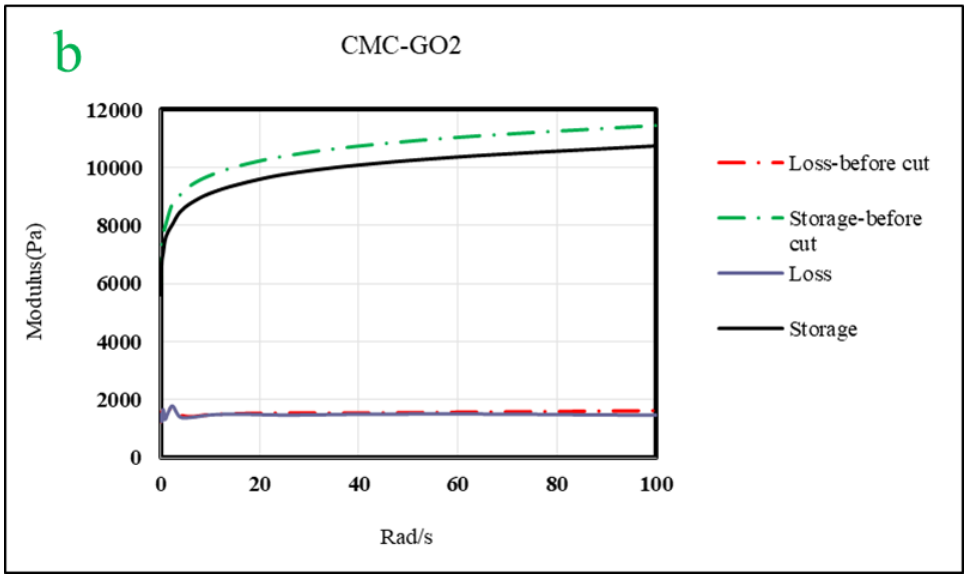
b
CMC-GO2
Modulus(Pa)
12000
10000
8000
6000
4000
2000
0
0
20
40
60
80
100
Rad/s
Loss-before cut
Storage-before cut
Loss
Storage

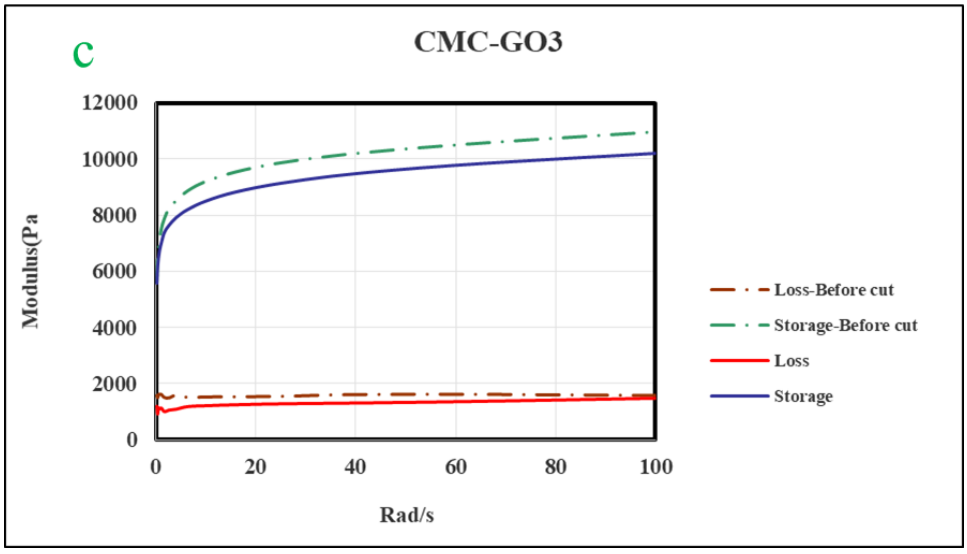

Figure 4. 15 Rheological properties of CMC hydrogels with different GO concentrations before and after the cut and healing

4.9 Electrical properties of the prepared conductive hydrogels

Conductivity is one of the most critical parameters that make the developed hydrogels promising candidates for sensors [161]. As reported previously [85], cellulosic hydrogels can endow ion and electron transportation pathways with the incorporation of conductive materials.

Table 4.1 shows the electrical conductivity of the hydrogels containing various amounts of GO and RGO measured at room temperature through the two-point probe resistivity measurements, in which the two probes of a multimeter were connected to two points (at a fixed distance of 1cm) on a sample via copper wires. The electrical conductivity of CMC was around 7×10^{-5} S/cm, which suggests a non-conducting material. The electrical conductivities for the hydrogels generally rise as the nanomaterials (GO or RGO) amount increased because of the contributions from the conductive components.

As can be seen, the electrical conductivity of the CMC-GO1 hydrogel is about 2.1×10^{-3} S/cm, which shows that the incorporation of GO improved the electrical conductivity of CMC. The addition of more GO caused a further increase in conductivity up to 5.8×10^{-3}S/cm for CMC-GO2, which was about 2.7-fold higher than that of CMC-GO1 and 82-times higher than that of CMC hydrogels. Due to an improvement in the sheet-to-sheet contact of GO, it eventually promotes the formation of a continuous 3D network of the conductive particles[162]. The conductivity was slightly increased to 7.1×10^{-3} S/cm at 3mg/ml loading (CMC-GO3).

Furthermore, the effect of the RGO concentrations on the electrical conductivity of the composite hydrogels was also explored. Results demonstrated that the electrical conductivities of the hydrogels were significantly enhanced when RGO was incorporated. The CMC-RGO1 hydrogel possesses a conductivity of 1.1×10^{-2} S/cm, which was approximately 5.2 times greater than that of CMC-GO1 and 157 times greater than that of CMC hydrogel. CMC-RGO2 achieved the maximum electrical conductivity at 4.4×10^{-2} S/cm. It can be attributed to an increase in the contact between two neighboring RGO layers and the homogeneous distribution and penetration of RGO, leading to an ideal 3D interconnected conducting network[82]. The electrical test results illustrated that with higher contents of RGO (≥2 mg/ml), more RGO agglomerations occurred in the RGO solution during the preparation process due to van der Waals interactions among RGO neighboring nanosheets[140]. It caused a slight decrease in conductivity. The agglomeration and poor distribution of RGO at higher content may prevent the completion of an intimate contacting network of RGO in the CMC networks [163].

The conductivity test findings presented that the electrical conductivities of hydrogels containing RGO are much greater than those hydrogels containing GO. It may be related to the abundant oxygen-containing groups, such as hydroxyl, carboxyl, and epoxy, on the surface of GO.

Consequently, the conjugated structure of the graphene may be disrupted, and the resistance enlarges[163].

It was also interesting to note that the self-healed CMC-RGO2 hydrogel showed the highest conductivity of about 2.9×10^{-2} S/cm. It was shown that a 9 h healing time resulted in a nearly full restoration of the electrical properties, which verified the self-healing process. Other healed samples also exhibited electrical conductivities ranging from 1.6×10^{-4}S/cm to 0.621×10^{-2} S/cm. It reveals that the developed hydrogels can not only repair their mechanical damages but also restore their electrical conductivity to a certain level. These results demonstrated their great potential for practical applications such as self-healing electronics and sensors.

Table 4. 1. The electrical conductivity of hydrogel samples

Samples	Conductivity (S/cm)	Conductivity S/cm (After Cut)
CMC-GO1	2.1×10^{-3}	1.6×10^{-4}
CMC-GO2	5.8×10^{-3}	2.9×10^{-4}
CMC-GO3	7.1×10^{-3}	6.3×10^{-4}
CMC-RGO1	1.1×10^{-2}	0.16×10^{-2}
CMC-RGO2	4.4×10^{-2}	2.9×10^{-2}
CMC-RGO3	1.8×10^{-2}	0.621×10^{-2}

4.10 Ammonia gas sensing tests

The capability of the developed hydrogels to detect ammonia gas was explored. The prepared conductive hydrogel-based sensor and the ammonia gas detecting system are presented in Figure 16.

The results were shown in Figure 17. Before exposure to the target gas, the resistance of a sample was monitored for 100 s in the air to get a stable initial resistance value (R0). Then, the conductive hydrogel sample was exposed to the testing gas.

As shown in Figure 17, the CMC-RGO sensors displayed good sensitivity to NH_3. It can be seen that, upon exposure of the CMC-RGO hydrogels to ammonia gas, an instant sharp increase in relative resistance variation can be observed. When CMC-RGO1 was exposed to the ammonia gas at 30 ppm, the R_{rel} value of the CMC-RGO1 reached about 73% after 18 min. The value remained steady for the next 10 minutes, indicating that the hydrogel sensor absorbed saturated ammonia gas. It can be seen that the R_{rel} value decreases with the decline in ammonia gas concentration. The resistance change was obtained at 46% and 20% for the gas content of 15 ppm and 7.5 ppm, respectively, after 20 min.

As shown in Figure 18, when the CMC-RGO2 hydrogel sensor was exposed to ammonia vapor of 7.5 ppm, the sensor's resistance variation increased and peaked at 40%. It took the sensor 8 min to reach a stable signal when it was exposed to 15 ppm ammonia gas. The R_{rel} of CMC-RGO2 reached 88% after 6.6 min when the sensor was exposed to 30ppm ammonia gas. As shown in Figure 18c, the response resistance variance increases from 25% to 78%, with the NH_3 concentration increased from 7.5 ppm to 30 ppm. Among all CMC- RGO sensors, CMC-RGO2 exhibited the fastest sensing responses, as shown by the sharp increase in resistance variance upon exposure to ammonia gas and reaching a stable value within 6.6 min. It indicates that the CMC-RGO2 hydrogel is maximum sensitivity of 88% to ammonia gas.

The mechanism of the hydrogel sensors can be explained as follows: The resistance change of RGO-CMC hydrogels may be due to charge transfer between RGO and adsorbed gas elements [10]. The positive charge transfer between RGO-CMC hydrogels and NH_3 leads to decreased

carrier (hole) concentration in the hydrogel sensors and increases the resistance of the sensors [164]. The oxygen-containing groups such as residual carboxylic and epoxide groups are electron-withdrawing and produce some holes in the conduction band, making RGO behave as a p-type semiconductor[165]. Besides, the excellent sensitivity in ammonia gas detection is related to the formation of hydrogen bonds between these gas molecules and a large number of oxygenated functional groups, including hydroxyl and carboxylic on the polymer chains of CMC and RGO. The formation of hydrogen bonds promoted the adsorption of gaseous ammonia on the hydrogels[9].

Ammonia gas sensoring tests were also performed on CMC-GO hydrogels. As shown in Figure 19a, it took almost 16 min for the CMC-GO1 hydrogel to reach a stable resistance variance upon exposure to ammonia gas. Compared to CMC-RGO hydrogels, CMC-GO hydrogel sensors showed a much slower response. It may be caused by the declined oxygen functional groups on GO after being reduced to RGO. The less defective sites on RGO act as active regions to adsorb gas molecules, boosting the gas sensitivity[164,166]. The most critical challenge of GO sensing stability is the existence of more oxygen-containing functional groups, which adsorb analyte gas molecules[167]. The oxygen functional groups of GO render it too electrically insulating for conductance-based sensors[168]. The gas sensing results for CMC-GO showed lots of fluctuation on the value of resistance variation for GO2 and GO3. It may be attributed to increased hydroxyl and carboxyl groups when GO content increased[169]. The stability is important for the accuracy of a practical gas sensor.

It is known that ammonia gas is poor solvents for cellulose. Therefore, the cellulose matrix has no noticeable swelling upon exposure to ammonia gas [170]. The water evaporation induced instability is a common concern for many hydrogel-based devices. Results showed a very small

increase in resistance variation after 30 min upon exposure to air (Figure 17a). Therefore, water evaporation of hydrogels did not affect the sensitivity of the hydrogel sensors. However, to further remove the low influence of humidity, the prepared hydrogel gas sensor may be encapsulated by a porous and hydrophobic membrane in future work.

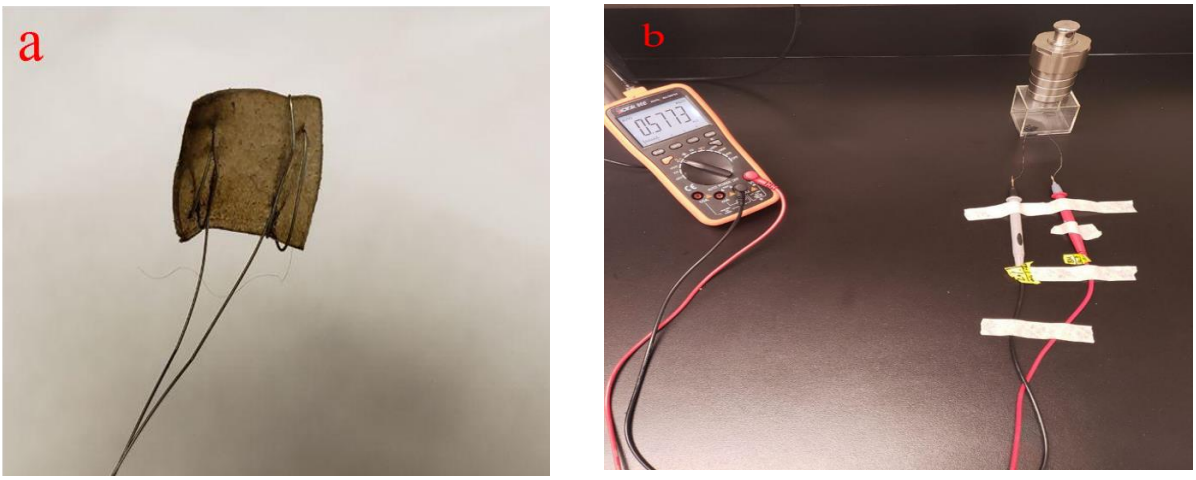

Figure 4. 16 The CMC/RGO-2 gas sensor (a) and the sealed system of the ammonia detector (b)

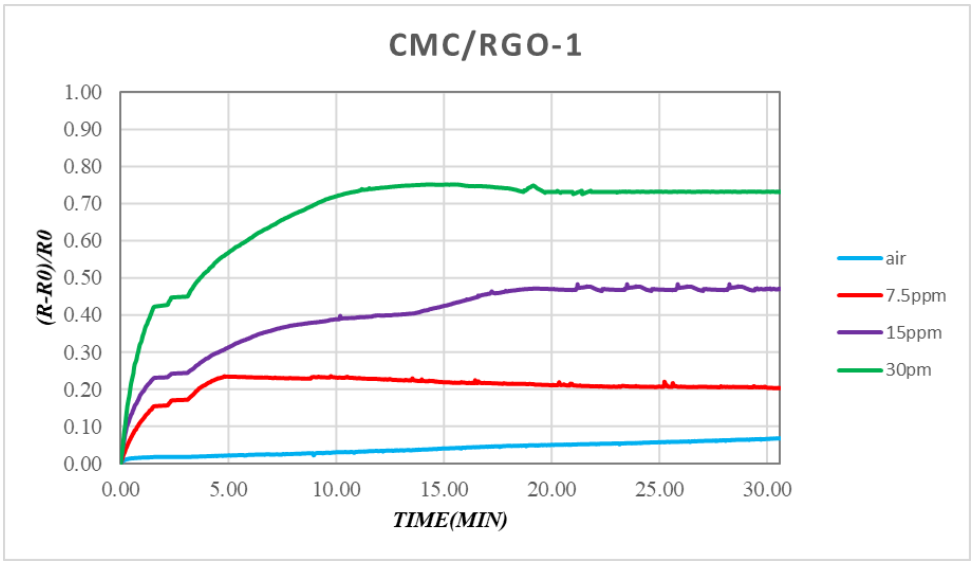
CMC/RGO-1
1.00
0.90
0.80
0.70
0.60
0.50
0.40
0.30
0.20
0.10
0.00
(R-R0)/R0
0.00
5.00
10.00
15.00
20.00
25.00
30.00
TIME(MIN)
air
7.5ppm
15ppm
30pm

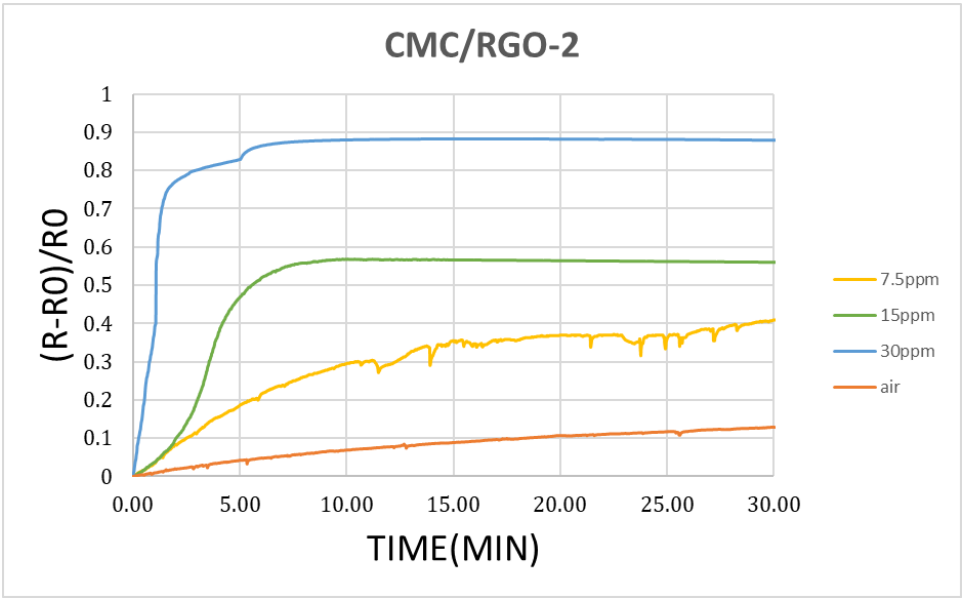
CMC/RGO-2
1
0.9
0.8
0.7
0.6
0.5
0.4
0.3
0.2
0.1
0
(R-R0)/R0
0.00
5.00
10.00
15.00
20.00
25.00
30.00
TIME(MIN)
7.5ppm
15ppm
30ppm
air

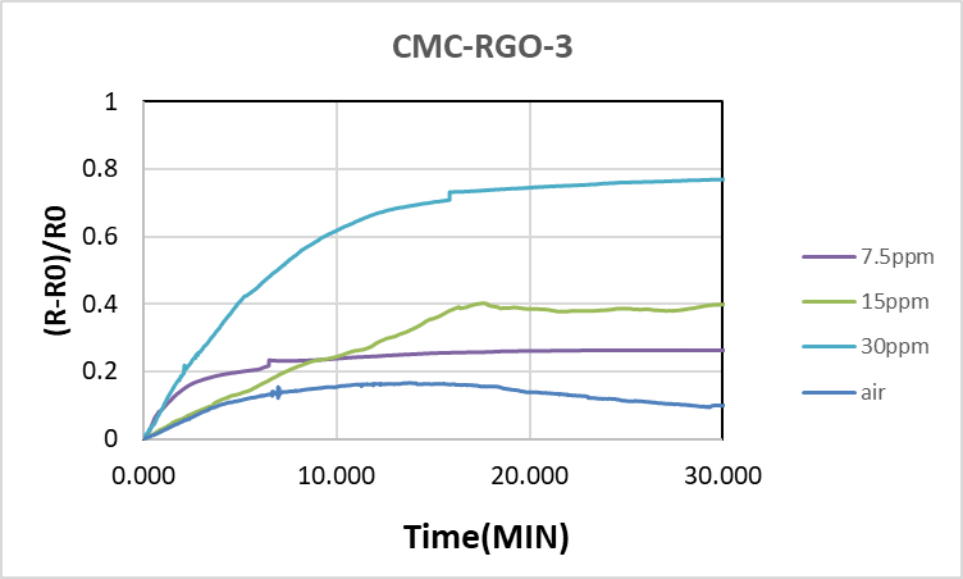

Figure 4. 17 Resistance variance of CMC-RGO sensors upon exposure to ammonia gas released from ammonia gas with different concentrations.

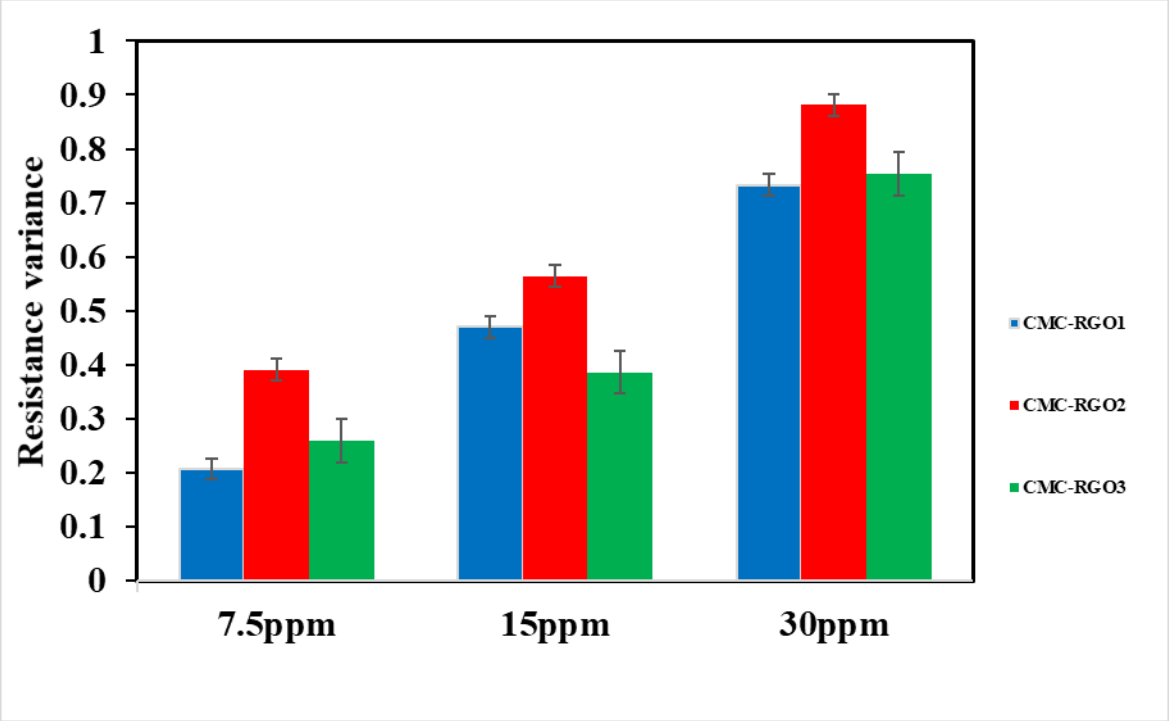

Figure 4. 18 Resistance variance of CMC-RGO hydrogels upon exposure to various ammonia gas contents.

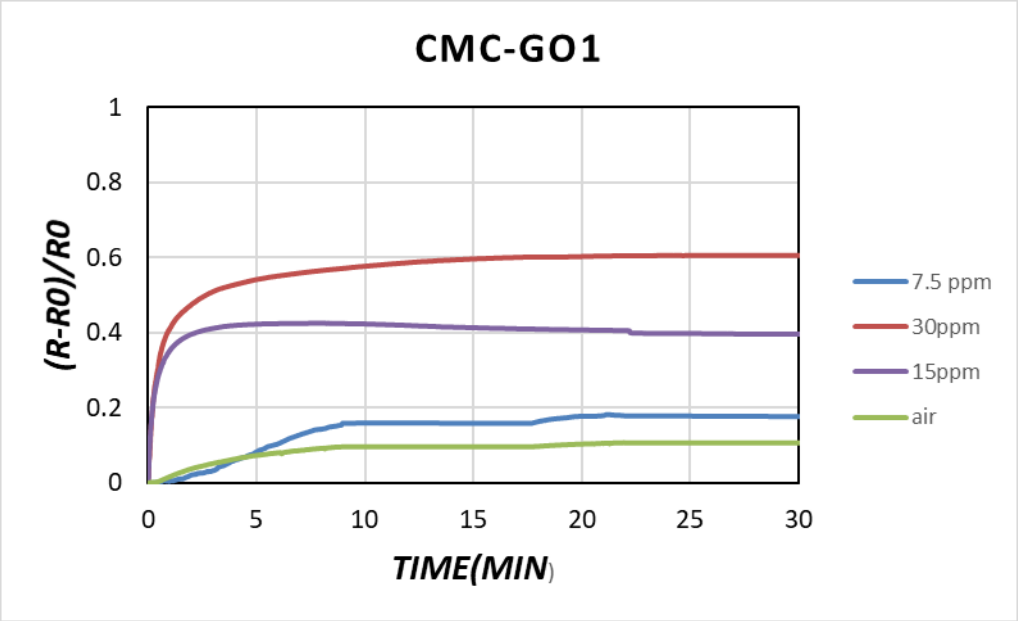
CMC-GO1
1
0.8
0.6
0.4
0.2
0
(R-R0)/R0
0
5
10
15
20
25
30
TIME(MIN)
7.5 ppm
30ppm
15ppm
air

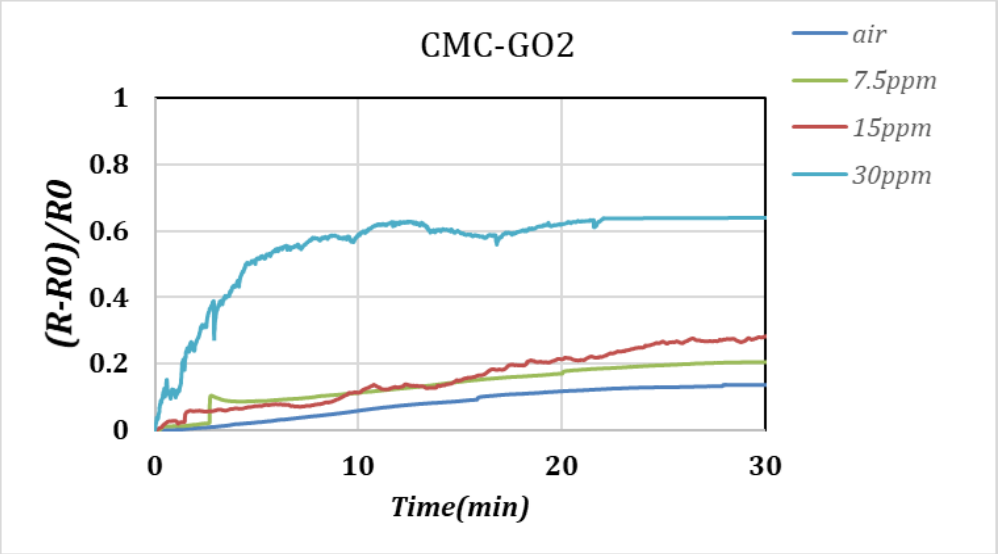
CMC-GO2
1
0.8
0.6
0.4
0.2
0
(R-R0)/R0
0
10
20
30
Time(min)
air
7.5ppm
15ppm
30ppm

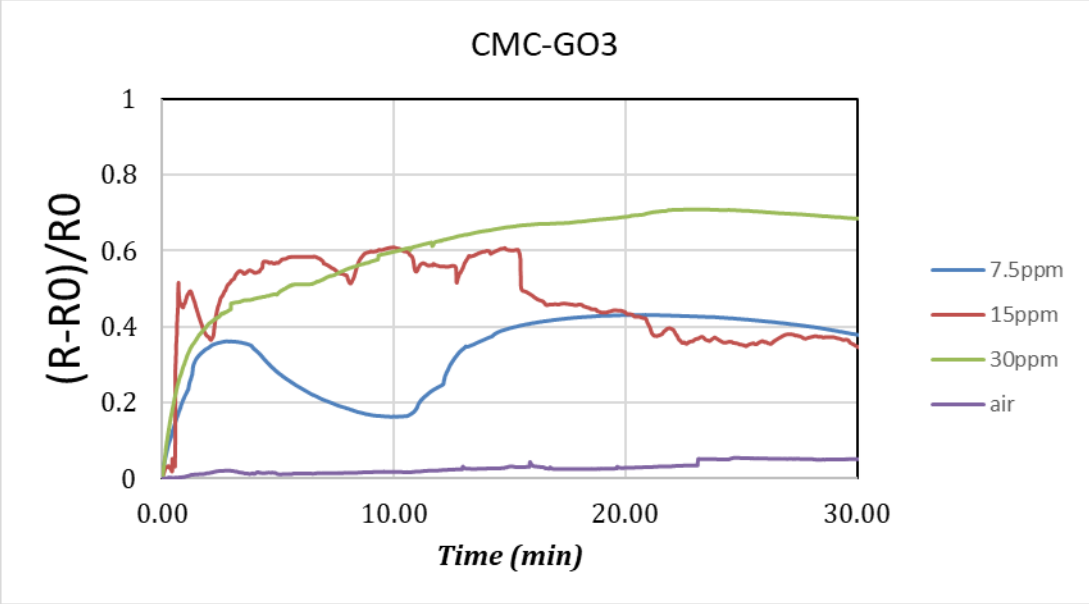

Figure 4. 19 Resistance variance of CMC-GO sensors upon exposure to ammonia gas released from ammonia gas with different concentrations.

4.11 Summary

A novel flexible, self-healable, and conductive hydrogel-based gas sensor was successfully fabricated by a simple two-step method. Conductive nanomaterials of RGO/Or GO were loaded into a cost-effective and non-toxic CMC hydrogel network, which make the hydrogels very sensitive upon exposure to ammonia gas. The prepared CMC-RGO hydrogels benefited from superior mechanical and electrical properties, exceptional self-healing ability, and highly gas-sensing performance, cost-effectiveness, and sustainability, making them promising materials for practical gas sensor applications.

Chapter 5: Conclusion and Future Work

In the present study, we developed a novel flexible, self-healable, and conductive hybrid hydrogel that is highly sensitive to ammonia gas at ambient temperature. Electro-conductive CMC hydrogels were fabricated via a facile and green approach by incorporating the conductive RGO/or GO into a cost-effective and non-toxic CMC matrix using citric acid as a cross-linker. The chemistry and morphology of the resulting hydrogels were characterized using FTIR and SEM. Mechanical, rheological, and conductivity tests were conducted to evaluate the hydrogels.

The 3D CMC hydrogel network was formed as a result of intra- and inter-molecular hydrogen bondings among constituents and hydrophobic interactions between the basal planes of conductive components (RGO/GO) and hydrophobic regions of CMC. Although all components are negatively charged, hydrogen bondings and hydrophobic interactions overcome the electrostatic repulsions and yield a physically cross-linked hydrogel with tunable mechanical properties. Morphological studies showed both CMC-RGO and CMC-GO hydrogels possess a homogeneous microporous and interconnected structure with pore sizes in the range of 100–200 μm. It demonstrated a well-dispersion and good miscibility of these conductive nanomaterials in the CMC network. The mechanical properties of both CMC-GO and CMC-RGO hydrogels are significantly improved due to the incorporation of GO and RGO, respectively.

With the incorporation of GO at a low ratio of 2mg/ml, the tensile strength of the composite hydrogels was dramatically enhanced by about 130% compared to those of pristine CMC hydrogels. Also, the maximum tensile fracture stress of CMC-rGO2 was almost 2.15 times greater than that of the pristine CMC hydrogel. The remarkable enhancement in the mechanical strength was endowed by GO and RGO nanosheets that acted as reinforcing nanofillers for the composite hydrogels. Rheological tests on the hydrogels demonstrate a more stable hydrogel network with dominant elastic behavior. The addition of GO or RGO endows the cellulose hydrogel an

outstanding self-healing ability without the need for external stimuli. The self-healing process can be achieved by physical entanglement and hydrogen bonding among CMC and the conductive components. The effect of conductive agents on self-healing capacity was investigated. The CMC hydrogels showed 63% healing efficiency in stress and 65% recovery in tensile strain. For CMC-GO2 hydrogel, these values considerably increased, with a healing efficiency of 91.2 % in the tensile stress and 94% in the tensile strain. When RGO was loaded, the obtained hydrogels showed 88.7% healing efficiency in stress and 86% recovery in tensile strain. The rheology tests further proved the excellent self-healing performance of the prepared hydrogels. The healing efficiency in storage moduli ranged from 76% to 93% by varying the RGO loading. The electrical properties can be tuned by altering the ratios of the nanomaterials. The prepared conductive CMC hydrogels showed superb conductivity, with CMC-RGO2 achieved the highest electrical conductivity at 4.4 $\times 10^{-2}$ S/cm.

Interestingly, the hydrogels showed sufficient restoration of the electrical properties after the self-healing process. CMC-RGO hydrogel sensors exhibit high sensitivity and desirable stability to ammonia gas. Upon exposure of CMC-RGO2 hydrogel to ammonia gas, the sensor response increases sharply and reaches a steady-state in about 6.6 min. The excellent sensitivity in ammonia gas detection is due to charge transfer between RGO and adsorbed gas elements and the formation of hydrogen bonds between the ammonia gas and many oxygenated functional groups on hydrogels' surface. The room-temperature sensing operation brings low energy consumption and thermal safety. The most critical challenge of GO-CMC hydrogel is the degree of functionalization with oxygenous functional groups, which deteriorates sensing stability. The oxygen functional groups of GO render it too electrically insulating for conductance-based sensors.

In short, we developed a flexible, self-healable, and conductive RGO-CMC hydrogel, which demonstrates excellent mechanical properties and remarkable self-healing capacity and gas-sensing performance, making it promising for practical applications in ammonia gas sensors. The unique advantages of the developed hydrogels include exceptional mechanical and electrical properties, remarkable self-healing capacity and highly gas-sensing performance, cost-effective and environmental friendliness,

A novel hydrogel-based wearable electronic biosensor is becoming a great alternative to traditional biosensors to monitor and manage human health. The RGO-CMC hydrogel can be developed into wearable biosensors to be used as electronic noses to precisely detect ammonia, which is a notorious toxic industrial pollutant and has serious adverse effects on human well-being. Also, the gas sensor's reusability will be investigated in future work to lower the cost of production. Integration of several vital features into a hydrogel has been a trend to broaden their practical application. Imparting 3D printability, conductivity, and eco-friendly and intrinsic self-healing ability will expand their service life and lower production costs. To fabricate the conductive gas sensor with a complex structure, the 3D printability of the conductive hydrogels can be explored by manipulating the various parameters, such as CMC concentrations. These efforts can be the focus of future research and development of the current work.

References

[1] X. Guan, M. Avci-Adali, E. Alarçin, H. Cheng, S.S. Kashaf, Y. Li, A. Chawla, H.L. Jang, A. Khademhosseini, Development of hydrogels for regenerative engineering, Biotechnol. J. 12 (2017) 10.1002/biot.201600394. https://doi.org/10.1002/biot.201600394.

[2] Y. Guo, J. Bae, F. Zhao, G. Yu, Functional Hydrogels for Next-Generation Batteries and Supercapacitors, Trends Chem. (2019). https://doi.org/10.1016/j.trechm.2019.03.005.

[3] L. Cao, M. Yang, D. Wu, F. Lyu, Z. Sun, X. Zhong, H. Pan, H. Liu, Z. Lu, Biopolymer-chitosan based supramolecular hydrogels as solid state electrolytes for electrochemical energy storage, Chem. Commun. (2017). https://doi.org/10.1039/c6cc08658f.

[4] J. Bae, J. Park, S. Kim, H. Cho, H.J. Kim, S. Park, D.S. Shin, Tailored hydrogels for biosensor applications, J. Ind. Eng. Chem. (2020). https://doi.org/10.1016/j.jiec.2020.05.001.

[5] K.M. Rao, A. Kumar, S.S. Han, Polysaccharide-based magnetically responsive polyelectrolyte hydrogels for tissue engineering applications, J. Mater. Sci. Technol. (2018). https://doi.org/10.1016/j.jmst.2017.10.003.

[6] M.C. Koetting, J.T. Peters, S.D. Steichen, N.A. Peppas, Stimulus-responsive hydrogels: Theory, modern advances, and applications, Mater. Sci. Eng. R Reports. (2015). https://doi.org/10.1016/j.mser.2015.04.001.

[7] A. Aldalbahi, P. Feng, N. Alhokbany, T. Ahamad, S.M. Alshehri, Synthesis, characterization, and CH4-sensing properties of conducting and magnetic biopolymer nano-composites, J. Environ. Chem. Eng. (2016). https://doi.org/10.1016/j.jece.2016.05.028.

[8] R. Dimatteo, N.J. Darling, T. Segura, In situ forming injectable hydrogels for drug delivery and wound repair, Adv. Drug Deliv. Rev. (2018). https://doi.org/10.1016/j.addr.2018.03.007.

[9] J. Wu, Z. Wu, S. Han, B.R. Yang, X. Gui, K. Tao, C. Liu, J. Miao, L.K. Norford, Extremely Deformable, Transparent, and High-Performance Gas Sensor Based on Ionic Conductive Hydrogel, ACS Appl. Mater. Interfaces. (2019). https://doi.org/10.1021/acsami.8b17437.

[10] J. Wu, K. Tao, J. Miao, L.K. Norford, Improved Selectivity and Sensitivity of Gas Sensing Using a 3D Reduced Graphene Oxide Hydrogel with an Integrated Microheater, ACS Appl. Mater. Interfaces. (2015). https://doi.org/10.1021/acsami.5b09695.

[11] Y. Jian, W. Hu, Z. Zhao, P. Cheng, H. Haick, M. Yao, W. Wu, Gas Sensors Based on Chemi-Resistive Hybrid Functional Nanomaterials, Nano-Micro Lett. (2020). https://doi.org/10.1007/s40820-020-0407-5.

[12] R. Tian, S. Wang, X. Hu, J.-G. Zheng, P. Ji, J. Lin, J. Zhang, M. Xu, J. Bao, S. Zuo, H. Zhang, W. Zhang, J. Wang, L. Yu, Novel approaches for highly selective, room-temperature gas sensors

based on atomically dispersed non-precious metals, J. Mater. Chem. A. (2020). https://doi.org/10.1039/d0ta05775d.

[13] H. Nazemi, A. Joseph, J. Park, A. Emadi, Advanced micro-and nano-gas sensor technology: A review, Sensors (Switzerland). (2019). https://doi.org/10.3390/s19061285.

[14] R. Alrammouz, J. Podlecki, P. Abboud, B. Sorli, R. Habchi, A review on flexible gas sensors: From materials to devices, Sensors Actuators, A Phys. (2018). https://doi.org/10.1016/j.sna.2018.10.036.

[15] H. Long, A. Harley-Trochimczyk, T. Pham, Z. Tang, T. Shi, A. Zettl, C. Carraro, M.A. Worsley, R. Maboudian, High Surface Area MoS2/Graphene Hybrid Aerogel for Ultrasensitive NO2 Detection, Adv. Funct. Mater. (2016). https://doi.org/10.1002/adfm.201601562.

[16] Y. Guo, T. Wang, F. Chen, X. Sun, X. Li, Z. Yu, P. Wan, X. Chen, Hierarchical graphene-polyaniline nanocomposite films for high-performance flexible electronic gas sensors, Nanoscale. (2016). https://doi.org/10.1039/c6nr02540d.

[17] K. Liu, S. Wei, L. Song, H. Liu, T. Wang, Conductive Hydrogels - A Novel Material: Recent Advances and Future Perspectives, J. Agric. Food Chem. (2020). https://doi.org/10.1021/acs.jafc.0c00642.

[18] W. Zhang, P. Feng, J. Chen, Z. Sun, B. Zhao, Electrically conductive hydrogels for flexible energy storage systems, Prog. Polym. Sci. (2018). https://doi.org/10.1016/j.progpolymsci.2018.09.001.

[19] Z. Ma, W. Shi, K. Yan, L. Pan, G. Yu, Doping engineering of conductive polymer hydrogels and their application in advanced sensor technologies, Chem. Sci. (2019). https://doi.org/10.1039/c9sc02033k.

[20] L. Tang, S. Wu, J. Qu, L. Gong, J. Tang, A review of conductive hydrogel used in flexible strain sensor, Materials (Basel). (2020). https://doi.org/10.3390/ma13183947.

[21] M. Nazouri, A. Seifzadeh, E. Masaeli, Characterization of polyvinyl alcohol hydrogels as tissue-engineered cartilage scaffolds using a coupled finite element-optimization algorithm, J. Biomech. (2020). https://doi.org/10.1016/j.jbiomech.2019.109525.

[22] Y. Shi, L. Pan, B. Liu, Y. Wang, Y. Cui, Z. Bao, G. Yu, Nanostructured conductive polypyrrole hydrogels as high-performance, flexible supercapacitor electrodes, J. Mater. Chem. A. (2014). https://doi.org/10.1039/c4ta00484a.

[23] R.S.H. Wong, K. Dodou, Effect of drug loading method and drug physicochemical properties on the material and drug release properties of poly (ethylene oxide) hydrogels for transdermal delivery, Polymers (Basel). (2017). https://doi.org/10.3390/polym9070286.

[24] J.N. Haigh, Y.M. Chuang, B. Farrugia, R. Hoogenboom, P.D. Dalton, T.R. Dargaville, Hierarchically Structured Porous Poly(2-oxazoline) Hydrogels, Macromol. Rapid Commun.

(2016). https://doi.org/10.1002/marc.201500495.

[25] R. Bhadani, U.K. Mitra, Synthesis and Studies on Water Swelling Behaviour of Polyacrylamide Hydrogels, Macromol. Symp. (2016). https://doi.org/10.1002/masy.201600051.

[26] M. Mahinroosta, Z. Jomeh Farsangi, A. Allahverdi, Z. Shakoori, Hydrogels as intelligent materials: A brief review of synthesis, properties and applications, Mater. Today Chem. (2018). https://doi.org/10.1016/j.mtchem.2018.02.004.

[27] P. Mohammadzadeh Pakdel, S.J. Peighambardoust, Review on recent progress in chitosan-based hydrogels for wastewater treatment application, Carbohydr. Polym. (2018). https://doi.org/10.1016/j.carbpol.2018.08.070.

[28] R. Song, M. Murphy, C. Li, K. Ting, C. Soo, Z. Zheng, Current development of biodegradable polymeric materials for biomedical applications, Drug Des. Devel. Ther. (2018). https://doi.org/10.2147/DDDT.S165440.

[29] Z. Shi, X. Gao, M.W. Ullah, S. Li, Q. Wang, G. Yang, Electroconductive natural polymer-based hydrogels, Biomaterials. (2016). https://doi.org/10.1016/j.biomaterials.2016.09.020.

[30] F. Ullah, M.B.H. Othman, F. Javed, Z. Ahmad, H.M. Akil, Classification, processing and application of hydrogels: A review, Mater. Sci. Eng. C. (2015). https://doi.org/10.1016/j.msec.2015.07.053.

[31] R.J. Moon, A. Martini, J. Nairn, J. Simonsen, J. Youngblood, Cellulose nanomaterials review: Structure, properties and nanocomposites, Chem. Soc. Rev. (2011). https://doi.org/10.1039/c0cs00108b.

[32] S. Wang, A. Lu, L. Zhang, Recent advances in regenerated cellulose materials, Prog. Polym. Sci. (2016). https://doi.org/10.1016/j.progpolymsci.2015.07.003.

[33] S.M.F. Kabir, P.P. Sikdar, B. Haque, M.A.R. Bhuiyan, A. Ali, M.N. Islam, Cellulose-based hydrogel materials: chemistry, properties and their prospective applications, Prog. Biomater. (2018). https://doi.org/10.1007/s40204-018-0095-0.

[34] A. Gandini, The Surface and In-Depth Modification of Cellulose Fibers, Adv. Polym. Sci. (2015). https://doi.org/10.1007/12.

[35] N.S.V. Capanema, A.A.P. Mansur, H.S. Mansur, A.C. de Jesus, S.M. Carvalho, P. Chagas, L.C. de Oliveira, Eco-friendly and biocompatible cross-linked carboxymethylcellulose hydrogels as adsorbents for the removal of organic dye pollutants for environmental applications, Environ. Technol. (United Kingdom). (2018). https://doi.org/10.1080/09593330.2017.1367845.

[36] K.J. De France, T. Hoare, E.D. Cranston, Review of Hydrogels and Aerogels Containing Nanocellulose, Chem. Mater. (2017). https://doi.org/10.1021/acs.chemmater.7b00531.

[37] R. Curvello, V.S. Raghuwanshi, G. Garnier, Engineering nanocellulose hydrogels for biomedical

applications, Adv. Colloid Interface Sci. (2019). https://doi.org/10.1016/j.cis.2019.03.002.

[38] D.M. Nascimento, Y.L. Nunes, M.C.B. Figueirêdo, H.M.C. De Azeredo, F.A. Aouada, J.P.A. Feitosa, M.F. Rosa, A. Dufresne, Nanocellulose nanocomposite hydrogels: Technological and environmental issues, Green Chem. (2018). https://doi.org/10.1039/c8gc00205c.

[39] M.T. Islam, M.M. Alam, A. Patrucco, A. Montarsolo, M. Zoccola, Preparation of Nanocellulose: A Review, AATCC J. Res. (2014). https://doi.org/10.14504/ajr.1.5.3.

[40] D. Miyashiro, R. Hamano, K. Umemura, A review of applications using mixed materials of cellulose, nanocellulose and carbon nanotubes, Nanomaterials. (2020). https://doi.org/10.3390/nano10020186.

[41] Z. Shi, W. Zhao, S. Li, G. Yang, Self-powered hydrogels induced by ion transport, Nanoscale. (2017). https://doi.org/10.1039/c7nr02962d.

[42] J.H. Min, M. Patel, W.G. Koh, Incorporation of conductive materials into hydrogels for tissue engineering applications, Polymers (Basel). (2018). https://doi.org/10.3390/polym10101078.

[43] Y. Zhao, B. Liu, L. Pan, G. Yu, 3D nanostructured conductive polymer hydrogels for high-performance electrochemical devices, Energy Environ. Sci. (2013). https://doi.org/10.1039/c3ee40997j.

[44] Hydrogels for Biomedical Applications: Cellulose, Chitosan, and Protein/Peptide Derivatives, Gels. (2017). https://doi.org/10.3390/gels3030027.

[45] D. Trache, M.H. Hussin, C.T. Hui Chuin, S. Sabar, M.R.N. Fazita, O.F.A. Taiwo, T.M. Hassan, M.K.M. Haafiz, Microcrystalline cellulose: Isolation, characterization and bio-composites application—A review, Int. J. Biol. Macromol. (2016). https://doi.org/10.1016/j.ijbiomac.2016.09.056.

[46] K. Bethke, S. Palantöken, V. Andrei, M. Roß, V.S. Raghuwanshi, F. Kettemann, K. Greis, T.T.K. Ingber, J.B. Stückrath, S. Valiyaveettil, K. Rademann, Functionalized Cellulose for Water Purification, Antimicrobial Applications, and Sensors, Adv. Funct. Mater. (2018). https://doi.org/10.1002/adfm.201800409.

[47] B. Tosh, Esterification and etherification of cellulose: Synthesis and application of cellulose derivatives, in: Cellul. Cellul. Deriv. Synth. Modif. Appl., 2015.

[48] K. Radotić, M. Mićić, Methods for Extraction and Purification of Lignin and Cellulose from Plant Tissues, in: 2016. https://doi.org/10.1007/978-1-4939-3185-9_26.

[49] T. Gurunathan, S. Mohanty, S.K. Nayak, A review of the recent developments in biocomposites based on natural fibres and their application perspectives, Compos. Part A Appl. Sci. Manuf. (2015). https://doi.org/10.1016/j.compositesa.2015.06.007.

[50] S. Ummartyotin, H. Manuspiya, A critical review on cellulose: From fundamental to an approach

on sensor technology, Renew. Sustain. Energy Rev. (2015). https://doi.org/10.1016/j.rser.2014.08.050.

[51] M. Börjesson, G. Westman, Crystalline Nanocellulose — Preparation, Modification, and Properties, in: Cellul. - Fundam. Asp. Curr. Trends, 2015. https://doi.org/10.5772/61899.

[52] H. Kargarzadeh, M. Ioelovich, I. Ahmad, S. Thomas, A. Dufresne, Methods for Extraction of Nanocellulose from Various Sources, in: Handb. Nanocellulose Cellul. Nanocomposites, 2017. https://doi.org/10.1002/9783527689972.ch1.

[53] D. Mudgil, The Interaction Between Insoluble and Soluble Fiber, in: Diet. Fiber Prev. Cardiovasc. Dis. Fiber's Interact. between Gut Micoflora, Sugar Metab. Weight Control Cardiovasc. Heal., 2017. https://doi.org/10.1016/B978-0-12-805130-6.00003-3.

[54] R.D.S. Bezerra, P.R.S. Teixeira, A.S.N.M. Teixeira, C. Eiras, J.A. Osajima, E.C.S. Filho, Chemical Functionalization of Cellulosic Materials — Main Reactions and Applications in the Contaminants Removal of Aqueous Medium, in: Cellul. - Fundam. Asp. Curr. Trends, 2015. https://doi.org/10.5772/61431.

[55] L. Vlaia, G. Coneac, I. Olariu, V. Vlaia, D. Lupuleasa, Cellulose-Derivatives-Based Hydrogels as Vehicles for Dermal and Transdermal Drug Delivery, in: Emerg. Concepts Anal. Appl. Hydrogels, 2016. https://doi.org/10.5772/63953.

[56] J.H. Kim, B.S. Shim, H.S. Kim, Y.J. Lee, S.K. Min, D. Jang, Z. Abas, J. Kim, Review of nanocellulose for sustainable future materials, Int. J. Precis. Eng. Manuf. - Green Technol. (2015). https://doi.org/10.1007/s40684-015-0024-9.

[57] A.J. Onyianta, M. Dorris, R.L. Williams, Aqueous morpholine pre-treatment in cellulose nanofibril (CNF) production: comparison with carboxymethylation and TEMPO oxidisation pre-treatment methods, Cellulose. (2018). https://doi.org/10.1007/s10570-017-1631-0.

[58] P.R. Sharma, A. Chattopadhyay, S.K. Sharma, L. Geng, N. Amiralian, D. Martin, B.S. Hsiao, Nanocellulose from Spinifex as an Effective Adsorbent to Remove Cadmium(II) from Water, ACS Sustain. Chem. Eng. (2018). https://doi.org/10.1021/acssuschemeng.7b03473.

[59] H. Liimatainen, T. Suopajärvi, J. Sirviö, O. Hormi, J. Niinimäki, Fabrication of cationic cellulosic nanofibrils through aqueous quaternization pretreatment and their use in colloid aggregation, Carbohydr. Polym. (2014). https://doi.org/10.1016/j.carbpol.2013.12.042.

[60] Y. Okahisa, Y. Furukawa, K. Ishimoto, C. Narita, K. Intharapichai, H. Ohara, Comparison of cellulose nanofiber properties produced from different parts of the oil palm tree, Carbohydr. Polym. (2018). https://doi.org/10.1016/j.carbpol.2018.06.089.

[61] A. Isogai, Wood nanocelluloses: Fundamentals and applications as new bio-based nanomaterials, J. Wood Sci. (2013). https://doi.org/10.1007/s10086-013-1365-z.

[62] A. Ilyas Rushdana, M. Sapuan Salit, M. Lamin Sanyang, M. Ridzwan Ishak, Nanocrystalline Cellulose As Reinforcement For Polymeric Matrix Nanocomposites And Its Potential Applications: A Review, Curr. Anal. Chem. (2017). https://doi.org/10.2174/1573411013666171003155624.

[63] R.M.A. Domingues, M.E. Gomes, R.L. Reis, The potential of cellulose nanocrystals in tissue engineering strategies, Biomacromolecules. (2014). https://doi.org/10.1021/bm500524s.

[64] N. Lavoine, L. Bergström, Nanocellulose-based foams and aerogels: Processing, properties, and applications, J. Mater. Chem. A. (2017). https://doi.org/10.1039/c7ta02807e.

[65] H. Charreau, M. L. Foresti, A. Vazquez, Nanocellulose Patents Trends: A Comprehensive Review on Patents on Cellulose Nanocrystals, Microfibrillated and Bacterial Cellulose, Recent Pat. Nanotechnol. (2013). https://doi.org/10.2174/1872210511307010056.

[66] D. Klemm, F. Kramer, S. Moritz, T. Lindström, M. Ankerfors, D. Gray, A. Dorris, Nanocelluloses: A new family of nature-based materials, Angew. Chemie - Int. Ed. (2011). https://doi.org/10.1002/anie.201001273.

[67] J. Araki, M. Wada, S. Kuga, T. Okano, Birefringent Glassy Phase of a Cellulose Microcrystal Suspension, Langmuir. (2000). https://doi.org/10.1021/la9911180.

[68] W. Treesuppharat, P. Rojanapanthu, C. Siangsanoh, H. Manuspiya, S. Ummartyotin, Synthesis and characterization of bacterial cellulose and gelatin-based hydrogel composites for drug-delivery systems, Biotechnol. Reports. (2017). https://doi.org/10.1016/j.btre.2017.07.002.

[69] X. Gao, Z. Shi, A. Lau, C. Liu, G. Yang, V. V. Silberschmidt, Effect of microstructure on anomalous strain-rate-dependent behaviour of bacterial cellulose hydrogel, Mater. Sci. Eng. C. (2016). https://doi.org/10.1016/j.msec.2016.01.042.

[70] E.Y.X. Loh, N. Mohamad, M.B. Fauzi, M.H. Ng, S.F. Ng, M.C.I. Mohd Amin, Development of a bacterial cellulose-based hydrogel cell carrier containing keratinocytes and fibroblasts for full-thickness wound healing, Sci. Rep. (2018). https://doi.org/10.1038/s41598-018-21174-7.

[71] X. Gao, Z. Shi, C. Liu, G. Yang, I. Sevostianov, V. V. Silberschmidt, Inelastic behaviour of bacterial cellulose hydrogel: In aqua cyclic tests, Polym. Test. (2015). https://doi.org/10.1016/j.polymertesting.2015.03.021.

[72] F. Esa, S.M. Tasirin, N.A. Rahman, Overview of Bacterial Cellulose Production and Application, Agric. Agric. Sci. Procedia. (2014). https://doi.org/10.1016/j.aaspro.2014.11.017.

[73] L. Fang, L. Zhao, X. Liang, H. Xiao, L. Qian, Effects of oxidant and dopants on the properties of cellulose/PPy conductive composite hydrogels, J. Appl. Polym. Sci. (2016). https://doi.org/10.1002/app.43759.

[74] X. Shi, Y. Hu, K. Tu, L. Zhang, H. Wang, J. Xu, H. Zhang, J. Li, X. Wang, M. Xu,

Electromechanical polyaniline-cellulose hydrogels with high compressive strength, Soft Matter. (2013). https://doi.org/10.1039/c3sm51490k.

[75] D. Xu, L. Fan, L. Gao, Y. Xiong, Y. Wang, Q. Ye, A. Yu, H. Dai, Y. Yin, J. Cai, L. Zhang, Micro-Nanostructured Polyaniline Assembled in Cellulose Matrix via Interfacial Polymerization for Applications in Nerve Regeneration, ACS Appl. Mater. Interfaces. (2016). https://doi.org/10.1021/acsami.6b03555.

[76] Z. Sun, L. Yang, J. Zhao, W. Song, Natural Cellulose-Full-Hydrogels Bioinspired Electroactive Artificial Muscles: Highly Conductive Ionic Transportation Channels and Ultrafast Electromechanical Response, J. Electrochem. Soc. (2020). https://doi.org/10.1149/1945-7111/ab732e.

[77] G.K. Knopf, D. Sinar, Flexible hydrogel actuated graphene-cellulose biosensor for monitoring pH, in: Proc. - IEEE Int. Symp. Circuits Syst., 2017. https://doi.org/10.1109/ISCAS.2017.8050613.

[78] I. Hussain, S.M. Sayed, S. Liu, O. Oderinde, M. Kang, F. Yao, G. Fu, Enhancing the mechanical properties and self-healing efficiency of hydroxyethyl cellulose-based conductive hydrogels via supramolecular interactions, Eur. Polym. J. (2018). https://doi.org/10.1016/j.eurpolymj.2018.05.025.

[79] J. Li, L. Fang, W.R. Tait, L. Sun, L. Zhao, L. Qian, Preparation of conductive composite hydrogels from carboxymethyl cellulose and polyaniline with a nontoxic crosslinking agent, RSC Adv. (2017). https://doi.org/10.1039/c7ra10788a.

[80] R. Barras, I. Cunha, D. Gaspar, E. Fortunato, R. Martins, L. Pereira, Printable cellulose-based electroconductive composites for sensing elements in paper electronics, Flex. Print. Electron. (2017). https://doi.org/10.1088/2058-8585/aa5ef9.

[81] H. Rastin, B. Zhang, J. Bi, K. Hassan, T.T. Tung, D. Losic, 3D printing of cell-laden electroconductive bioinks for tissue engineering applications, J. Mater. Chem. B. (2020). https://doi.org/10.1039/d0tb00627k.

[82] Y. Chen, K. Lu, Y. Song, J. Han, Y. Yue, S.K. Biswas, Q. Wu, H. Xiao, A skin-inspired stretchable, self-healing and electro-conductive hydrogel with a synergistic triple network for wearable strain sensors applied in human-motion detection, Nanomaterials. (2019). https://doi.org/10.3390/nano9121737.

[83] C. Chen, Y. Wang, T. Meng, Q. Wu, L. Fang, D. Zhao, Y. Zhang, D. Li, Electrically conductive polyacrylamide/carbon nanotube hydrogel: reinforcing effect from cellulose nanofibers, Cellulose. (2019). https://doi.org/10.1007/s10570-019-02710-8.

[84] V. Kuzmenko, E. Karabulut, E. Pernevik, P. Enoksson, P. Gatenholm, Tailor-made conductive inks from cellulose nanofibrils for 3D printing of neural guidelines, Carbohydr. Polym. (2018).

https://doi.org/10.1016/j.carbpol.2018.01.097.

[85] C. Zheng, Y. Yue, L. Gan, X. Xu, C. Mei, J. Han, Highly stretchable and self-healing strain sensors based on nanocellulose-supported graphene dispersed in electro-conductive hydrogels, Nanomaterials. (2019). https://doi.org/10.3390/nano9070937.

[86] Q. Ding, X. Xu, Y. Yue, C. Mei, C. Huang, S. Jiang, Q. Wu, J. Han, Nanocellulose-Mediated Electroconductive Self-Healing Hydrogels with High Strength, Plasticity, Viscoelasticity, Stretchability, and Biocompatibility toward Multifunctional Applications, ACS Appl. Mater. Interfaces. (2018). https://doi.org/10.1021/acsami.8b09656.

[87] K. Liu, L. Chen, L. Huang, Y. Ni, Z. Xu, S. Lin, H. Wang, A facile preparation strategy for conductive and magnetic agarose hydrogels with reversible restorability composed of nanofibrillated cellulose, polypyrrole, and Fe3O4, Cellulose. 25 (2018) 4565–4575. https://doi.org/10.1007/s10570-018-1889-x.

[88] K. Liu, X. Pan, L. Chen, L. Huang, Y. Ni, J. Liu, S. Cao, H. Wang, Ultrasoft Self-Healing Nanoparticle-Hydrogel Composites with Conductive and Magnetic Properties, ACS Sustain. Chem. Eng. 6 (2018) 6395–6403. https://doi.org/10.1021/acssuschemeng.8b00193.

[89] F. Lin, R. Zheng, J. Chen, W. Su, B. Dong, C. Lin, B. Huang, B. Lu, Microfibrillated cellulose enhancement to mechanical and conductive properties of biocompatible hydrogels, Carbohydr. Polym. 205 (2019) 244–254. https://doi.org/https://doi.org/10.1016/j.carbpol.2018.10.037.

[90] G. Nyström, A. Mihranyan, A. Razaq, T. Lindström, L. Nyholm, M. Strømme, A nanocellulose polypyrrole composite based on microfibrillated cellulose from wood, J. Phys. Chem. B. (2010). https://doi.org/10.1021/jp911272m.

[91] Y. Li, H. Zhu, Y. Wang, U. Ray, S. Zhu, J. Dai, C. Chen, K. Fu, S.-H. Jang, D. Henderson, T. Li, L. Hu, Cellulose-Nanofiber-Enabled 3D Printing of a Carbon-Nanotube Microfiber Network, Small Methods. (2017). https://doi.org/10.1002/smtd.201700222.

[92] K.M.O. Håkansson, I.C. Henriksson, C. de la Peña Vázquez, V. Kuzmenko, K. Markstedt, P. Enoksson, P. Gatenholm, Solidification of 3D Printed Nanofibril Hydrogels into Functional 3D Cellulose Structures, Adv. Mater. Technol. (2016). https://doi.org/10.1002/admt.201600096.

[93] M. Bordoni, E. Karabulut, V. Kuzmenko, V. Fantini, O. Pansarasa, C. Cereda, P. Gatenholm, 3D Printed Conductive Nanocellulose Scaffolds for the Differentiation of Human Neuroblastoma Cells, Cells. (2020). https://doi.org/10.3390/cells9030682.

[94] Y. Li, H. Zhang, S. Ni, H. Xiao, In situ synthesis of conductive nanocrystal cellulose/polypyrrole composite hydrogel based on semi-interpenetrating network, Mater. Lett. (2018). https://doi.org/10.1016/j.matlet.2018.08.115.

[95] X. Liang, B. Qu, J. Li, H. Xiao, B. He, L. Qian, Preparation of cellulose-based conductive

hydrogels with ionic liquid, React. Funct. Polym. (2015). https://doi.org/10.1016/j.reactfunctpolym.2014.11.002.

[96] F. Hoeng, J. Bras, E. Gicquel, G. Krosnicki, A. Denneulin, Inkjet printing of nanocellulose-silver ink onto nanocellulose coated cardboard, RSC Adv. (2017). https://doi.org/10.1039/c6ra23667g.

[97] M. Alizadehgiashi, A. Gevorkian, M. Tebbe, M. Seo, E. Prince, E. Kumacheva, 3D-Printed Microfluidic Devices for Materials Science, Adv. Mater. Technol. (2018). https://doi.org/10.1002/admt.201800068.

[98] H.H. Hsu, Y. Liu, Y. Wang, B. Li, G. Luo, M. Xing, W. Zhong, Mussel-Inspired Autonomously Self-Healable All-in-One Supercapacitor with Biocompatible Hydrogel, ACS Sustain. Chem. Eng. (2020). https://doi.org/10.1021/acssuschemeng.9b07250.

[99] S. Liu, Y. Zheng, Y. Sun, L. Su, L. Yue, Y. Sen Wang, J. Feng, J. Fan, An oxygen tolerance conductive hydrogel anode membrane for use in a potentially implantable glucose fuel cell, RSC Adv. (2016). https://doi.org/10.1039/c6ra22702c.

[100] M. Mashkour, M. Rahimnejad, M. Mashkour, G. Bakeri, R. Luque, S.E. Oh, Application of Wet Nanostructured Bacterial Cellulose as a Novel Hydrogel Bioanode for Microbial Fuel Cells, ChemElectroChem. (2017). https://doi.org/10.1002/celc.201600868.

[101] Z. Shi, S. Zang, F. Jiang, L. Huang, D. Lu, Y. Ma, G. Yang, In situ nano-assembly of bacterial cellulose-polyaniline composites, RSC Adv. (2012). https://doi.org/10.1039/c1ra00719j.

[102] J. Huang, D. Li, M. Zhao, P. Lv, L. Lucia, Q. Wei, Highly stretchable and bio-based sensors for sensitive strain detection of angular displacements, Cellulose. (2019). https://doi.org/10.1007/s10570-019-02313-3.

[103] J. Huang, M. Zhao, Y. Cai, M. Zimniewska, D. Li, Q. Wei, A Dual-Mode Wearable Sensor Based on Bacterial Cellulose Reinforced Hydrogels for Highly Sensitive Strain/Pressure Sensing, Adv. Electron. Mater. (2020). https://doi.org/10.1002/aelm.201900934.

[104] H. Zhu, Z. Fang, C. Preston, Y. Li, L. Hu, Transparent paper: Fabrications, properties, and device applications, Energy Environ. Sci. (2014). https://doi.org/10.1039/c3ee43024c.

[105] M. Sakata, C. Hongo, T. Matsumoto, T. Nishino, Cellulose nanofiber nanocomposites with aligned silver nanoparticles AU - Ito, Hiroaki, Nanocomposites. (2019) 1–11. https://doi.org/10.1080/20550324.2018.1556912.

[106] Y. Wang, Y. Zhu, Y. Xue, J. Wang, X. Li, X. Wu, Y. Qin, W. Chen, Sequential in-situ route to synthesize novel composite hydrogels with excellent mechanical, conductive, and magnetic responsive properties, Mater. Des. (2020) 108759. https://doi.org/https://doi.org/10.1016/j.matdes.2020.108759.

[107] Q. Wang, J. Sun, Q. Yao, C. Ji, J. Liu, Q. Zhu, 3D printing with cellulose materials, Cellulose.

(2018). https://doi.org/10.1007/s10570-018-1888-y.

[108] P. Parandoush, D. Lin, A review on additive manufacturing of polymer-fiber composites, Compos. Struct. (2017). https://doi.org/10.1016/j.compstruct.2017.08.088.

[109] X. Wang, M. Jiang, Z. Zhou, J. Gou, D. Hui, 3D printing of polymer matrix composites: A review and prospective, Compos. Part B Eng. (2017). https://doi.org/10.1016/j.compositesb.2016.11.034.

[110] T.D. Ngo, A. Kashani, G. Imbalzano, K.T.Q. Nguyen, D. Hui, Additive manufacturing (3D printing): A review of materials, methods, applications and challenges, Compos. Part B Eng. (2018). https://doi.org/10.1016/j.compositesb.2018.02.012.

[111] J.Y. Lee, J. An, C.K. Chua, Fundamentals and applications of 3D printing for novel materials, Appl. Mater. Today. (2017). https://doi.org/10.1016/j.apmt.2017.02.004.

[112] H. Li, C. Tan, L. Li, Review of 3D printable hydrogels and constructs, Mater. Des. (2018). https://doi.org/10.1016/j.matdes.2018.08.023.

[113] J.T. Belter, A.M. Dollar, Strengthening of 3D printed fused deposition manufactured parts using the fill compositing technique, PLoS One. (2015). https://doi.org/10.1371/journal.pone.0122915.

[114] K. Markstedt, J. Sundberg, P. Gatenholm, 3D Bioprinting of Cellulose Structures from an Ionic Liquid, 3D Print. Addit. Manuf. (2014). https://doi.org/10.1089/3dp.2014.0004.

[115] Y. Jiang, J. Zhou, C. Feng, H. Shi, G. Zhao, Y. Bian, Rheological behavior, 3D printability and the formation of scaffolds with cellulose nanocrystals/gelatin hydrogels, J. Mater. Sci. (2020). https://doi.org/10.1007/s10853-020-05128-x.

[116] S. Sultan, A.P. Mathew, 3D printed porous cellulose nanocomposite hydrogel scaffolds, J. Vis. Exp. (2019). https://doi.org/10.3791/59401.

[117] L. Dai, T. Cheng, C. Duan, W. Zhao, W. Zhang, X. Zou, J. Aspler, Y. Ni, 3D printing using plant-derived cellulose and its derivatives: A review, Carbohydr. Polym. (2019). https://doi.org/10.1016/j.carbpol.2018.09.027.

[118] J.S. Park, T. Kim, W.S. Kim, Conductive Cellulose Composites with Low Percolation Threshold for 3D Printed Electronics, Sci. Rep. (2017). https://doi.org/10.1038/s41598-017-03365-w.

[119] S.S. Athukoralalage, R. Balu, N.K. Dutta, N.R. Choudhury, 3D bioprinted nanocellulose-based hydrogels for tissue engineering applications: A brief review, Polymers (Basel). (2019). https://doi.org/10.3390/polym11050898.

[120] S. Sultan, G. Siqueira, T. Zimmermann, A.P. Mathew, 3D printing of nano-cellulosic biomaterials for medical applications, Curr. Opin. Biomed. Eng. (2017). https://doi.org/10.1016/j.cobme.2017.06.002.

[121] J. Chen, Q. Peng, T. Thundat, H. Zeng, Stretchable, Injectable, and Self-Healing Conductive Hydrogel Enabled by Multiple Hydrogen Bonding toward Wearable Electronics, Chem. Mater.

(2019). https://doi.org/10.1021/acs.chemmater.9b01239.

[122] M.L. Oyen, Mechanical characterisation of hydrogel materials, Int. Mater. Rev. (2014). https://doi.org/10.1179/1743280413Y.0000000022.

[123] T.A. Khattab, S. Dacrory, H. Abou-Yousef, S. Kamel, Development of microporous cellulose-based smart xerogel reversible sensor via freeze drying for naked-eye detection of ammonia gas, Carbohydr. Polym. (2019). https://doi.org/10.1016/j.carbpol.2019.01.067.

[124] N.R. Tanguy, M. Thompson, N. Yan, A review on advances in application of polyaniline for ammonia detection, Sensors Actuators, B Chem. (2018). https://doi.org/10.1016/j.snb.2017.11.008.

[125] L. Wang, H. Huang, S. Xiao, D. Cai, Y. Liu, B. Liu, D. Wang, C. Wang, H. Li, Y. Wang, Q. Li, T. Wang, Enhanced sensitivity and stability of room-temperature NH3 sensors using core-shell CeO2 nanoparticles@cross-linked PANI with p-n heterojunctions, ACS Appl. Mater. Interfaces. (2014). https://doi.org/10.1021/am503286h.

[126] Y. Wang, Q. Chang, R. Zhan, K. Xu, Y. Wang, X. Zhang, B. Li, G. Luo, M. Xing, W. Zhong, Tough but self-healing and 3D printable hydrogels for E-skin, E-noses and laser controlled actuators, J. Mater. Chem. A. (2019). https://doi.org/10.1039/c9ta04248b.

[127] H. Bai, K. Sheng, P. Zhang, C. Li, G. Shi, Graphene oxide/conducting polymer composite hydrogels, J. Mater. Chem. (2011). https://doi.org/10.1039/c1jm13918e.

[128] H. Golmohammadi, E. Morales-Narváez, T. Naghdi, A. Merkoçi, Nanocellulose in Sensing and Biosensing, Chem. Mater. (2017). https://doi.org/10.1021/acs.chemmater.7b01170.

[129] T. Abel, B. Ungerböck, I. Klimant, T. Mayr, Fast responsive, optical trace level ammonia sensor for environmental monitoring, Chem. Cent. J. (2012). https://doi.org/10.1186/1752-153X-6-124.

[130] H. Zhi, J. Gao, L. Feng, Hydrogel-Based Gas Sensors for NO2 and NH3, ACS Sensors. (2020). https://doi.org/10.1021/acssensors.9b02383.

[131] M. Tomczykowa, M.E. Plonska-Brzezinska, Conducting polymers, hydrogels and their composites: Preparation, properties and bioapplications, Polymers (Basel). (2019). https://doi.org/10.3390/polym11020350.

[132] R. Ghosh, A. Midya, S. Santra, S.K. Ray, P.K. Guha, Chemically reduced graphene oxide for ammonia detection at room temperature, ACS Appl. Mater. Interfaces. (2013). https://doi.org/10.1021/am4019109.

[133] Q. Zhu, S. Liu, J. Sun, J. Liu, C.J. Kirubaharan, H. Chen, W. Xu, Q. Wang, Stimuli-responsive cellulose nanomaterials for smart applications, Carbohydr. Polym. (2020). https://doi.org/10.1016/j.carbpol.2020.115933.

[134] H.H. Hsu, A. Khosrozadeh, B. Li, G. Luo, M. Xing, W. Zhong, An Eco-Friendly,

Nanocellulose/RGO/in Situ Formed Polyaniline for Flexible and Free-Standing Supercapacitors, ACS Sustain. Chem. Eng. (2019). https://doi.org/10.1021/acssuschemeng.8b04947.

[135] W.J. Zheng, J. Gao, Z. Wei, J. Zhou, Y.M. Chen, Facile fabrication of self-healing carboxymethyl cellulose hydrogels, Eur. Polym. J. (2015). https://doi.org/10.1016/j.eurpolymj.2015.06.013.

[136] H. Si, H. Luo, G. Xiong, Z. Yang, S.R. Raman, R. Guo, Y. Wan, One-step in situ biosynthesis of graphene oxide-bacterial cellulose nanocomposite hydrogels, Macromol. Rapid Commun. (2014). https://doi.org/10.1002/marc.201400239.

[137] M.B. Heaney, Electrical conductivity and resistivity, in: Electr. Meas. Signal Process. Displays, 2003. https://doi.org/10.1201/9780203009406.

[138] S. Bhadra, C. Narvaez, D.J. Thomson, G.E. Bridges, Non-destructive detection of fish spoilage using a wireless basic volatile sensor, Talanta. (2015). https://doi.org/10.1016/j.talanta.2014.12.017.

[139] C. Li, S. Zhang, M. Hu, C. Xie, Nanostructural ZnO based coplanar gas sensor arrays from the injection of metal chloride solutions: Device processing, gas-sensing properties and selectivity in liquors applications, Sensors Actuators, B Chem. (2011). https://doi.org/10.1016/j.snb.2010.11.008.

[140] A.T. Smith, A.M. LaChance, S. Zeng, B. Liu, L. Sun, Synthesis, properties, and applications of graphene oxide/reduced graphene oxide and their nanocomposites, Nano Mater. Sci. (2019). https://doi.org/10.1016/j.nanoms.2019.02.004.

[141] R. Tarcan, O. Todor-Boer, I. Petrovai, C. Leordean, S. Astilean, I. Botiz, Reduced graphene oxide today, J. Mater. Chem. C. (2020). https://doi.org/10.1039/c9tc04916a.

[142] Z. Bo, X. Shuai, S. Mao, H. Yang, J. Qian, J. Chen, J. Yan, K. Cen, Green preparation of reduced graphene oxide for sensing and energy storage applications, Sci. Rep. (2014). https://doi.org/10.1038/srep04684.

[143] S. Pei, H.M. Cheng, The reduction of graphene oxide, Carbon N. Y. (2012). https://doi.org/10.1016/j.carbon.2011.11.010.

[144] S.H. Yu, J. Cho, K.M. Sim, J.U. Ha, D.S. Chung, Morphology-Driven High-Performance Polymer Transistor-based Ammonia Gas Sensor, ACS Appl. Mater. Interfaces. (2016). https://doi.org/10.1021/acsami.6b00471.

[145] M. Rasoulzadeh, H. Namazi, Carboxymethyl cellulose/graphene oxide bio-nanocomposite hydrogel beads as anticancer drug carrier agent, Carbohydr. Polym. (2017). https://doi.org/10.1016/j.carbpol.2017.03.014.

[146] X. Yu, D. Kang, Y. Hu, S. Tong, M. Ge, C. Cao, W. Song, One-pot synthesis of porous magnetic cellulose beads for the removal of metal ions, RSC Adv. (2014).

https://doi.org/10.1039/c4ra05601a.

[147] X. Chen, S. Zhou, L. Zhang, T. You, F. Xu, Adsorption of heavy metals by graphene oxide/cellulose hydrogel prepared from NaOH/urea aqueous solution, Materials (Basel). (2016). https://doi.org/10.3390/MA9070582.

[148] A. Pettignano, A. Charlot, E. Fleury, Solvent-free synthesis of amidated carboxymethyl cellulose derivatives: Effect on the thermal properties, Polymers (Basel). (2019). https://doi.org/10.3390/polym11071227.

[149] T.F. Emiru, D.W. Ayele, Controlled synthesis, characterization and reduction of graphene oxide: A convenient method for large scale production, Egypt. J. Basic Appl. Sci. (2017). https://doi.org/10.1016/j.ejbas.2016.11.002.

[150] M. Xu, Q. Huang, X. Wang, R. Sun, Highly tough cellulose/graphene composite hydrogels prepared from ionic liquids, Ind. Crops Prod. (2015). https://doi.org/10.1016/j.indcrop.2015.03.004.

[151] J. Liu, C. Zhang, D. Miao, S. Sui, F. Deng, C. Dong, L. Zhang, P. Zhu, Preparation and characterization of carboxymethylcellulose hydrogel fibers, J. Eng. Fiber. Fabr. (2018). https://doi.org/10.1177/155892501801300302.

[152] R. Atif, I. Shyha, F. Inam, Mechanical, thermal, and electrical properties of graphene-epoxy nanocomposites-A review, Polymers (Basel). (2016). https://doi.org/10.3390/polym8080281.

[153] J.M. Zuidema, C.J. Rivet, R.J. Gilbert, F.A. Morrison, A protocol for rheological characterization of hydrogels for tissue engineering strategies, J. Biomed. Mater. Res. - Part B Appl. Biomater. (2014). https://doi.org/10.1002/jbm.b.33088.

[154] B. von Lospichl, S. Hemmati-Sadeghi, P. Dey, T. Dehne, R. Haag, M. Sittinger, J. Ringe, M. Gradzielski, Injectable hydrogels for treatment of osteoarthritis – A rheological study, Colloids Surfaces B Biointerfaces. (2017). https://doi.org/10.1016/j.colsurfb.2017.07.073.

[155] A. Islam, M. Riaz, T. Yasin, Structural and viscoelastic properties of chitosan-based hydrogel and its drug delivery application, Int. J. Biol. Macromol. (2013). https://doi.org/10.1016/j.ijbiomac.2013.04.044.

[156] E.B. Souto, S.A. Wissing, C.M. Barbosa, R.H. Müller, Evaluation of the physical stability of SLN and NLC before and after incorporation into hydrogel formulations, Eur. J. Pharm. Biopharm. (2004). https://doi.org/10.1016/j.ejpb.2004.02.015.

[157] J.J. Roberts, A. Earnshaw, V.L. Ferguson, S.J. Bryant, Comparative study of the viscoelastic mechanical behavior of agarose and poly(ethylene glycol) hydrogels, J. Biomed. Mater. Res. - Part B Appl. Biomater. (2011). https://doi.org/10.1002/jbm.b.31883.

[158] N.A. Sirajuddin, M.S.M. Jamil, M.A.S.M. Lazim, Effect of cross-link density and the healing

efficiency of self-healing poly(2-hydroxyethyl methacrylate) hydrogel, E-Polymers. (2014). https://doi.org/10.1515/epoly-2014-0036.

[159] A. Khabibullin, M. Alizadehgiashi, N. Khuu, E. Prince, M. Tebbe, E. Kumacheva, Injectable Shear-Thinning Fluorescent Hydrogel Formed by Cellulose Nanocrystals and Graphene Quantum Dots, Langmuir. (2017). https://doi.org/10.1021/acs.langmuir.7b02906.

[160] J. Tang, M.U. Javaid, C. Pan, G. Yu, R.M. Berry, K.C. Tam, Self-healing stimuli-responsive cellulose nanocrystal hydrogels, Carbohydr. Polym. (2020). https://doi.org/10.1016/j.carbpol.2019.115486.

[161] Q. Peng, J. Chen, T. Wang, X. Peng, J. Liu, X. Wang, J. Wang, H. Zeng, Recent advances in designing conductive hydrogels for flexible electronics, InfoMat. (2020). https://doi.org/10.1002/inf2.12113.

[162] J. Phiri, L.S. Johansson, P. Gane, T. Maloney, A comparative study of mechanical, thermal and electrical properties of graphene-, graphene oxide- and reduced graphene oxide-doped microfibrillated cellulose nanocomposites, Compos. Part B Eng. (2018). https://doi.org/10.1016/j.compositesb.2018.04.018.

[163] Y. Liu, L. Xia, Q. Zhang, H. Guo, A. Wang, W. Xu, Y. Wang, Structure and properties of carboxymethyl cotton fabric loaded by reduced graphene oxide, Carbohydr. Polym. (2019). https://doi.org/10.1016/j.carbpol.2019.03.028.

[164] J. Wu, K. Tao, J. Miao, L.K. Norford, Enhanced gas sensing by 3D water steamed graphene hydrogel, Solid. State. Electron. (2017). https://doi.org/10.1016/j.sse.2017.10.004.

[165] W. Yuan, A. Liu, L. Huang, C. Li, G. Shi, High-performance NO2 sensors based on chemically modified graphene, Adv. Mater. (2013). https://doi.org/10.1002/adma.201203172.

[166] N. Sharma, V. Sharma, R. Vyas, M. Kumari, A. Kaushal, R. Gupta, S.K. Sharma, K. Sachdev, A new sustainable green protocol for production of reduced graphene oxide and its gas sensing properties, J. Sci. Adv. Mater. Devices. (2019). https://doi.org/10.1016/j.jsamd.2019.07.005.

[167] S. Prezioso, F. Perrozzi, L. Giancaterini, C. Cantalini, E. Treossi, V. Palermo, M. Nardone, S. Santucci, L. Ottaviano, Graphene oxide as a practical solution to high sensitivity gas sensing, J. Phys. Chem. C. (2013). https://doi.org/10.1021/jp3085759.

[168] P.G. Su, S.L. Peng, Fabrication and NO2 gas-sensing properties of reduced graphene oxide/WO3 nanocomposite films, Talanta. (2015). https://doi.org/10.1016/j.talanta.2014.09.034.

[169] K. Toda, R. Furue, S. Hayami, Recent progress in applications of graphene oxide for gas sensing: A review, Anal. Chim. Acta. (2015). https://doi.org/10.1016/j.aca.2015.02.002.

[170] H. Qi, J. Liu, J. Pionteck, P. Pötschke, E. Mäder, Carbon nanotube-cellulose composite aerogels for vapour sensing, Sensors Actuators, B Chem. (2015). https://doi.org/10.1016/j.snb.2015.02.067.